EUROPEAN COMMISSION

nuclear science and technology

Large-scale Experiments on Core Degradation, Melt Retention and Coolability

(LACOMERA)

Contract No: FIR1-CT2002-40157
(Duration: 1 September 2002 to 31 August 2006)

Final report

Work performed as part of the European Atomic Energy Community's R&T specific programme
Nuclear Energy 1998-2002, key action Nuclear Fission Safety
(Fifth Framework Programme)
Area: Operational safety of existing installations

2007

Directorate-General for Research
Euratom

Project coordinator

A. Miassoedov, H. Alsmeyer, B. Fluhrer, W. Hering, C. Homann, L. Meyer,
L. Sepold, M. Steinbrück, J. Stuckert
Forschungszentrum Karlsruhe, Germany (FZK)

Project partners

J. Birchley, T. Haste
Paul Scherrer Institut, Switzerland (PSI)

C. Caroli, M. Cranga, F. Fichot
Institut de radioprotection et de sûreté nucléaire, France (IRSN)

Z. Hozer, I. Nagy, P. Windberg
Atomic Energy Research Institute, Hungary (AEKI)

I. Ivanov, G. Dubleva
Technical University of Sofia, Bulgaria (TUS)

D. Popov
Kozloduy NPP Plc, Bulgaria

G. Sdouz, R. Mayrhofer
ARC Seibersdorf Research GmbH, Austria (ARC)

P. Groudev, R. Gencheva, A. Stefanova
Institute for Nuclear Research and Nuclear Energy, Sofia, Bulgaria (INRNE)

CONTENTS

EXECUTIVE SUMMARY

The LACOMERA project [1-5] at Forschungszentrum Karlsruhe (FZK) was a TALI action which started in September 2002 and had a duration of four years. The overall objective of the project was to offer research institutions from the EU Member States (except Germany) and Associated States access to four large-scale experimental facilities (QUENCH, LIVE, DISCO, and COMET) which could be used to investigate core-melt scenarios from the beginning of core degradation to melt formation and relocation in the vessel, possible melt dispersion to the reactor cavity, and finally corium concrete interaction and corium coolability in the reactor cavity.

The use of these experimental facilities was a remarkable option with high value. The project brought interested partners of different European Member States together in the area of severe accident analysis and control, with the goal of increasing public confidence in the use of nuclear energy. Moreover, partners from the newly Associated States were included as far as possible. Therefore, the needs of Eastern, as well as Western, reactors were considered in the LACOMERA project. The project offered a unique opportunity to get involved in the networks and activities supporting VVER safety and for Eastern experts to get access to large-scale experimental facilities in a Western research organisation to improve understanding of material properties and core behaviour under severe accident conditions.

As a result of three calls for proposals, the following eight experiments were defined and conducted during the project lifetime:

- QUENCH-L1: This experiment was proposed by the KFKI Atomic Energy Research Institute Budapest, Hungary (AEKI), and supported by Paul Scherrer Institut, Switzerland (PSI), and was intended to investigate the air ingression impact on core degradation. The test has provided unique data for the investigation of air ingress phenomenology in conditions as representative as possible of the reactor case regarding the source term.
- QUENCH-L2: This experiment was proposed by the Institute for Nuclear Research and Nuclear Energy, Sofia, Bulgaria (INRNE), and supported by PSI. The main objective of the test is to study the boil-off behaviour of a flooded bundle - a challenging task with a completely new objective not investigated before. The test is of a generic interest for all reactor types, provided a link between the severe accident and design basis areas, and delivers oxidation and thermal hydraulic data at high temperatures.
- COMET-L1: This experiment investigates the situation of a basement attack by the simulated corium melt and brings together partners from the Institut de radioprotection et de sûreté nucléaire, France (IRSN), and Technical University of Sofia, Bulgaria (TUS). The open question which is addressed in this experiment is a long-term 2D concrete ablation in siliceous concrete cavity at intermediate decay heat power level with a top flooding phase after a phase of dry concrete erosion.
- COMET-L2: This experiment was proposed by ARC Seibersdorf Research GmbH and concentrates on the generic study of a long-term metal/concrete interaction in cylindrical cavity for intermediate and low decay heat levels through metal phase only. The results of the test are required for specific code validation (e.g. ASTEC).

- DISCO-L1: This experiment was proposed by IRSN and has been designed to investigate the fluid-dynamic and thermal processes during melt ejection out of a breach in the lower head of a French-type PWR pressure vessel at pressures below 2 MPa with an iron-alumina melt and nitrogen as a driver gas, thus, neglecting the chemical effects such as hydrogen generation and combustion.
- DISCO-L2: This experiment was proposed by the TUS in cooperation with the Kozloduy NPP and aimed at investigating the corium melt dispersion phenomena for the VVER-1000 reactor geometry, which has not been studied before, neither in the DISCO facility nor elsewhere.
- LIVE-L1: This experiment was proposed by TUS and was dedicated to investigate the core-melt behaviour in the lower plenum of the reactor pressure vessel and the influence of the cooling of the vessel outer surface with water in the conditions that may occur during core-meltdown accident in the WWER-1000 plant. The experiment provided important information on the melt pool behaviour during the stages of air circulation at the outer RPV surface with a subsequent flooding of the lower head.
- LIVE-L2: This experiment was proposed jointly by IRSN and Commissariat à l'énergie atomique (CEA) and has been designed to investigate the transient melt spreading along the RPV lower head wall, the shape of the final melt pool and its impact on the steady-state heat fluxes in the conditions that may occur during core-meltdown accident in LWRs.

Eight organisations from five EU Member States and Associated States having an excellent expertise on core degradation and melt behaviour under severe accident conditions were involved in the project, including plant operators, R&D organisations working on nuclear safety, and universities.

Activities within the LACOMERA project provided important links with other European projects, like PLINIUS and SARNET, and also with the PHEBUS programme, and thereby optimised its usefulness and dissemination of knowledge obtained in the project. Five LACOMERA tests are being used within the SARNET Network of Excellence (NoE) for the benchmarking of codes applied for safety assessment and planning of accident mitigation concepts.

Eleven papers based on the LACOMERA project results have been presented at international conferences; three papers ([3], [5], and [9]) will be published in *Journal of Nuclear Engineering and Design*.

1. Introduction

During the last years, the concern of nuclear safety experts has concentrated on residual safety problems associated with core quenching and melt retention during a severe reactor accident. The essential ones are:

1. that the quench process produces an excess of steam and hydrogen at surfaces where Zircaloy oxidation had previously been limited by steam starvation.
2. that the thermal stresses induced in the rapidly cooling material induce cracking and spalling of the protective oxide layer on the fuel-rod cladding. The new exposed metal can then react vigorously with the excess steam thus producing heat and hydrogen and leading to additional melt release. The increased temperatures and greater oxidation potential will accelerate the release of hydrogen and fission products.
3. that the addition of water will not stop the melt progression necessarily and instantaneously. In the Three Mile Island accident molten material moved towards the lower head following refill and the fact that the lower head was not penetrated in this case may have been fortuitous.
4. that the demonstration of in-vessel coolability of melt pools still does not have a profound basis, experimentally and theoretically. The knowledge about melt mass relocation from the core to the lower plenum, coolable debris bed formation and formation of gaps between solidified melt and RPV shell is rather poor.
5. that the melt mass pouring into the cavity after RPV failure strongly depends on the failure location of the lower head, pressure of the primary circuit, the geometry of the cavity and melt properties. Experimental evaluation has up to now only been performed with simulants at ambient temperature and must be extended to more representative reactor conditions.
6. that for the ex-vessel situations melt retention in the reactor cavity need to be verified as mitigation measure against long term Molten Core Concrete Interaction (MCCI) to delay or exclude basement penetration and major gas release into the containment. Furthermore, to be applicable to existing reactors, proposed core catcher concepts need further evaluation, improvements and verification.

Those issues were highlighted in series of experiments, both in-pile and out-of-pile (CORA, LOFT, BETA, MASCA, DISCO, MACE, COMET). Generally, computer models have difficulties in modelling the quenching behaviour and molten pool formation and cooling in the lower head even though the modelling has recently advanced considerably. Some models for the molten pool behaviour in the lower head have been developed, but until there is enough data to check the models with, they cannot be considered as reliable.

The overall objectives of the LACOMERA project are to offer research institutions from the EC access to large-scale experimental facilities which shall be used to increase the knowledge of the quenching of a degraded core and regaining melt coolability in the RPV, of possible melt dispersion to the cavity, of MCCI and of ex-vessel melt coolability. One major aspect is to understand how these events affect the safety of European reactors and how to deduce soundly-based accident management procedures. Specifically, the access to the large-scale facilities shall provide answers to the following questions:

1. What are the main factors governing the quantity of hydrogen production and melt generation during quenching?
2. What will be the time span of melt relocation to the lower plenum and what measures are needed to regain coolability?

3. Where will the melt be located after failure of the RPV under moderate pressure, with different failure positions? What is the pressure increase in the reactor pit, the sub-compartments and the containment due to thermal and chemical reactions (hydrogen production and burning)?
4. Is the experimental basis of MCCI sound enough to model long-term erosion rates and how can ex-vessel melt coolability be achieved?

2. Objectives and description of the project

Four large-scale facilities at FZK with a broad experience on severe accident research are offered to external partners from EU Member Countries or Associated States. These facilities are QUENCH, LIVE, DISCO-H, COMET. Their overall purpose is to investigate core-melt scenarios from the beginning of core degradation to melt formation and relocation in the vessel, possible melt dispersion to the reactor cavity, and finally corium concrete interaction and corium coolability in the reactor cavity. In all experiments, simulant material is used to investigate the behaviour of the core material. These simulant materials were especially chosen to be as close to the real core material for the important properties as possible. On the other hand, the use of the simulant material allows covering a wide and broad range of scenarios with the experiments in a relatively small time schedule and for relatively low budget/funding. The experiments, post-test investigations and special-effect tests can be performed under well-defined conditions and can be completely controlled.

The possible users were invited to make their own proposals of experiments for each of the large-scale facilities. Researchers were strongly supported if they wanted to participate in the experiments. On the other hand, due to the existing infrastructure, the personnel were able to perform experiments defined by partners without additional support of the possible partners if they did not have the ability to participate in the experiments.

The main thrust of this project was towards large-scale tests under prototypical conditions. These help in the understanding of core degradation and quenching, melt formation and relocation as well as melt coolability in real reactors in two ways – firstly directly by scaling-up and secondly indirectly by providing data for the improvement and validation of computer codes. Although the facilities can only perform experiments with simulant materials, the tests can be considered as prototypic since the selected materials represent in important physical properties the real core materials. The large masses used allow extrapolation to the reactor case. Moreover, the flexibility and variability of the facilities is high due to the rather simple handling. Pre-tests, parallel separate-effects tests and post-test analysis can be performed in one hand. These tests can be seen as complementary to tests with UO_2 in other research centres.

The work plan involved four work packages described below.

2.1. WP1: Large-scale Quench Tests (QUENCH)

Bundle experiments in the QUENCH facility [6], [7] are specifically designed to contribute to the reduction in uncertainties and increase in understanding of the quenching process that will be necessary if a proper assessment of the risk posed by quenching to full-scale power plants is to be reached.

The main component of the QUENCH test facility is the test section with the test bundle (

Fig. 1). Super-heated steam from the steam generator and super heater together with argon as a carrier gas enter the test bundle at the bottom. The argon, the steam not consumed, and the hydrogen produced in the zirconium-steam reaction, flow from the bundle outlet at the top through a water-cooled off-gas pipe to the condenser where the steam is separated from the non-condensable gases argon and hydrogen. The system pressure in the test section is around 0.2 MPa. QUENCH experiments can be terminated either by quenching with water from the bottom or from the top or by the injection of cold steam. The test section has a separate inlet at the bottom to inject water for quenching whereas the steam for cool down enters the test section through the same line that is used for the superheated steam during the previous phases.

The test bundle (

Fig. 2) is made up of 21 fuel-rod simulators, each with a length of approximately 2.5 m. Twenty fuel-rod simulators are heated electrically over a length of 1024 mm, the one unheated fuel-rod simulator is located in the centre of the test bundle. Heating is electric by 6 mm diameter tungsten heaters installed in the rod centre. Electrodes of molybdenum and copper connect the heaters with the cable leading to the DC electric power supply. The total heating power available is 70 kW distributed between two groups of heated rods. The distribution of the electric power within the two groups is as follows: 40 % of the power is released in the eight inner fuel-rod simulators, 60 % in the twelve outer fuel-rod simulators.

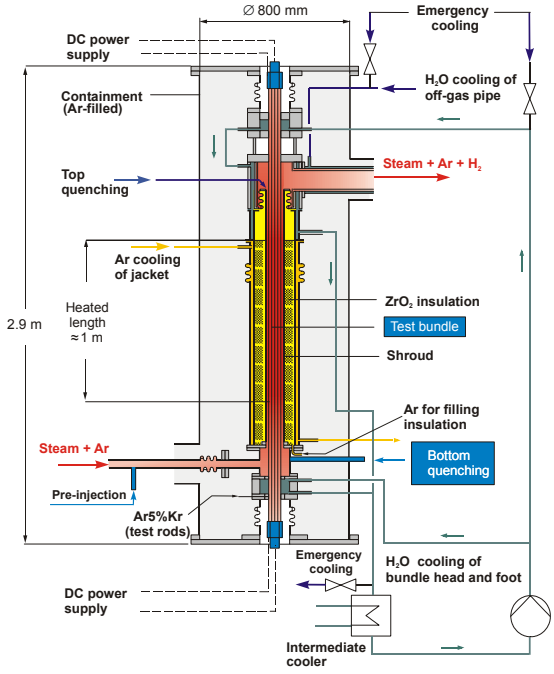

Fig. 1: QUENCH test section

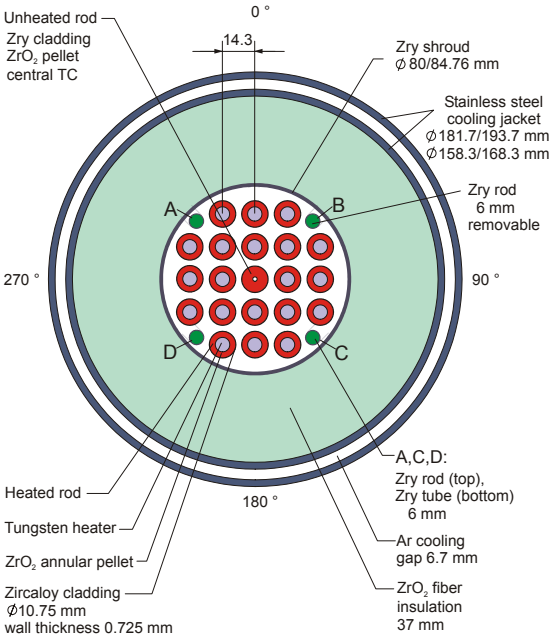

Fig. 2: Fuel-rod simulator bundle

The fuel-rod simulators are held in position by five grid spacers, four are made of Zircaloy and the one at the bottom of Inconel. The tungsten heaters are surrounded by annular ZrO_2 pellets. The rod cladding of the heated fuel-rod simulator is identical to that used in LWRs with respect to material and dimensions (Zircaloy-4, 10.75 mm outside diameter, 0.725 mm wall thickness). The heated rods are filled with Ar-5%Kr at a pressure of approx. 0.22 MPa. The krypton additive allows test rod failure to be detected by the mass spectrometer.

Hydrogen is analyzed by three different measurement systems: (1) a state-of-the-art mass spectrometer GAM300 located at the off-gas pipe about 2.7 m behind the test section, (2) a commercial-type hydrogen detection system ”Caldos 7G” located behind the off-gas pipe and

condenser, and (3) a second, simpler mass spectrometer “Prisma” installed close to the Caldos device.

For temperature measurements, the test bundle, shroud, and cooling jackets are equipped with thermocouples at different elevations and orientations: In the lower bundle region, i.e. up to 550 mm elevation, NiCr/Ni thermocouples with stainless steel sheath and an outside diameter of 1.0 mm are used for measurements of the rod cladding and shroud temperatures. The thermocouples in the hot zone are high-temperature thermocouples with W5Re/W26Re wires, HfO_2 insulation, and a duplex sheath of tantalum (inside) and Zircaloy (outside) with an outside diameter of 2.1 mm. Shroud thermocouples are mounted at the outer shroud surface between – 250 mm and 1250 mm.

The main parameters of the test programme are: quench medium, i. e. water or steam, fluid injection rate, extent of pre-oxidation at onset of quenching, and the starting temperature at initiation of water quenching or steam cool down.

2.1.1. QUENCH-L1 test

The experiment QUENCH-L1 was proposed by AEKI and supported by PSI. The test is intended to simulate air ingress during an anticipated accident in a spent fuel pool and its consequence on the fuel elements. In detail, it is assumed that water-cooling of the stored fuel elements is interrupted; the water inventory in the pool boils off, and oxidises the fuel rods. Eventually, the water level is so low that a flow path for air into the fuel elements is opened through holes in the lower part of the shroud. If the water boils off even in the region of the bundle foot, a larger path is opened below the shroud. The fuel element geometry is assumed intact up to this time.

The experiment has been performed on 21 July 2004. The results are presented in [8], [9] Main results of the experiment as well as the results of the post-test bundle examination obtained during the third year of the LACOMERA project are given below.

In common with the previous QUENCH experiments, the bundle was heated by a series of stepwise increases of electrical power from room temperature to ~ 600 °C in an atmosphere of flowing argon (3 g/s) and preheated steam (3 g/s). The bundle was stabilised at this temperature, the electrical power being ~ 4 kW.

In a first transient, the bundle was heated by power increase to about 1350 °C. This marked the start of the pre-oxidation phase (see also Fig. 3) to achieve a cladding oxidation of up to 600 μm.

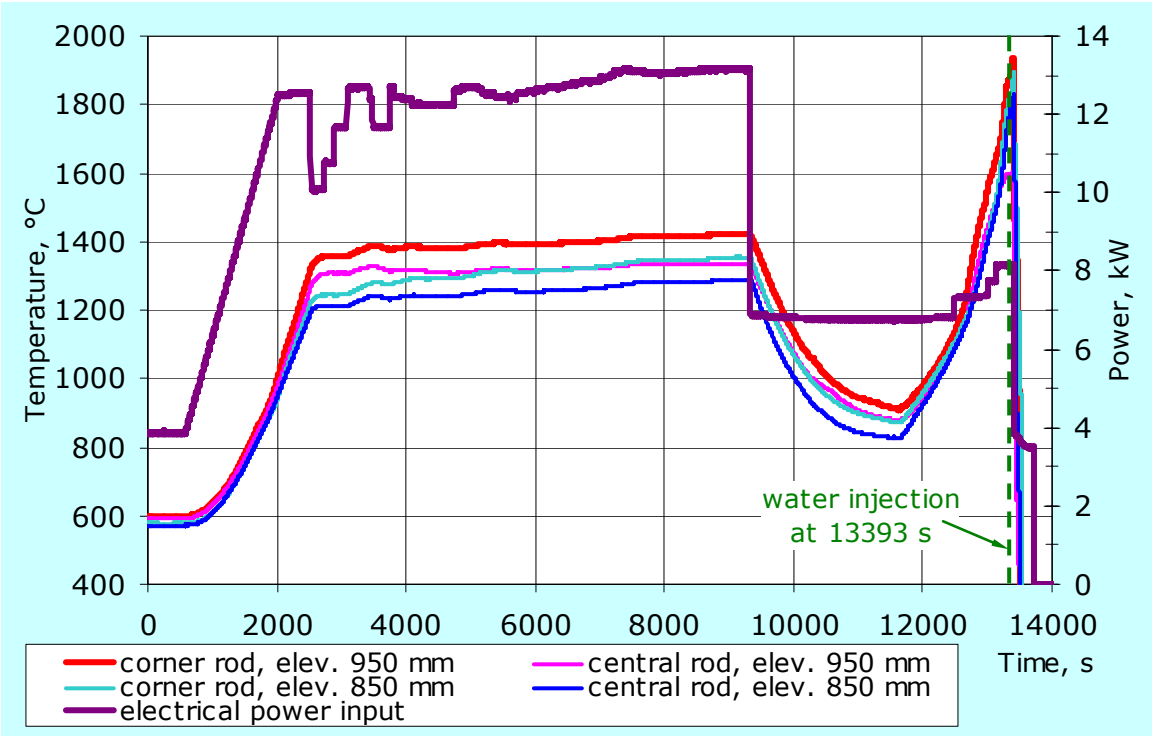

Fig. 3: QUENCH-L1 test overview

The power was controlled to maintain a more or less constant hydrogen production rate of about 5 mg/s after the peak value of 16 mg/s, caused by the previous heat-up. This procedure led to a slow increase in temperature to 1420 °C. This phase lasted ~ 6600 s. Since the oxide thickness could not be measured online, it was estimated on the basis of pre-test calculations [11] and online monitoring of hydrogen release. The total hydrogen release from the beginning of the test to this point was 48 g (Fig. 4).

To achieve an adequate duration of the subsequent air ingress phase, the bundle was then cooled to a maximum temperature of about 920 °C by decreasing the electrical power from 13.2 to 6.9 kW. The temperature was reached after 2400 s. Hydrogen generation dropped rather quickly to about 0.4 mg/s due to this cooling so that nearly no further oxidation occurred. Towards the end of this phase, the first corner rod was extracted from the test bundle to determine the maximum oxide layer thickness, which amounted to ~ 500 µm.

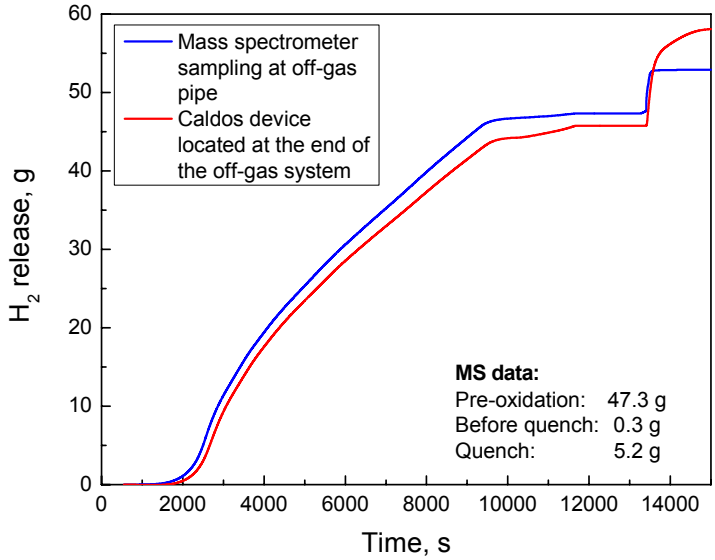

Fig. 4: Integral hydrogen release in QUENCH-L1 test

In the subsequent air ingress phase, the steam flow of 3 g/s was replaced by 1 g/s of air. This change had the immediate effect of reducing the heat transfer so that the temperatures began to rise again. The temperature increase was somewhat slower than expected, therefore the electrical power was increased stepwise to 8 kW. Due to this procedure, temperature and oxidation increased such that the heat release eventually drove the temperatures beyond the final target value of 1800 °C. The duration of this phase was ~ 900 s. Complete consumption of oxygen and partial consumption of nitrogen (about 0.1 g/s) were observed toward the end of this phase. The total uptakes of oxygen and nitrogen were about 84 and 8 g, respectively. However, N_2 uptake was noticeable only towards the end of the air ingress phase when the temperatures in the bundle increased significantly.

At the end of the air ingress phase the second corner rod was removed. An inspection of the two withdrawn corner rods indicated that pre-oxidation was as desired, i.e. the maximum oxide layer thickness prior to quenching amounted to more than 600 µm.

The reflood was initiated by turning off the air flow, switching the argon injection to the top of the bundle, rapidly filling the lower plenum of the test section and injecting 50 g/s of water. The power was reduced to 4 kW after a further 10 s to simulate decay heat. Right at the beginning of reflood, there was indication of a short and mild temperature excursion in the upper part of the bundle, leading to maximum measured temperatures of about 1930 °C at 950 mm elevation and to ~ 1130 °C at the levels above the heated zone. In other elevations the cooling was established almost immediately, and complete flooding of the bundle was achieved after about 300 s. A modest release of hydrogen, i.e. ~ 5 g was observed during the early part of the reflood. About 60 % or 5 g of the nitrogen previously taken up was released.

Detection of He by the mass spectrometer indicated a first small failure of a fuel-rod simulator after 20 min in the pre-oxidation phase and a much larger failure after 13 min in the intermediate cool down phase. A further increase in the measured helium concentration after quench initiation indicated an extended failure of cladding tubes during this highly transient phase.

The evaluation of the hydrogen release rates with help of the mass spectrometer data gives 47.3 g of total hydrogen generation up to the end of the pre-oxidation phase, 0.3 g shortly

before the quench phase, and 5.2 g of hydrogen release during the quench phase, hence about 53 g of H_2 in total.

After the experiment the QUENCH-L1 bundle and its shroud appear completely oxidised in the region between 750 and 1000 mm (Fig. 5). Besides oxidation, the shroud exhibits deformation and formerly molten zones partly due to an interaction with the ZrO_2 fibre insulation. The inner surface of the shroud shows a white oxide layer and some spots where nitride had formed by oxidation in air.

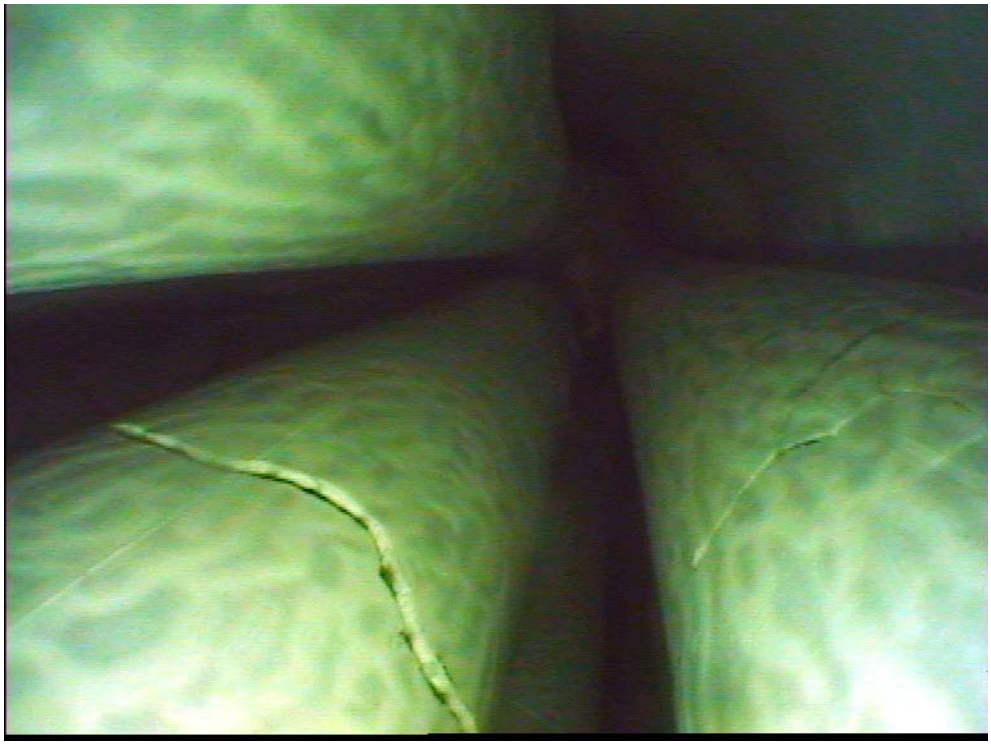

Fig. 5: Cracks in the oxidised fuel-rod cladding

Two corner rods, i.e. rod B (withdrawn after the steam pre-oxidation phase) and rod D (lower part withdrawn towards the end of the transient or air ingress phase), were evaluated meanwhile. A videoscope inspection of the bundle was performed, in which the optical system was inserted from the bottom into the bundle at the empty positions of corner rods B and D. The bundle was then filled with epoxy resin, and the cured block was cut into various slabs for the metallographic preparation of bundle cross sections at elevations of interest. The comprehensive post-test examinations of the bundle and, in particular, of the scale thickness profile measurements are in progress. Special attention is being paid to the degradation phenomena of cladding oxidation during the air ingress phase and to the bundle response on quenching.

Inspection by videoscope

The videoscope photographs in
Fig. 6 demonstrate stripes and spots on the shroud inner surface containing zirconium nitride (ZrN).

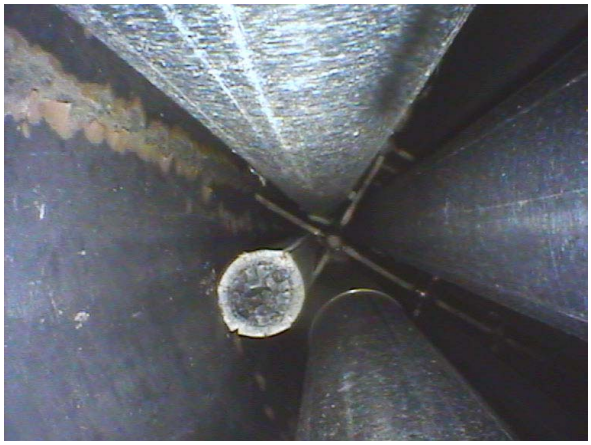

Videoscope inserted at corner rod position D, elevation 450 mm: axial stripe with ZrN on the shroud inner surface

Videoscope inserted at corner rod position B, elevation 650 mm: spots with ZrN on the shroud inner surface

Fig. 6: Videoscope photographs of the shroud inner surface

Metallographic examination with respect to ZrN formation at the shroud

Fig. 7 shows typical results of the metallographic investigations of axially extended stripes and spots of ZrN which had developed at the shroud at relatively cold elevations of 550 and 650 mm (maximum temperatures of about 1300 and 1350 K, respectively). In the radial direction, nitride formation is observed between the surface of the α-Zr(O) layer at the inside and the (spalled) zirconium oxide scale at the outside.

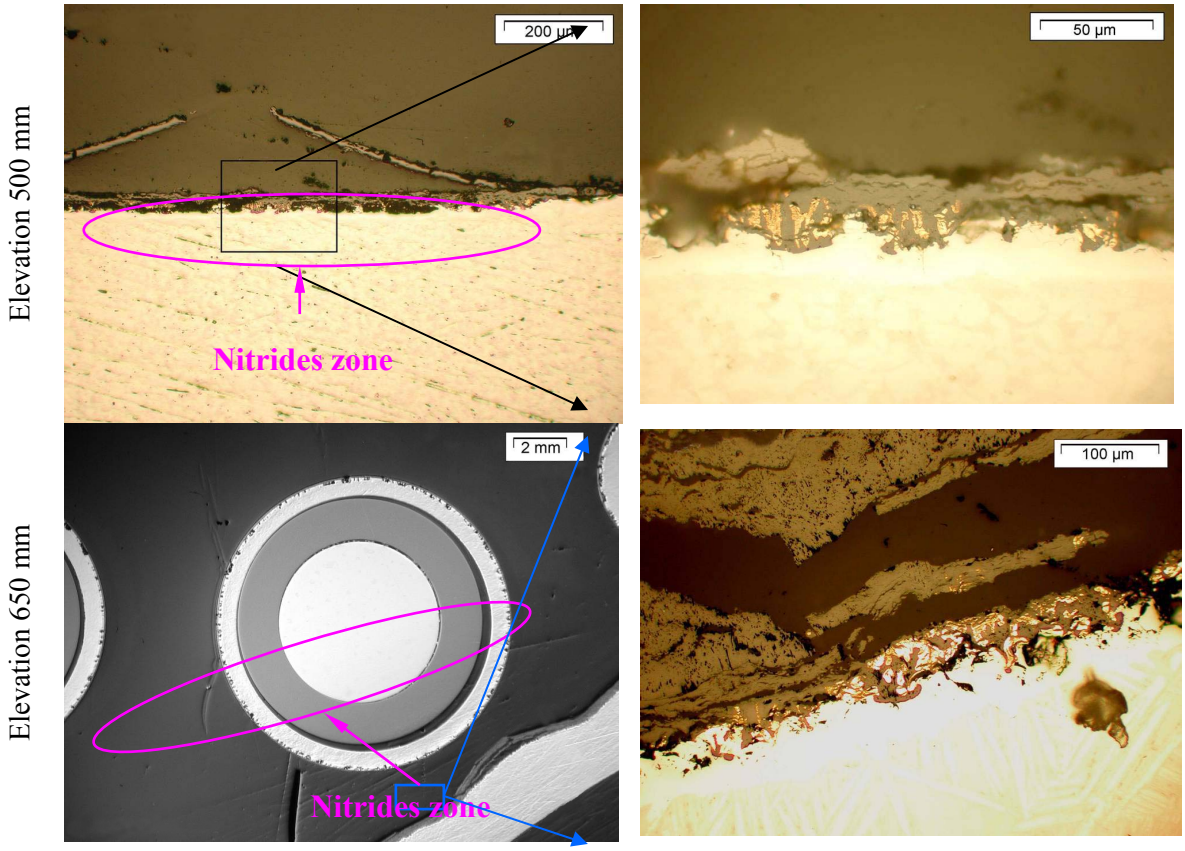

Fig. 7: Zr nitride formation on the boundary between friable (and partially spalled) ZrO_2 oxide layer at the outside and α-Zr(O) layer of the shroud inner surface

At higher elevations of the shroud, i.e. at 850 and 950 mm with maximum temperatures of about 2150 K, the oxide layer did not have a tendency to spalling. It contained embedded remnants of zirconium nitride as can be seen in
Fig. 8. There were also Zr nitride particles formed locally at the boundary between ZrO_2 scale and metallic layer.

Interpretation of the metallographic examination of the shroud

The shroud examination at the 500 and 650 mm elevations, performed complementarily to the videoscope inspection, covered the observed spots of oxide scale and the axially extended stripes which are of similar appearance. The axial weld seam of the shroud (at NW orientation) is covered by a thick post-transition oxide scale, characterized by lateral breakaway-related crack formation. The localized spots and stripes of the inner shroud surface (described above) are assumed to be related to scratches or local defects of the material existing prior to the test. Nevertheless, they can be interpreted as typical for air oxidation. At higher shroud elevations the advanced air exposure influenced oxidation at the whole internal surface.

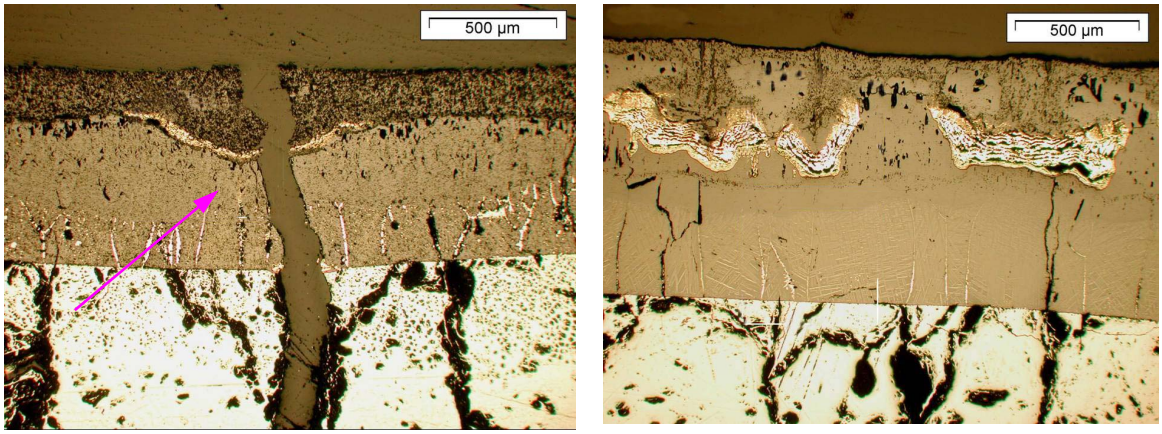

Fig. 8: Formation of Zr nitride on the inner shroud surface: a previously coherent nitride layer at the outside was converted into a porous oxide layer during quenching (left), otherwise Zr nitride cells were re-converted (during quenching) into a friable type of ZrO_2 scale (right)

Metallographic examination with respect to ZrN formation in the bundle

ZrN cell formation was observed at the surface of the rod claddings. These cells developed during the air ingress phase [10] can be seen at the surface of corner rod D withdrawn after the air ingress (**Fig. 9**). The metallographic examinations, which are now in progress, show that during quenching the nitride cells were partially re-converted into ZrO_2 oxide.

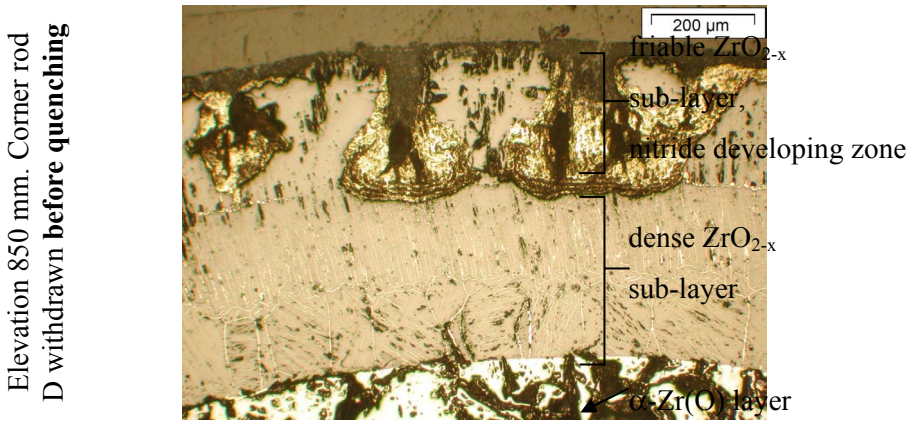

Fig. 9: Formation of nitride cells inside the ZrO_2 oxide layer at the outer surface of corner rod D before quenching

Evaluation of the oxide scale thickness

The lateral scale thickness distributions at the cross sections are rather flat but locally with a large scatter of the data. The axial oxide thickness profiles of the rod bundle are pronounced. At 800 mm elevation some of the rods show complete cladding conversion due to fast external oxidation of a molten cladding matrix and due to internal oxygen transfer from the pellets. Above this level, only local thickness results can be given because e. g. at 950 mm all claddings are gone after fragmentation and relocation. Within this axial region the oxidation of the shroud is seen to have continued. Above the 1000 mm level the extent of bundle oxidation is less. The surplus oxidation of corner rod D during air exposure compared to rod

B (without air exposure) was the reason for fracturing of rod D during pulling. The axial scale profile of rod D is comparable to that of the rod claddings.

The analysis of released aerosols described in [12] indicates that the oxides of structural materials (mainly Zr, Sn, and Fe) have been produced at high temperature and partially released from the bundle with the gas flow.

2.1.2. QUENCH-L2 test

The experiment QUENCH-L2 on boil-off and subsequent quenching is dedicated to investigate degraded core reflood situations with a rather low mass flow rate, which may occur if pumps cease and/or if low make-up systems are activated in the course of Accident Management Measures (AMM). The test conditions simulated a depressurised plant sequence in which the core would be essentially dried-out and with a limited steam flow due to boiling of residual water in contact with the hot structures in the lower plenum. The test was proposed by the Institute for Nuclear Research and Nuclear Energy, Sofia, Bulgaria, and supported by PSI.

Added value of the boil-off scenario

In integral experiments investigating delayed core reflood in the severe fuel damage SFD regime as a successful accident management procedure, the conditions inside the RPV prior to reflood initiation are represented only far above the water level.

Recent research results have shown that the transition of intact rod geometry to large debris pool formation is sensitive with respect to reflood success, e.g. it touches the feasibility of long-term core coolability. But so far, no integral experiment has been performed with a controlled steam mass flow rate into the core and a free water surface at the lower end of the test section, neither for reactor nor for non-power conditions. The axial temperature gradients are mainly controlled by convective heat losses; the lowest temperature is given by the fluid entrance temperature. Furthermore, this configuration would also allow the simulation of the short water swelling phase when saturated steam enters the water pool.

Another issue is the simulation of the dry-out and slow reflood process as expected in non-power accident situations, e.g. dry-out of a fuel element storage pool with subsequent reflood from the bottom. However, scenarios like the Paks incident require top flooding installation, which will be available later.

The 2 m long test section of the QUENCH facility offers the unique opportunity to simulate high temperatures as well as a water pool with an axial temperature gradient of up to 2000 K/m. Experiences from the previous test shows that the water level can be monitored with sufficient accuracy, the steam production can be controlled by extra heating, simulating the fuel element sections below water level and measured additionally by the mass spectrometer.

However, for such type of experiments know-how is lacking and extrapolation from design basis flooding experiments is risky. To reduce this uncertainty the pre-test analyses have to be extended using all available detailed code systems, offering the chance to establish a blind code benchmark as part of the SARNET activities.

Pre-test calculations

The scoping calculations have been performed at FZK/IRS with SCDAP/RELAP5. They were focused on the system behaviour in case of free water surface in the lower third of the bundle. Also they provided information about the steam rate to be expected by the heat release of the bundle alone and with an additional heater mounted on the shroud. In the scoping calculations, the feasibility of such an experiment was assessed and demonstrated.

From the scoping calculations the necessity of an additional heating system at the lower end of the test section as well as additional water injection of approx. 1 g/s became obvious. Without any additional water injection the test ends up in a steam starvation test which is not desired for QUENCH-L2. At the end of one calculation the steam produced is completely consumed in the lower half of the bundle. This is not representative for a dry-out or boil-off scenario since the decay heat in the lower core third produces sufficiently steam for the oxidation reaction in the upper third. Additional heater is necessary to compensate the temperature dependent energy release of the metallic heating system composed of Molybdenum and tungsten wires. Due to this effect, not sufficient heat is released in the lower electrode zone.

According to these requirements, major modifications in the QUENCH facility have been realized. The auxiliary heater has been designed and installed in the lower plenum of the test section, as can be seen in **Fig. 10** and **Fig. 11**.

Fig. 10: Stainless-steel auxiliary heater
.

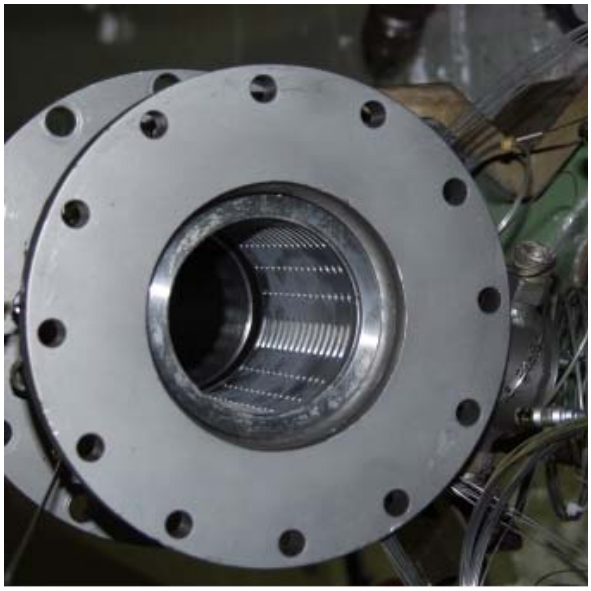

Fig. 11: Auxiliary heater element installed in the lower plenum of the QUENCH test section

Another important experimental parameter is the desired water level in the core. The wish is as low as possible, to use the full length of the fuel-rod bundle. Practically, due to the volume necessary to install such a device, the water level is limited to - 0.250 mm (collapsed water level). Below that level, the risk of melting the stainless steel heater is evident.

Therefore, both additional heating power as well and water inflow have to be considered simultaneously. As a first result, the power can vary between 2000 and 3000 W at an inflow rate of 1 g/s, keeping the level quasi stationary.

The QUENCH input deck was extended to simulate both features. The realisation in the QUENCH facility has to be discussed in detail after end of the pre-calculation phase, the need to position the auxiliary heater as low as possible became evident, because of the risk of failure in case a two phase fluid as a heat sink. Another advantage of a water level around – 0.3 m is that the representative bundle length is increased to approx. 1.8 m above the water pool with a depth of approx. 0.3 m.

For the mass spectrometers the carrier gas argon is injected at the upper end of the bundle during the whole test sequence. To ensure correct flow rates and velocities, the evaporation has to be controlled to achieve a quasi stationary steam flow rate. If the heater is coupled close to the fluid or to the shroud, a fast reaction of the evaporation and hence the water level in the bundle can be achieved.

In a next step, detailed pre-test calculations [13] were performed, to specify important parameters for the final test protocol. Furthermore, these calculations deliver information about the sensitivity of electrical power and auxiliary heating power, together with the additional mass inlet in the different test phases with respect to the desired test conduct.

Based on pre-test calculations performed initially with SCDAP/RELAP5 and later on with ASTEC V1.2 (July 2005) a draft test protocol was established. Results of a draft calculation are shown in
Fig. 12.

An input deck for ASTEC V1.1 was established and sent to INRNE for further pre-test calculations. The development of ASTEC input decks for the whole scenario are under way, to address the initial oxide layers correctly. The results are comparable to those obtained by SCDAP/RELAP5 except for the reflood phase, which has not yet been calculated with ASTEC V1.2.

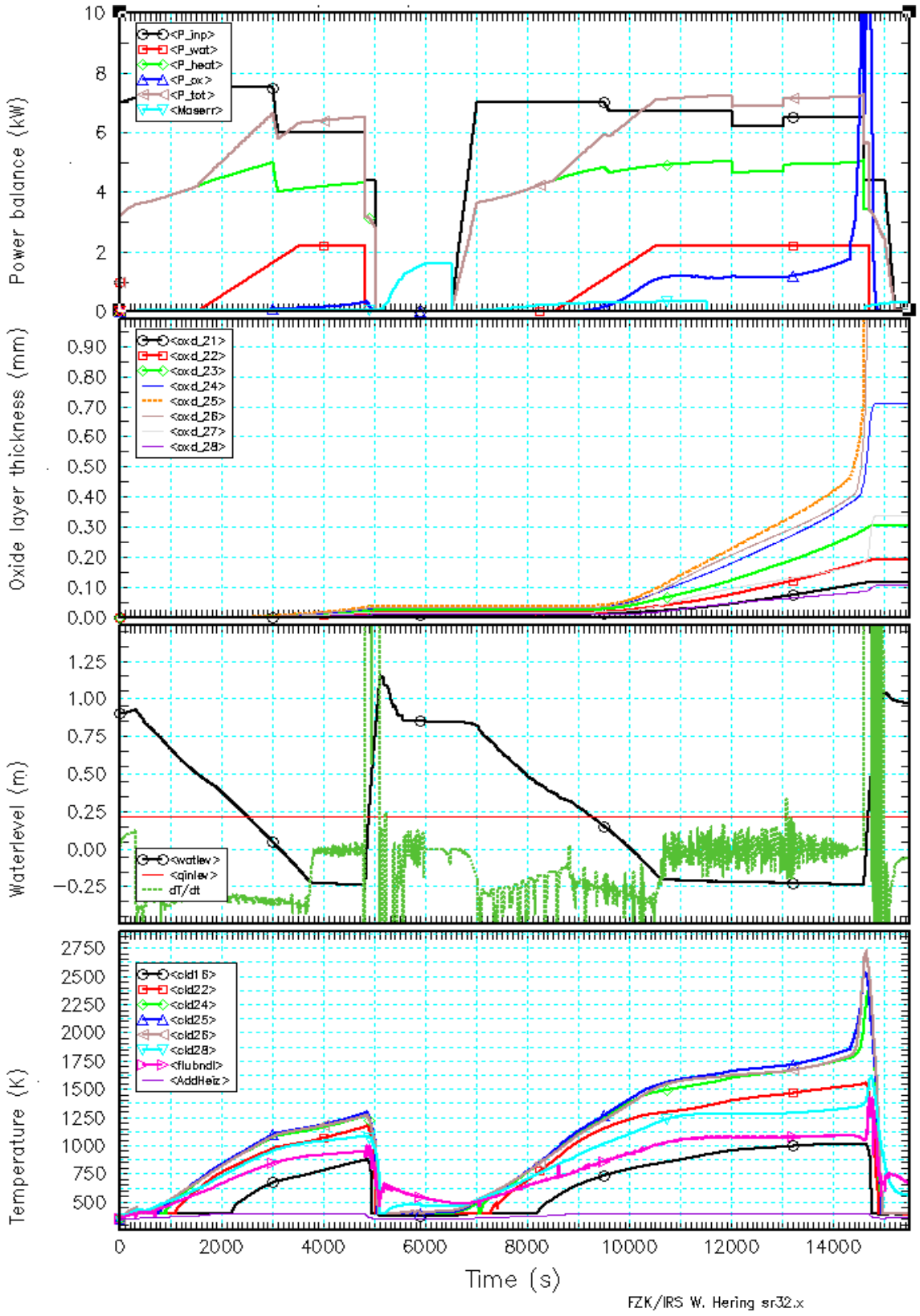

Fig. 12: Complete scenario including pre-test "Vorversuch" q-11v3 (up to 4800 s), a short refill phase and the Q-11 test: top: electrical and exothermal power, below: oxide layer thicknesses, collapsed water level and heat-up rate (dotted line), and bottom: temperature evolution in the upper third of the bundle

Test performance and key results

In contrast to all the previous QUENCH experiments, the bundle was initially filled with water and slowly evaporated. Among other facility changes, an auxiliary heater and an additional water injection system were installed in the lower plenum to maintain the evaporation rate at low water level without jeopardizing the bundle heating. To investigate the behaviour of the test section under such conditions, several pre-experiments were performed, simulating the early part of the experiment. In the last one, QUENCH-11v3, the bundle was heated-up to 1080 °C and flooded with the same reflood rate as foreseen in QUENCH-L2.

The pre-tests were important to check the functioning of the new components and facility control, to characterise the boil-off behaviour as well as to further improve pre-test calculations. The last trial also provided data on reflooding at temperatures pertinent to design basis conditions. There had been no damage to the bundle during the pre-tests but the QUENCH-L2 test started with an initial oxide layer thickness of approx. 20 μm (axial maximum) which had formed during the last pre-test.

The determination of the test protocol was based on numerous calculations with SCDAP/RELAP5, SCDAPSIM, MELCOR, and ASTEC; the last calculations were also based on the pre-experiments. They were prepared by FZK and performed in collaboration between INRNE, PSI, and FZK. To improve the test conduct further, calculated temperatures and hydrogen production rates were compared with the experimental data during the test.

The experiment started with an application of electrical bundle power of ~ 7 kW. This was initiation of a steady boil-off and a consequent top-down uncovery of the test bundle. To assure that water evaporated in the lower plenum the auxiliary heater was turned on and its power was increased step-wise to a maximum of 3 kW as the uncovery progressed and continued during reflood. In order to maintain a sufficient water level to keep the auxiliary heater covered and thus continue the steaming rate, water was injected into the lower plenum at a rate of ~ 1 g/s at 2575 s when the water level had fallen to 70 mm below the heated section of the bundle (**Fig. 13**). This enabled a nearly stable level as well as a constant steam flow to be maintained. This water injection was continued during the quench phase. As the temperatures increased, the onset of significant cladding oxidation was first detected at 4900 s with the maximum bundle temperatures at ~ 1160 °C (**Fig. 14**).

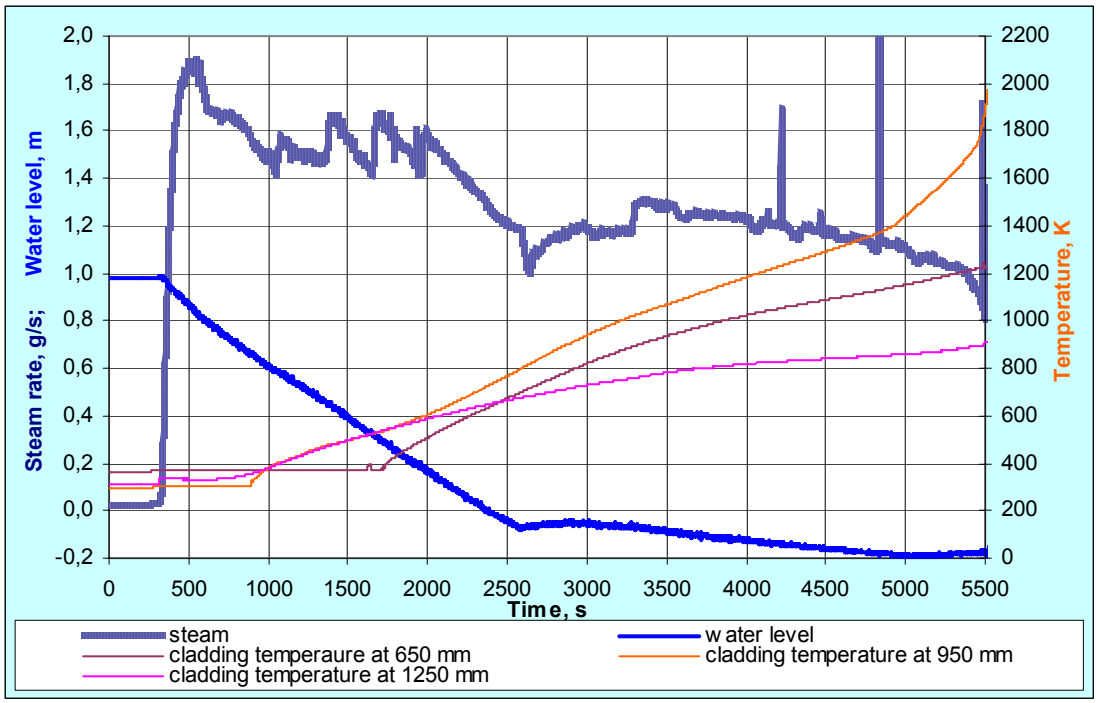

Fig. 13: Boil-off phase of the QUENCH-L2 test

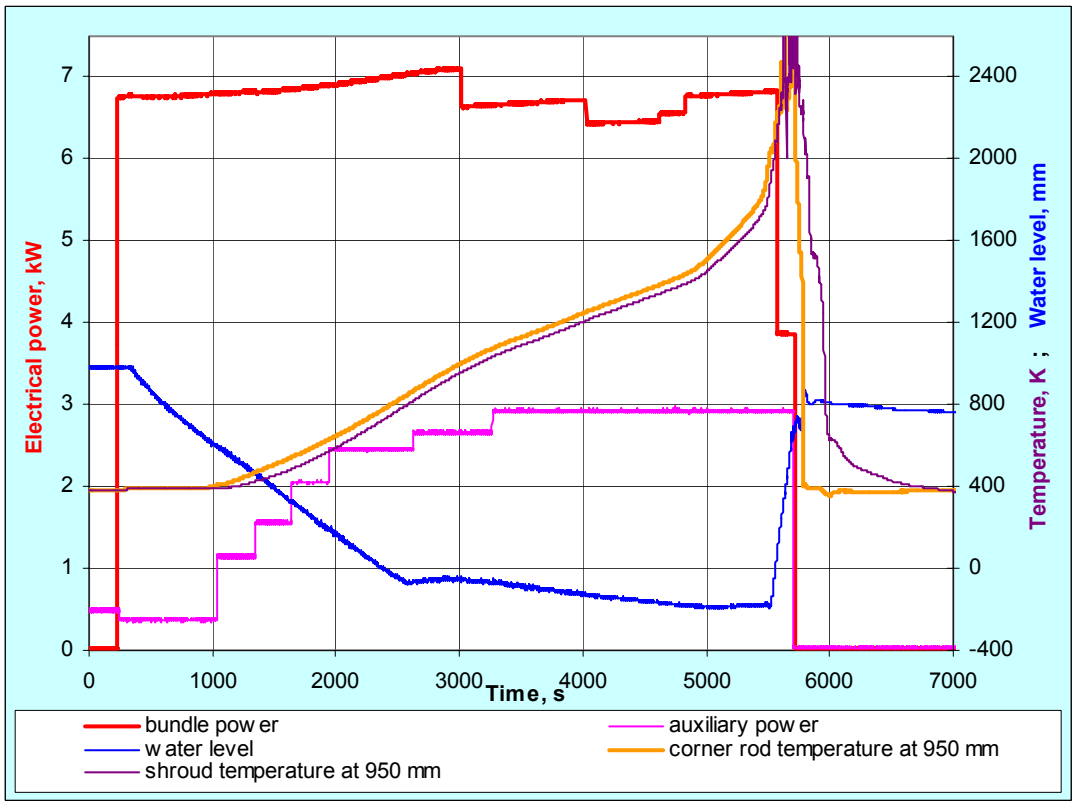

Fig. 14: Overview of the QUENCH-L2 test

As in previous experiments, one of the corner rods was removed for later inspection before reflood was to be initiated. Post-test examinations showed that the peak cladding oxidation after the transient prior to the reflood phase was about 170 µm, as shown in **Fig. 15**.

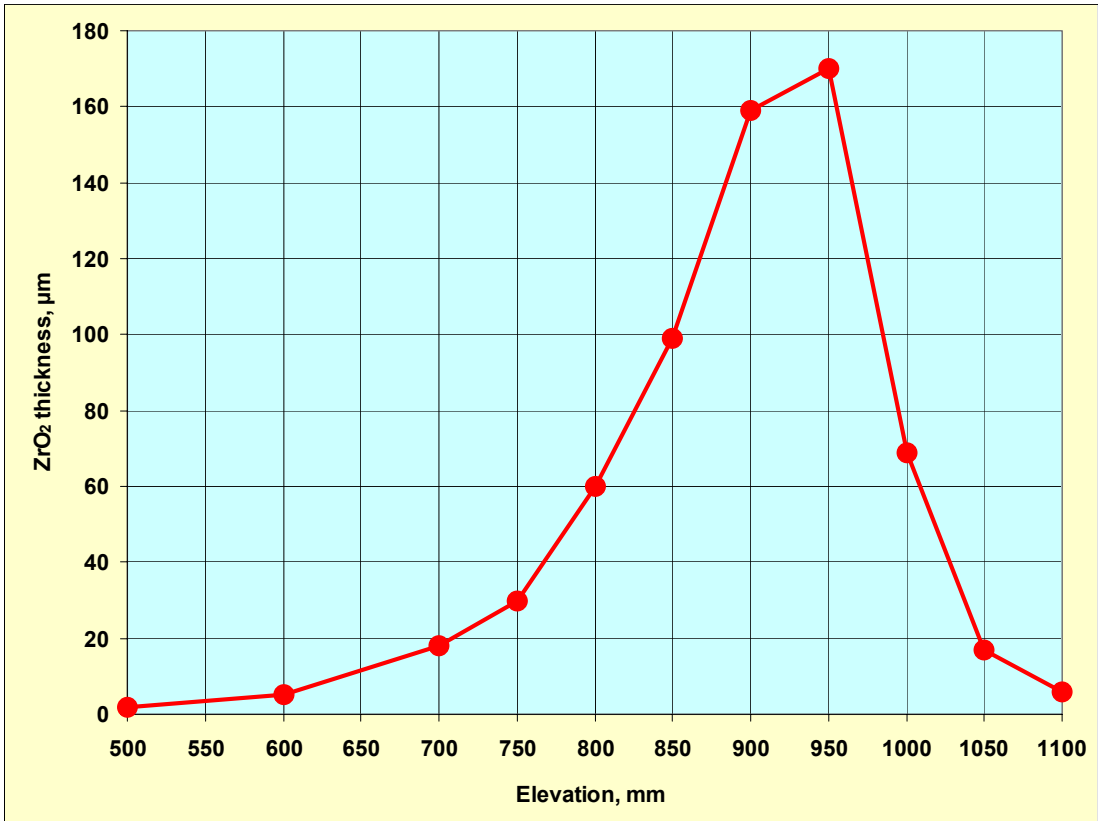

Fig. 15: Axial oxide layer profile of the corner rod in QUENCH-L2

As foreseen, the quench flow of 17 g/s water at 20 °C was initiated at 5500 s, when hydrogen generation reached 50 mg/s. The maximum observed temperature in the bundle at this time was 1770 °C (**Fig. 16**). Immediately following the injection of sub-cooled water into the lower plenum, there was indication of a temporary stagnation of the bundle exit flow and perturbations in the bundle temperature. With a certain delay, the water level in the lower plenum began to rise, reaching the bottom of the heated section after approximately 40 s.

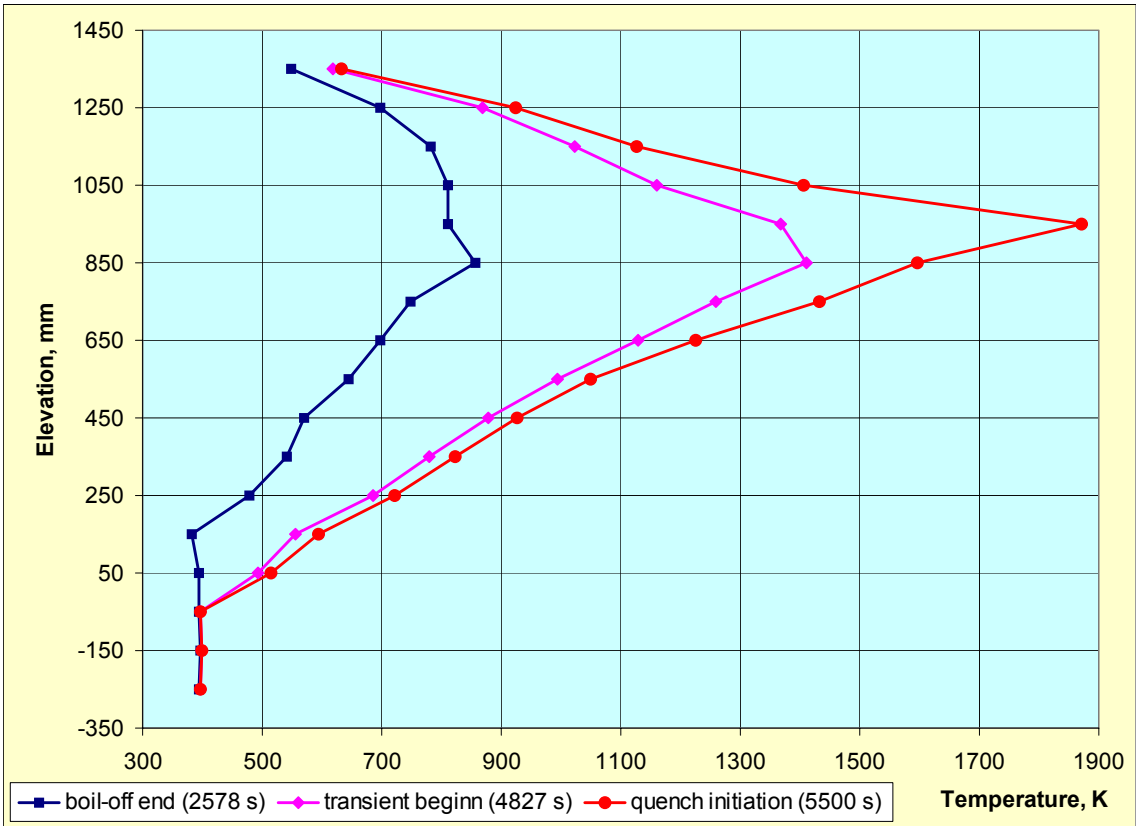

Fig. 16: Axial temperature profiles in QUENCH-L2

Three events occurred within a few seconds of the beginning of bundle quench. Failure of the heater rods was first indicated at 5563 s by detection of helium with the mass spectrometer and by a drop in helium rod pressure. There was indication of shroud failure at the same time by a drop in pressure in the annular region between the shroud and inner cooling jacket. Furthermore, it was at almost exactly this time that the hydrogen generation rate increased sharply, reaching a maximum of more than 700 mg/s for a short time, before gradually decreasing and eventually terminating during the next few minutes. It is not yet clear to what extent these three events are connected.

The bundle power was reduced to 3.9 kW, approximating effective decay heat levels, at 5573 s and later terminated at 5713 s. In contrast to lower elevations, the temperature escalation started above 800 mm, leading to enhanced hydrogen production and temperatures beyond 2100 °C, before final temperature decrease as in the lower part of the bundle. Locations above the heated section also showed an increase, apparently due to reverse heat transfer from the flow of very hot steam-gas mixture. Thermocouples at elevation 850 mm also showed local quenching, but delayed until 5800 s and only after the initial escalation.

Water level did not increase beyond about 800 mm. Experience from previous tests suggests that the shroud has failed at about that elevation so that the quench water leaked through the breach in the shroud. Locations above 850 mm were therefore slowly cooled down after terminating the electrical heating, reaching temperatures close to saturation only after a further 3000 s.

The total generation of hydrogen was in the region of 140 g (**Fig. 17**), of which more than 90 % was produced during the reflood phase. It is possible that the modest level of pre-oxidation, combined with the rather low reflood rate, led to conditions favourable for an enhanced oxidation during reflood.

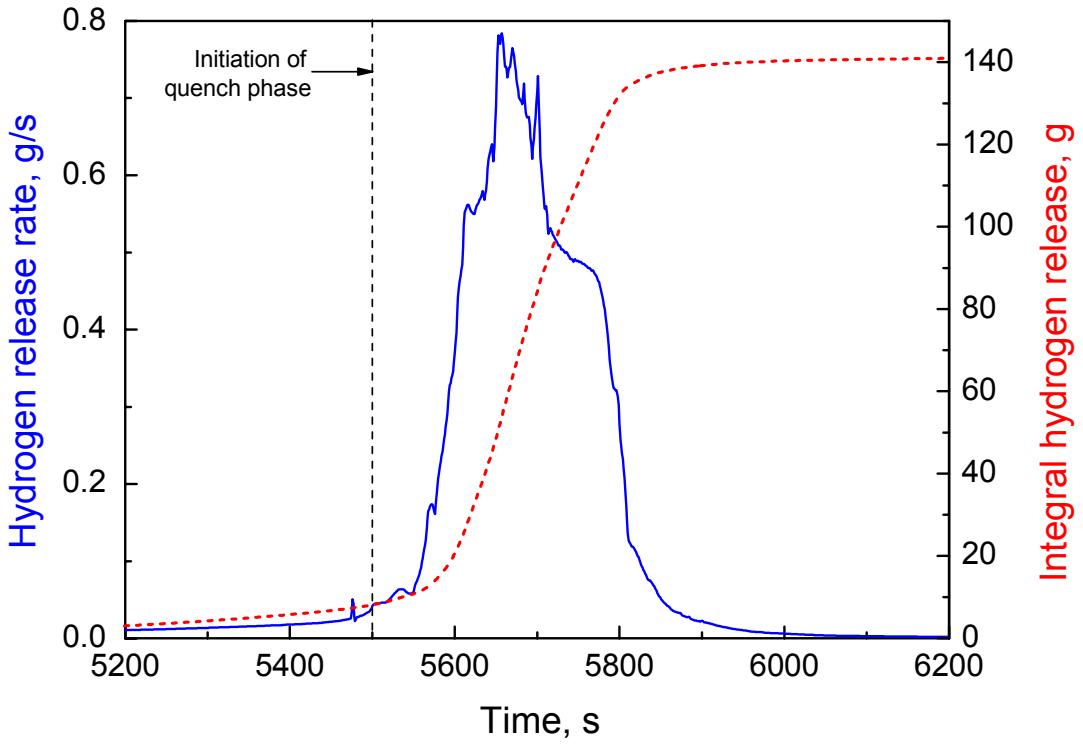

Fig. 17: Hydrogen release in the QUENCH-L2 test

The post-test analysis of the test bundle shows significant oxidation and fragmentation of the Zircaloy cladding from 800 mm elevation upwards (**Fig. 18**). The view into the bundle demonstrates severe melting and degradation of the bundle in this region. In addition a strong interaction between shroud and fuel-rod simulators as well as shroud and ZrO_2 fiber insulation took place.

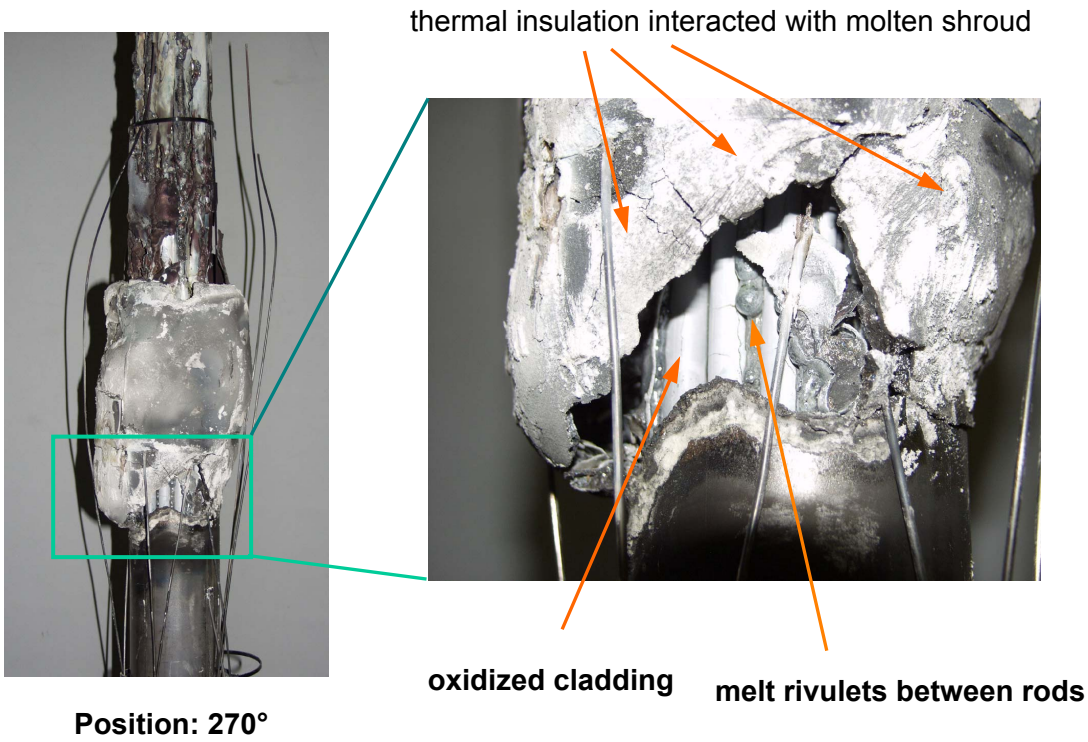

Fig. 18: Post-test view of the QUENCH-L2 bundle

2.2. WP2: Large-scale Tests on MCCI and Ex-vessel Melt Coolability (COMET)

The test facility (**Fig. 19**) is able to investigate different scenarios of molten core concrete interaction and the possibility of cooling the ex-vessel melt. It is presently used to investigate a core catcher concept, which is based on water injection into the core melt from below. Due to the resulting strong evaporation process, the melt is fragmented and forms a porous bed which is coolable and can be stabilised.

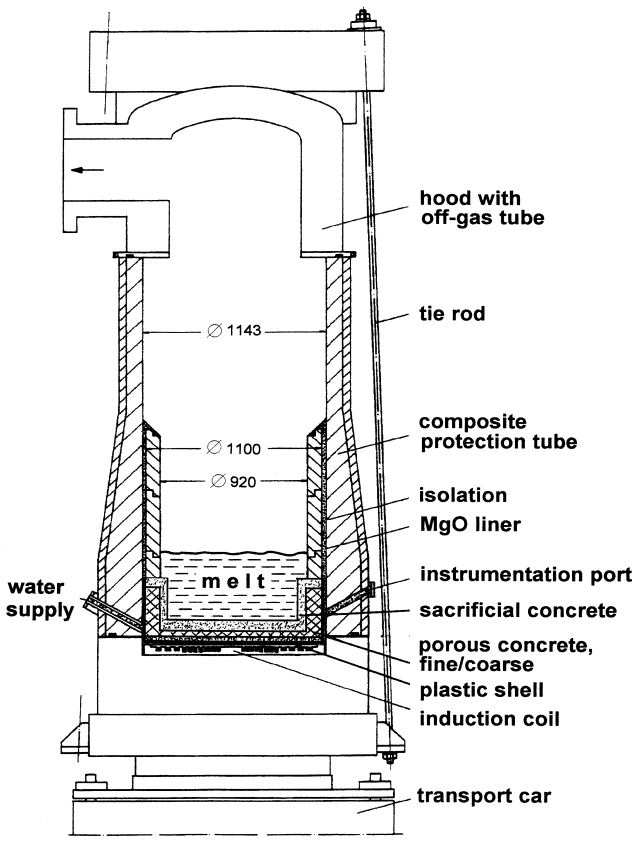

Fig. 19: Diagram of the COMET test facility

In these tests, the corium melt is simulated by Fe and Al_2O_3 melt with initial temperature of more than 2000 °C, which is produced by a thermite reaction in a special crucible. By using different oxide additives, the solidification temperature of the melt is lowered and the solidus-liquidus temperature range is increased. The melt is poured into the test device. Decay heat simulation throughout the test is achieved by an induction heating coil under the device, which is able to induce about 500 kW/m² into the melt. For cooling investigations, the experimental device may be fabricated of different layers. A first sacrificial concrete layer serves to lower the initially high temperature of the molten core. After erosion of this layer, the melt comes into contact with a specially designed porous water layer, which injects water into the melt from the bottom. As required, the cooling insert can be modified to allow, for example a longer phase of concrete erosion.

The test crucible itself is designed to withstand a pressure build-up of 20 bar, which might occur due to melt/water interactions at the initial phase of cooling. In the off-gas pipe, a complete system of aerosol and gas measurement is installed. Additionally, the water supply rate and the steam release rate are measured. In the specially-designed cooling device, thermocouples are installed to detect the erosion front progression in the upper concrete layer and to give temperature information at the lower, water-filled levels of the device.

Experiments in the COMET facility generally consist of the following phases:

- Up to 1000 kg of melt is generated in an external crucible by thermite reaction, resulting in steel melt (Fe + Cr, Ni, Zr) and oxide melt (Al_2O_3 + CaO + SiO_2 + FeO).

- Melt is then poured into test crucible, initial temperature 2000-2300 K, depending on type of generated melt. Steel melt is at the bottom, oxide on top (corresponding to reactor situation after admixture of eroded concrete).
- Steel fraction is continuously heated by electrical induction heating with total power from 100 to 500 kW (simulation of decay heat). Internal heating of the oxide phase is however not possible, oxide is heated by convection and conduction from the steel layer. Therefore, erosion in the actual experiments is mostly dominated by the metal phase.
- End of experiment defined by maximal concrete erosion.

The following types of concrete can be used in the COMET facility: siliceous, siliceous/limestone, limestone, serpentine ($Mg_3Si_2O_7 \cdot 2H_2O$ in Eastern plants), etc., possibly in combination with refractory ceramic liner.

Standard test results are: simulated decay power; temperature of melt; release rates, temperatures and composition of gases/steam/aerosols; erosion of concrete/structures; cooling rate by water and steam flow; pressures; video observation of melt surface and crust formation.

2.2.1. COMET-L1 test

The first experiment in COMET facility COMET-L1 investigates the situation of basement attack by the simulated corium melt and brings together partners from IRSN and TUS. The experiment was conducted on 10 July 2004. The open questions which are addressed in this experiment are

1. the long-term erosion of the concrete by a two component metal plus oxide melt during the absence of water, and
2. the consequence of top flooding when water is added to the surface of the hot melt during concrete erosion.

This experiment [14], [15] is complementary to the present OECD-CCI tests that are carried out at ANL [16] with pure oxidic corium.

The special objective of the first phase of this test is the 2D concrete erosion in a cylindrical concrete cavity, evaluating the lateral vs. axial erosion rates by a sustained heated, simulated corium melt. This shall allow improved predictions of time and location of the potential basement penetration. Heating of the melt is achieved by simulating the nuclear decay heat by inductive heating of the lower steel phase overlaid by an oxide phase which receives the heat by convective heat transfer from the steel layer. Layering of steel below the less dense oxide melt is typical for the long-term concrete erosion, where the addition of light oxides produced by concrete ablation will decrease the oxide layer density. The power density in the steel is maintained at a low power level representing late accident conditions. After substantial concrete erosion, it was planned to start the second phase of the test by adding water to the surface of the melt. Emphasis of the flooding process is on the potential retardation or stop of concrete erosion and on those processes that could generate a coolable corium bed, such as crust cracking and melt eruptions. Pre-calculations were performed by the partners to design the details of the test installation, and to delineate the decay power and the expected timing during the test.

The experiment was performed on 10 July 2004. The crucible was fabricated from siliceous concrete, outer dimensions 1100 mm diameter, and 1050 mm high (**Fig. 20** and **Fig. 21**). The inner cavity, to which the melt is supplied, has an initial inner diameter of 600 mm. The crucible was instrumented with 88 thermocouples positioned at well-defined locations in the concrete to detect the response of the concrete and the actual position of the erosion front (**Fig. 22**). Video and a high-tech infrared camera observe the surface of the melt from the hood of the crucible throughout the test. Chemical analysis and volume fluxes of the off-gas generated from the decomposing concrete are registered throughout the test.

The initial mass of the melt supplied to the crucible is 460 kg steel melt (90 w-% Fe, 10 w-% Ni), layer height 25 cm, plus 467 kg oxide melt (**Fig. 23**). The oxide, overlaying the metal melt, is 56 w-% Al_2O_3 plus 44 w-% CaO and was designed to have a wide freezing range with a low solidus temperature. The height of the oxide layer in the cavity without void corresponds to 55 cm. The melt was generated externally by a thermite reaction and poured into the cavity with an initial temperature of 1640 °C (**Fig. 24**). Because of the planned low internal heating rate, partial crust formation at the concrete interfaces was expected already during the first phase of the test. The power that could be deposited in the melt by induction heating was 120 kW after completion of the melt pour, rising to 160 kW at 958 s, when the electrical power supply failed and unfortunately could not be re-established.

The interaction of melt and concrete in the first period of the test until some 250 s is characterized by significant agitation and some splashing of the melt as shown in **Fig. 25**, caused by substantial gas release from the decomposing concrete. In this time period, axial and lateral erosion rates of the cavity are similar and mainly controlled by the initial overheat of the melt. With cool down of the melt to a stationary lower temperature as defined by the simulated decay power, and due to concurrent onset of crust formation in the metal phase, the erosion rate reduces. Based on the current analysis of the test data, downward erosion in this phase is more pronounced than radial erosion. Some eruptions, which occur during the stationary heating phase (**Fig. 26**), indicate sudden release of gas and melted concrete masses, which may have accumulated under a crusted metal melt, and penetrated or removed parts of the crust. This process correlates with a clear increase of the heating power, as heating efficiency improves when the metal phase comes closer to the induction coil.

Due to its low solidus temperature, the oxide melt remains liquid and well stirred with a relatively low viscosity. In some periods a thin surface crust forms, which is however removed when periods of more intense gas release occur. The erosive action of the oxide melt is minor, partly because of the low overheat of the oxide related to the “melting” temperature of the siliceous concrete.

After the unexpected end of heating at 959 s, the melt cools down only very slowly. Some flooding process are initiated by the operator after 3000 s, bringing water to the outer surface of the concrete crucible only, namely to its bottom and sidewall. This has, however, negligible influence on the melt in the crucible and the inner concrete structure, as heat conduction through the concrete is very small. Permanent flooding of the melt surface at 4770 s quenches the hot surface of the crusted melt, which is still hot and bright in the bulk. However, the registered temperature near the inner concrete interface are 1100 to 1200 °C at that time and show no significant change due to the presence of water on the crusted surface (**Fig. 27**). Very slow reduction of this temperature to 400-600 °C at 28 000 s shows that cool down is controlled by transient heat conduction, and water ingression through suspected cracks is not effective.

To determine the melt temperature during the experiment, an infrared video camera was installed on top of the hood of the crucible at a distance of ~ 2.5 m from the melt surface. This camera operates in the shortwave spectrum from 3.4 to 5.0 µm to produce a video film and, every 15 s, up to 240 high precision thermal images of the melt surface during 60 min. The camera utilizes a 3.9 micron flame suppression filter and is placed behind a 3 mm thick sapphire window which has a transmission coefficient of ~ 0.9 at the considered wavelength. As for any IR system, to derive the temperature or the emitted radiation from the surface, assumptions have been made for the emissivity of the surface. Recordings of the infrared camera have been used to determine initial melt temperature during the melt release (**Fig. 28** and **Fig. 29**) and evolution of the melt surface temperature (**Fig. 30**). In addition, bulk temperature of the oxide melt can be estimated when fresh material was transported to the surface, e.g. by released gases. IR registration gives however no quantitative information when water is added to the surface of the melt.

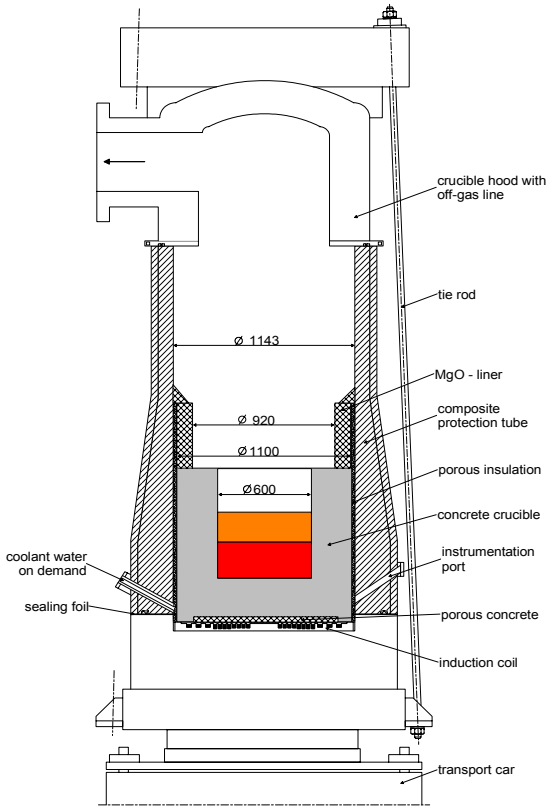

Fig. 20: COMET-L1 test rig

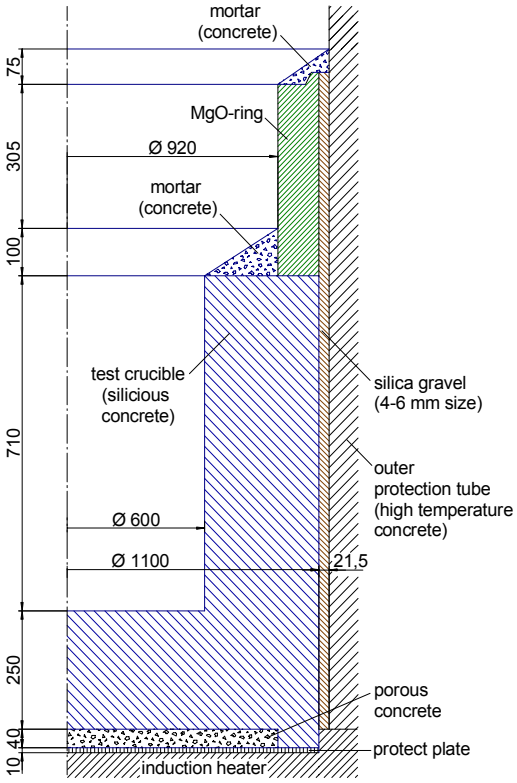

Fig. 21: COMET-L1 crucible

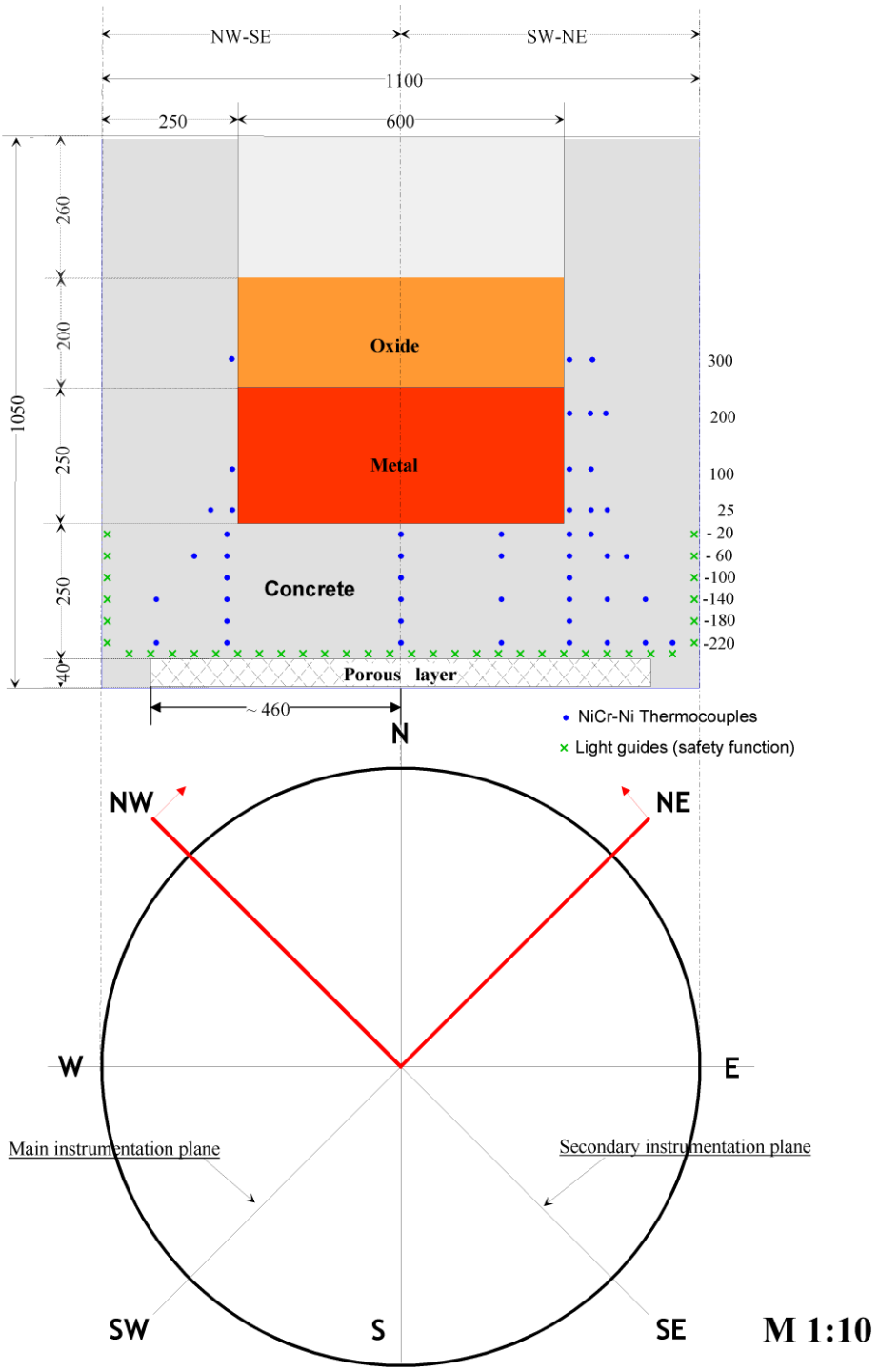

Fig. 22: Dimensions and instrumentation plan of COMET-L1 crucible
Right side: main instrumentation plane, representing left and right side of plane SW-NE
Left side: secondary instrumentation plane, representing left and right side of plane NW-SE
x indicates light guides which switch off the decay heat simulation when melt interrupts light guide (safety function)

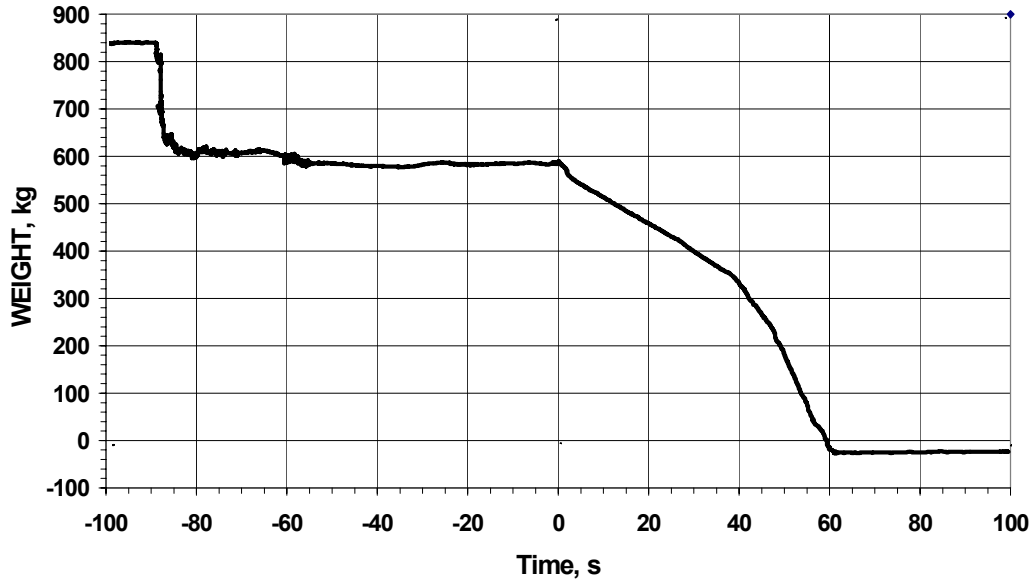

Fig. 23: Weight of thermite reaction tank during thermite reaction and release of the melt (registered by pen writer). The decrease of the weight after ignition of the thermite at 90 s is due to some unexpected error in the measurement system and leads to an increased mass of oxide poured to the test vessel

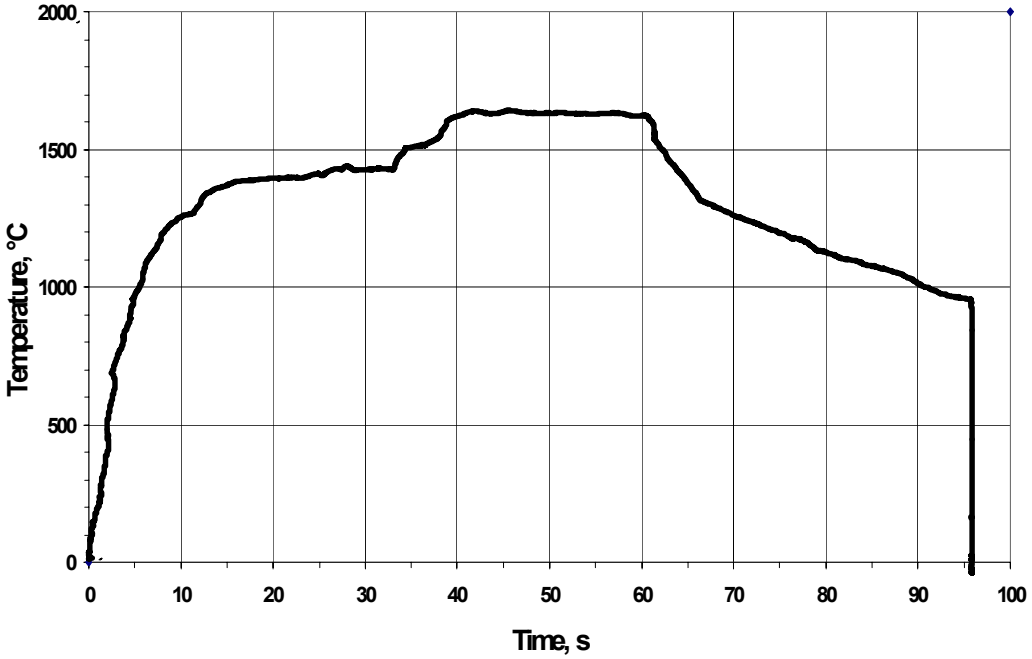

Fig. 24: Initial temperature of the melt measured in the spout by W-Re thermo-couple

Fig. 25: Interaction of melt and concrete in the beginning of the test

Fig. 26: Interaction of melt and concrete during stationary heating phase

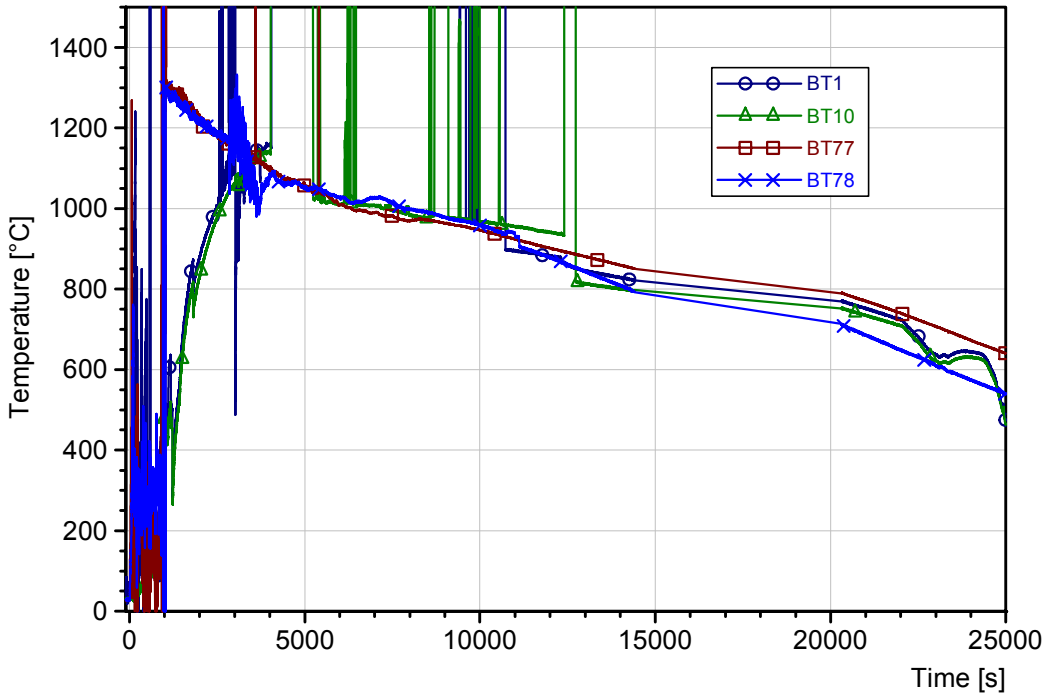

Fig. 27: Temperatures measured near the concrete surface

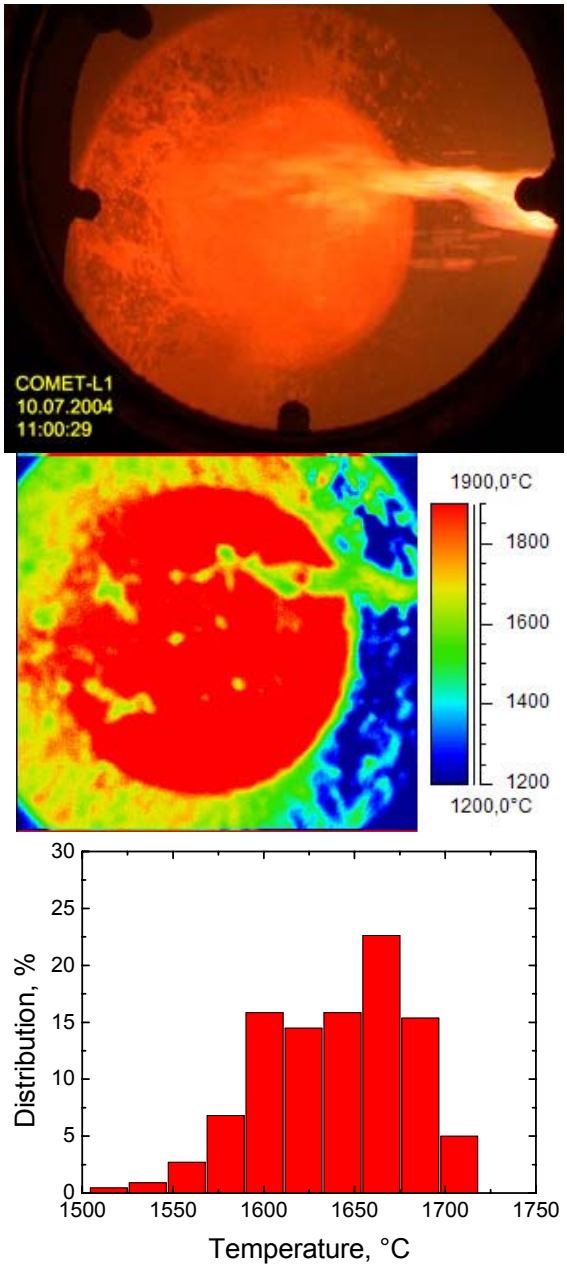

Fig. 28: Temperature of the metallic melt

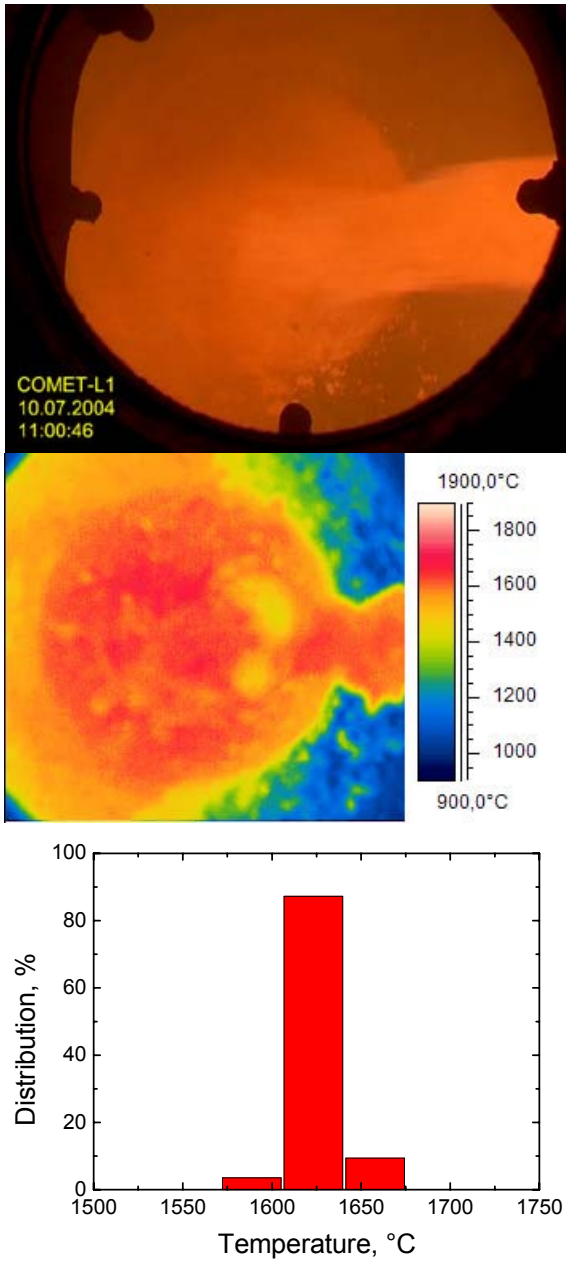

Fig. 29: Temperature of the oxidic melt

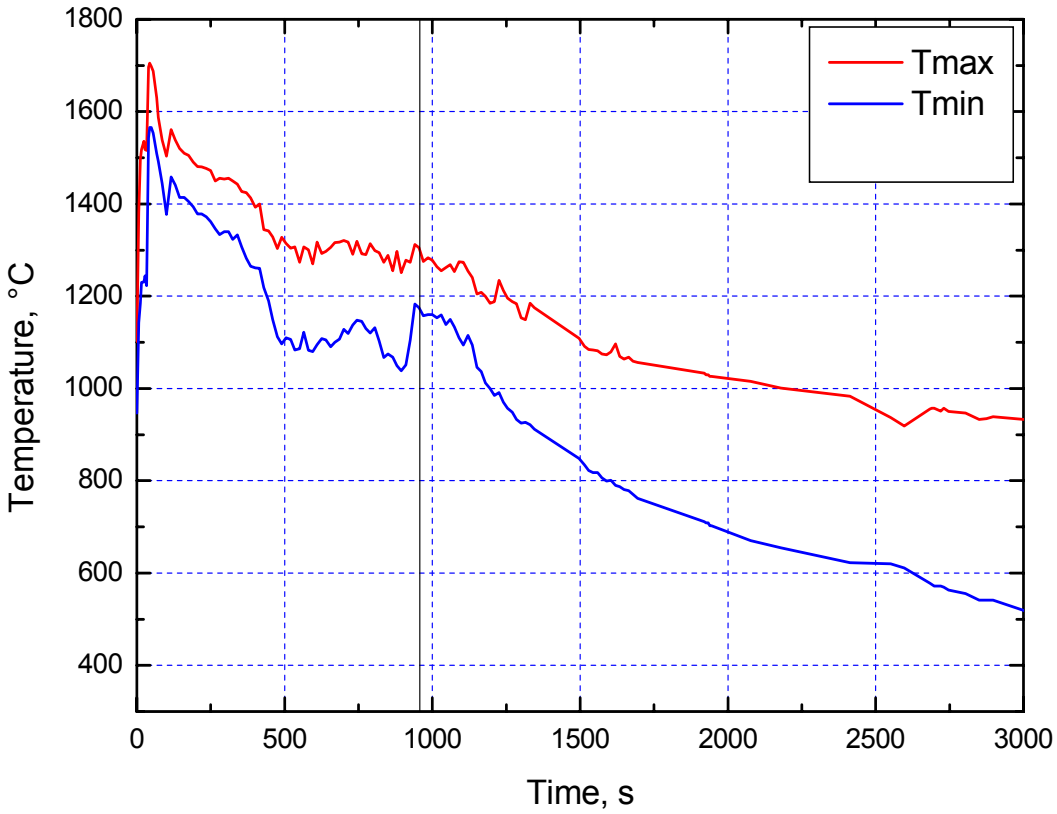

Fig. 30: Evolution of melt surface temperatures in the COMET-L1 test

2.2.2. COMET-L2 test

The COMET-L2 experiment [17] was planned to fulfil the proposal of ARC Seibersdorf Research GmbH, Austria. It concentrated on generic studies of long-term metal/concrete interaction in cylindrical cavity for intermediate and low decay heat levels through metal phase only. The experiment [18] is designed to answer the following questions: investigation of a long-term MCCI of metallic corium in cylindrical siliceous concrete cavity under dry conditions with decay heat simulation of intermediate power during test phase 1, and subsequently at reduced power during test phase 2. Downward and sideward cavity erosion rates, cavity shape, and related processes have been observed. The test uses a heated metal melt that is covered by an inevitable oxide layer. Decay heat is simulated in the metal melt by electrical inductive heating.

From the experience of the COMET-L1 experiment [14], special consideration was given to the rating of internal heating of the melt, which simulates the nuclear decay heat by induction heating of the metal phase. The power, which can be transferred by induction heating, is limited by the relatively small electromagnetic efficiency of the induction coil, which is strongly reduced for thicker basements. The goal is, to avoid the formation of a stable interface crust in phase 1 of the test by supplying sufficient decay power, and to observe the onset of possible crust formation and its consequences when in phase 2 of the test the simulated decay power is reduced.

The experiment was conducted on 5 February 2005. A short overview of the main test parameters is provided in
Table 1.

Parameter	Specification
Corium simulant	Metal (Fe + Ni) and oxide (Al_2O_3 + CaO)
Melt formation	Thermite reaction
Initial temperature of the melt	1750 to 1800 °C
Initial melt mass	430 kg metal + 35 kg oxide
Radial erosion limit	250 mm
Axial erosion limit	170 mm
Concrete type	Standard siliceous concrete
Initial cavity dimension	D_i = 595 mm, H_i = 615 mm
Simulated decay heat	Induction heating at approx. 200-250 kW
Facility pressure	Atmospheric
Cover gas	Argon
Flow rate of the cover gas	50 m^3/h main flow and 2 x 8 m^3/h from windows
Criteria for phase 1	250 kW heating until 13 cm downward erosion during the dry phase
Criteria for phase 2	200 kW heating until 17 cm
Criteria for test termination	1) Contact of the melt with a light guide 2) 25 cm radial erosion 3) Porous concrete at the bottom reached

Table 1: Specifications for the COMET-L2 experiment

Geometry and instrumentation of the crucible is shown in
Fig. 31. All indicated thermocouples are of the type NiCr-Ni. They fail at ~ 1350 °C, and therefore operate until melting of the concrete does occur. Their failure indicates arrival of the melt front. These thermocouples are however unable to measure the temperature of the melt. Important is that the thermocouples give sufficient information during the test about the actual position of the melt front. Therefore, the instrumentation is arranged in two perpendicular planes, namely SW-NE and NW-SE. The total number of NiCr-Ni thermocouples is 90. Additional safety relevant instrumentation in form of light guides is located in the outer sections of the crucible. If they are destroyed by the arriving melt, heating is switched off immediately, and the melt cools down.

With the given dimensions of the inner cavity, the mass of the metallic melt is selected to fill the cavity – without void – with 250 mm. The steel height decreases during the test when radial cavity erosion proceeds. This means, that for a radial erosion from 600 mm to e. g. 900 mm the height of the steel is reduced to 44 %, that is from 250 mm to 111 mm. Initially, no oxide shall be present on top of the steel melt, but would build up due to accumulation of the concrete decomposition products throughout the test.

After careful preparation of the test and check of all measurement and control systems, inertisation of the test rig by argon cover gas flow started 30 min before pour of the melt. The mixed and pre-heated thermite powder was ignited in the external vessel 90 seconds before the pouring. The thermite reaction was completed after 33 seconds. After further 57 s to allow separation of the metal and the oxide phases, 465 kg of the melt was discharged into the concrete vessel. Release of the melt to the concrete cavity took 18 s. The melt consisted of 430 kg steel and 35 kg oxide.

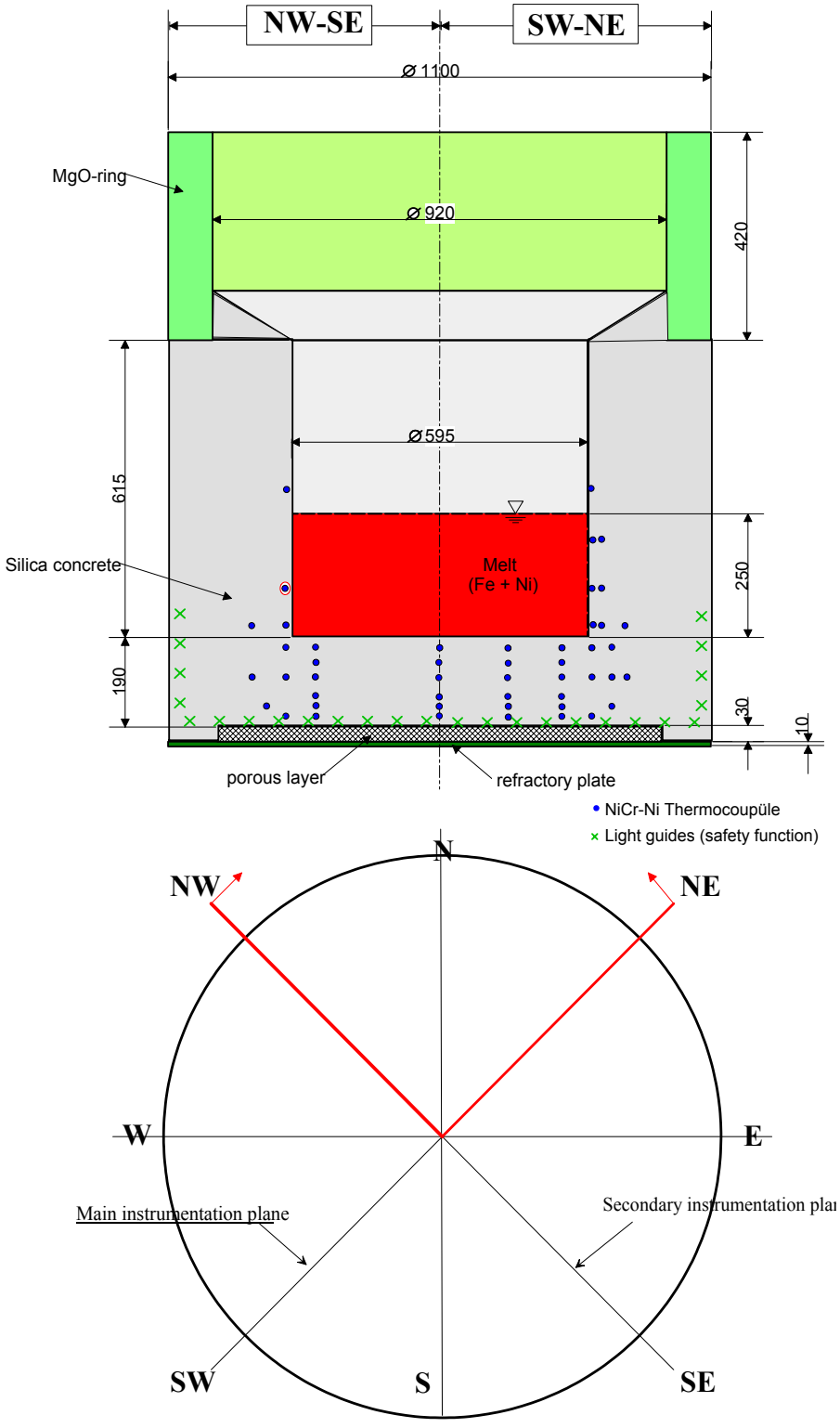

Fig. 31: Dimensions and instrumentation plan of the COMET-L2 crucible
Right side: main instrumentation plane, representing left and right side of plane SW-NE
Left side: secondary instrumentation plane, representing left and right side of plane NW-SE
x indicates light guides which switch off the decay-heat simulation when melt interrupts light guide (safety function)

The most significant events during the test are listed in Table 2.

Hour	Time [s]	Event
10:57:20	- 160	Induction system started, voltage 2.0 kV
10:58:30	- 90	Ignition of thermite, completion of thermite burn after 33 s
10:59:40	- 20	Operator increases induction voltage to 2.6 kV as specified
11:00:00	0	After count-down according to plan, start of melt pour. Full melt jet released, hits inner wall of MgO tube and rim of upper crucible, and rapidly flows to bottom of crucible. Initial temperature of melt ~ 1760 ± 20 °C. Gas measurement system fails: Scan function not operating. No chemical gas composition measured throughout the test.
11:00:18	18	Pour of 465 kg melt (~ 430 kg metal melt + 35 kg oxide melt) completed. Residual oxide melt poured into slag wagon.
11.00:28	28	Spout to position 2
11:00:31	31	Command to close crucible hood. Melt has very low viscosity. Intense agitation of melt surface. Some melt splashed to upper crucible rim and to inner MgO tube, from which the melt flows back to the central crucible. (Remaining melt film at the wall forms a nearly closed, solid steel sheet, as recognized by post test analysis). No difference observable between metal and oxide melt phases – phases might be mixed. Slight aerosols in crucible until 90 s
11:00:50	50	160 kW net power, hood of crucible locked
11:01:00	60	intense melt agitation ongoing with low viscosity
11:01:30	90	189/1250 kW net/total induction heating power at 2.61 kV lower than expected. Inductor voltage remains unchanged until 570 s, as no further voltage increase possible. Future power increase is due to increase of heating efficiency by smaller distance to the induction coil. Strong agitation of the melt equally distributed over melt surface, but nevertheless small splash-out of melt only. Melt surface has low viscosity, corresponding to the expected steel melt. Very clear video of the crucible, aerosols nearly zero. Small H2-flame at end of off-gas line.
11:02:20	140	170/1240 kW net/total heating power at 2.61 kV. Clear video of the crucible. Surface of melt covered by a layer of oxide melt (higher viscosity than before), may be due to ongoing concrete erosion. Intense agitation ongoing. No aerosols throughout the further test. H2 burn of off-gas ended.
11:03:00	180	189/ 1260 kW net/total heating power at 2.61 kV, strong melt agitation, viscosity of upper oxidic melt layer increased. Gas flow from the eroding concrete determines the flow pattern of the turbulent melt: Upwards at the cylinder wall, downwards in the center. Off-gas with condensing steam
11:03:20	200	Downward erosion of concrete between – 30 and – 60 mm.
11:04:00	240	194/1280 kW at 2.61 kV. Oxidic melt surface more viscous strongly agitated. Off-gas has low content of condensing steam.
11:05:00	300	200/1280 kW at 2.61 kV. Gas release evenly distributed over oxidic melt surface. Some eruptions eject melt, partly metallic, to rim of concrete crucible. Low off-gas flow
11:05:30	330	Erosion approaches - 60 mm, further increase of viscosity and some reduction of melt agitation.
11:06:30	390	217/1290 kW at 2.61 kV, oxide melt has higher viscosity, upper oxidic melt layer includes some bright metallic droplets, splash-out of melt reduced with exception of some more vigorous events, low condensing steam in off-gas
11:07:30	450	227/1300 kW at 2.61 kV. Gas release evenly distributed over oxidic melt surface. Gas bubble transports hot melt from the bulk to the surface. Increased steam flow at off-gas tube, no increase of gas release visible in crucible.

11:08:10	490	250/1320 kW at 2.61 kV, planned net power achieved
11:08:20	500	244/1300 kW at 2.61 kV. Power input to the melt does not show high frequency fluctuations since the early test phase. This indicates stable coupling of the metal melt to the induction field and minor metal relocation. Period of stronger melt agitation and some stronger melt eruptions. Low off-gas flow. Temperature in the lower crucible, displayed at operator's desk, is still unchanged (at room temperature).
11:09:20	560	260 kW. Significant eruption of metal melt in south of crucible. This results in temporary increase of the heating efficiency. Start of manual reduction of induction voltage by operator.
11:09:50	590	240/1160 kW at 2.42 kV. Still some periods of higher melt eruptions. Melt approaches – 90 mm level.
11:10:55	655	Further reduction of induction voltage due to steady increase of heating efficiency. 250/1100 kW at 2.36 kV. Intense agitation ongoing. Gas flow equally distributed over melt surface. Oxide melt has higher viscosity and transports some dispersed metal droplets. Temperature in porous layer under crucible still near room temperature. Low off-gas flow.
11:11:50	710	Power reduction from 268 to 250 kW. Melt further on well agitated with some metal droplets. Melt approaches –130 mm level.
11:12:30	750	Power reduction from 268 to 250 kW/1050 kW at 2.26 kV. Oxide melt has lower viscosity with stronger agitation.
11:13:40	820	-130 mm level eroded. Start of Phase 2 of the test: Power reduction to 200 kW target value: 200/714 kW at 1.86 kV. Ejection of some metal melt.
11:14:30	870	Power reduction to 200 kW/695 kW at 1.80kV. Melt well agitated, increased viscosity of oxide, no more metal droplets visible. Low off-gas flow, -170 mm eroded as indicated by failure of BT 58
11:15:45	945	Again power reduction to 200 kW. Decision to continue heating until light guides are destroyed by melt.
11:16:10	970	205/626 kW at 1.69 kV. Melt is well agitated, oxide more viscous with some metal droplets. Air flow through porous layer under crucible still cold, indicating that melt did not yet penetrate the lower bottom.
11:16:55	1015	Heating switched-off automatically by failure of light guide CX 4. No further heating takes place, as melt reached the lower bottom. Agitation of melt by gases continues. Condensing steam in off-gas flow.
11:18:20	1100	Air flow in porous layer still cold (20 °C), melt and surface still liquid, outer crucible as indicated on operator panel still at 30°C only.
11:18:40	1120	Light guide CX 4 repeats failure signal (was possibly "repaired")
11:19:14	1154	Light guide CX 3 interrupted, both failed light guides are located in N hemisphere. Ongoing gas bubbles transport hot melt from the bulk to the surface.
11:20:50	1250	Oxide surface near cylinder wall forms dark crust, central surface still bright and liquid, and further on agitated by gas bubbles. Bulk of melt still at high temperatures. Low off-gas flow.
11:22:00	1320	Dark ring of crust broadening. Bright central surface of melt reduced to some 30 cm diameter
11:22:20	1340	Cooling of bottom of concrete crucible activated by supply of coolant water to N and S of the porous concrete layer under the crucible. Continuous coolant flow from 1.5 to 0.65 l/s, coolant water shows no temperature increase. Cooling does not initiate intense processes in crucible or melt. Off-gas flow with condensing steam.
11:24:00	1440	Bottom cooling ongoing with 0.62 l/s driven by 3 m water overhead.
11:24:10	1450	Surface of melt dark, only center bright and still liquid
		Tape changed
11:25:00	1500	Remaining hot spot in the center of ~10 cm dia with release of gas bubbles. Surface crust smooth and gas tight

11:26:40	1600	Bottom flooding ongoing with 0.69 l/s, central surface still bright, off-gas with condensing steam. Maximum downward erosion occurred probably in SW
11:28:50	1730	All light guides under crucible failed by contact with the hot melt/regulus
11:30:00	1800	Bottom flooding ongoing with 0.66 l/s, with minor increase of the water temperature only. No water visible in upper crucible.
11:31:00	1860	Surface of oxide covered by dark crust, some hot lines probably due to cracks indicate the hot temperatures in the bulk of the oxide melt
11:31:40	1900	Lights in crucible on, fine glass whiskers visible above the dry surface, Surface crust is convex, smooth, and closed. Steam flow in off-gas seems ongoing.
11:33:20	2000	Water inflow to porous concrete interrupted. Water level in outer annulus of the concrete crucible, which was filled with water up to 70 cm, slowly reduces to 10 cm. Existence of water in the annulus indicates cracks which allow permeation of water from the porous sublayer to the annulus.
11:34:12	2052	Water inflow to porous concrete resumed, resulting in 0.72 l/s. Only small increase of water temperature (20.4°C). Thermocouple BT 34-37 in lower crucible show ~ 70°C. Melt evidently stopped close to the porous layer, no further erosion of concrete expected.
11:37:10	2230	Water inflow to porous bottom layer is 0,69 l/s, water level in annulus 64 cm due to leakage from bottom layer. Small leakage of water from outer crucible, where instrumentation lines are introduced; this leakage confirms that annulus is flooded.
11:40:00	2400	some hot spots still visible through the upper oxide crust, central part of the oxide still hot, bottom cooling continued
11:45:00	2700	Direct water supply to annulus started with the goal to flood the surface of the melt by overflow from the annulus.
11:45:05	2705	Water enters surface of melt, strong foaming
11:46:10	2770	Surface of melt practically covered with foaming water in moderate pool boiling, convex crust, total water flow to bottom and annulus 1.04 l/s
11:48:00	2880	Surface of crust covered by 10 to 20 cm water layer, moderate pool boiling, steam in off-gas
11:50:00	3000	Further activities directed to cool the melt and to extract the energy, keeping the outer test rig and the induction coil sufficiently cool
11:56:40	3400	Melt flooded, total water inflow to bottom and sidewall ~0.52 l/s, minor boiling in water layer, measured water level in the annulus is 73 cm, condensing steam flow in off-gas
12:00:00	3600	Water level in crucible raised up to 10 cm below upper rim of the Mg0 ring, minor boiling, gases are released from water layer in east and to minor extend in west, temperature measured at the lower melt/concrete interface still 1200°C typical. Extraction of heat strongly limited by conduction through remaining concrete at bottom and side, and through crust at upper surface. Crucible is completely enclosed by water.
12:03:50	3830	Shower head activated to add water from the crucible hood
12:10:00	4200	Stop of flooding through shower head
12:14:00	4440	Drainage of water from the upper water layer through the melt to the porous concrete layer is not successful: No cracks in the solidifying melt or at the melt/concrete interface, which allow passage of water. Very small steam flow in the off-gas.
12:22:00	4920	Again activation of shower head
12:36:40	5800	End of experiment declared, temperatures at melt/concrete interface in lower crucible still 1000-1100 °C
		Further flooding and draining to remove the heat, crucible remains flooded for long- term heat removal over the rest of the day to extract the energy

Table 2: Sequence of COMET-L2 as observed during the test

Melt stream and melt surface temperatures

As in the QUENCH-L1 experiment, an infrared video camera was installed on top of the hood of the crucible at a distance of ~ 2.5 m from the melt surface. To determine the temperature of the melt pour stream the following assumptions have been made. Different estimates for the spectral emittance of the molten iron performed in the steel industry come up with an emissivity value of 0.2-0.5 depending on temperature and wavelength. Taking into account the conditions of the COMET-L2 test and the operating spectrum of the IR camera, a value of 0.3 has been chosen for the current analysis.

Two thermal images of the iron melt stream have been taken 11 and 15 seconds after the start of the pouring process. These thermal images, corresponding visual pictures, and temperature histograms of the melt pouring process in the COMET-L2 test are shown in **Fig. 32**.

Thermographic analysis shows that the estimated temperatures of the melt stream are within a range of 1600-1850 °C with a distinct maximum at 1700-1750 °C. The lighter areas in the thermograms represent the oxide film on the iron melt surface at the bottom of the crucible. It has a higher emissivity, which consequently results in artificially high measured temperatures. The melt stream temperature estimates are in a fairly good agreement with the values measured by a W/Re thermocouple (compare **Fig. 33**) positioned in the spout. However, it is noted that the emissivity of a pour stream, which is one of the crucial factors for the correct estimation of the surface temperature, can be very different from the emissivity of the native material. Moreover, the thermographic analysis becomes even more difficult due to the aerosols from MCCI absorbing part of the IR radiation and due to the oxide films higher emissivity on the stream surface.

Assuming the associated emissivity for the initial melt as 0.7 and for pure SiO_2 as 0.92, further temperatures of the melt surface were determined for later phases of the experiment using the infrared video camera. The evolution of the maximum measured temperatures of the melt surface is shown in **Fig. 34**. However, it is noted that when water is added into the porous concrete layer, the infrared measurements are no longer reliable because of the vapour absorption.

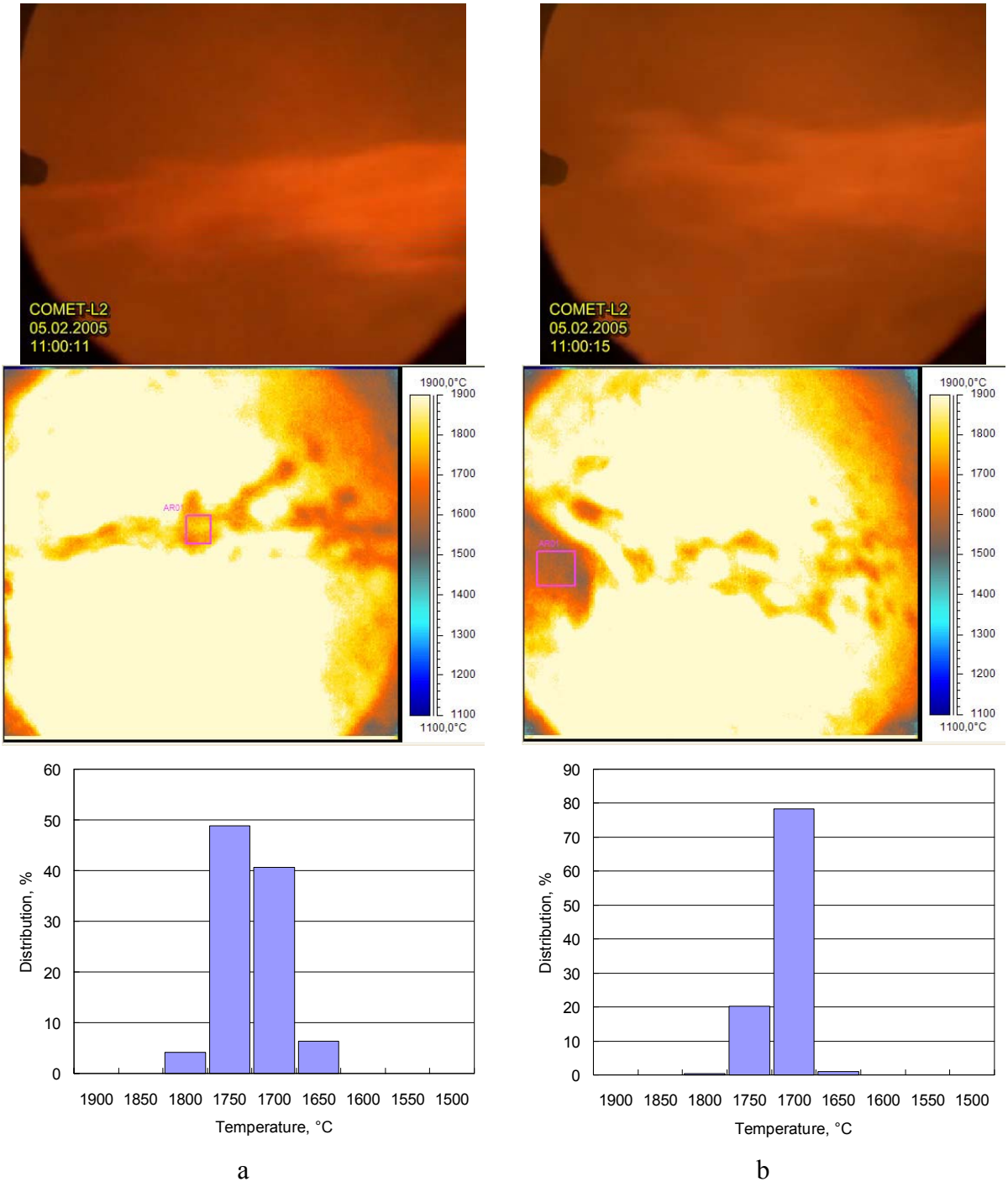

Fig. 32: Iron melt stream a) 11 s and b) 15 s after the onset of the melt pouring. Visual pictures, corresponding thermograms, and temperature distribution

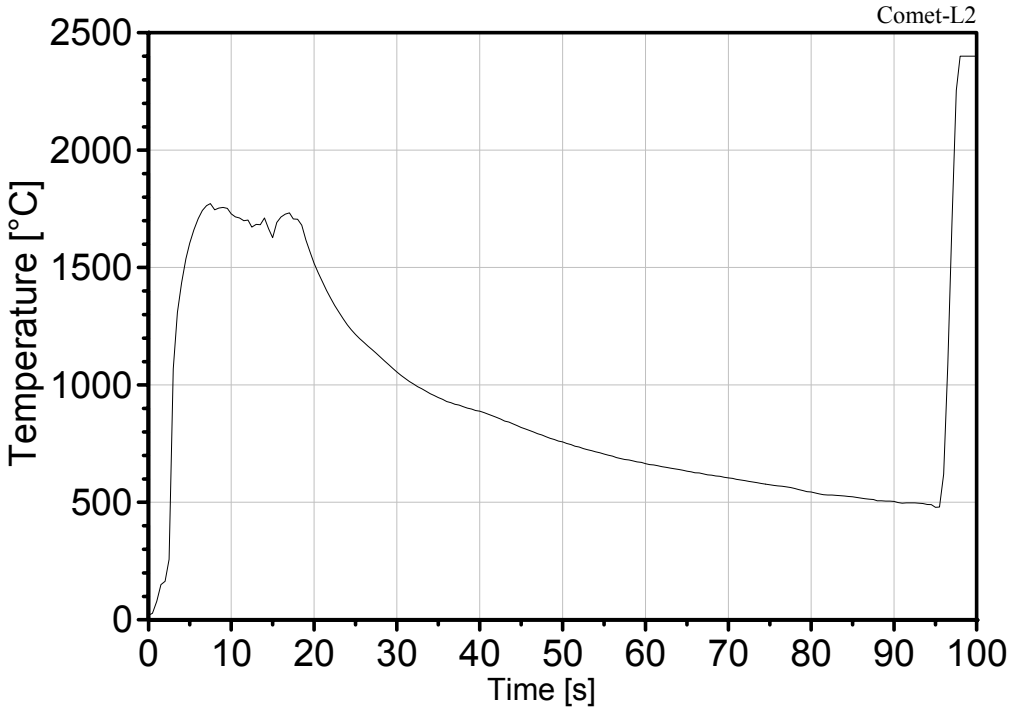

Fig. 33: Melt temperature in the spout

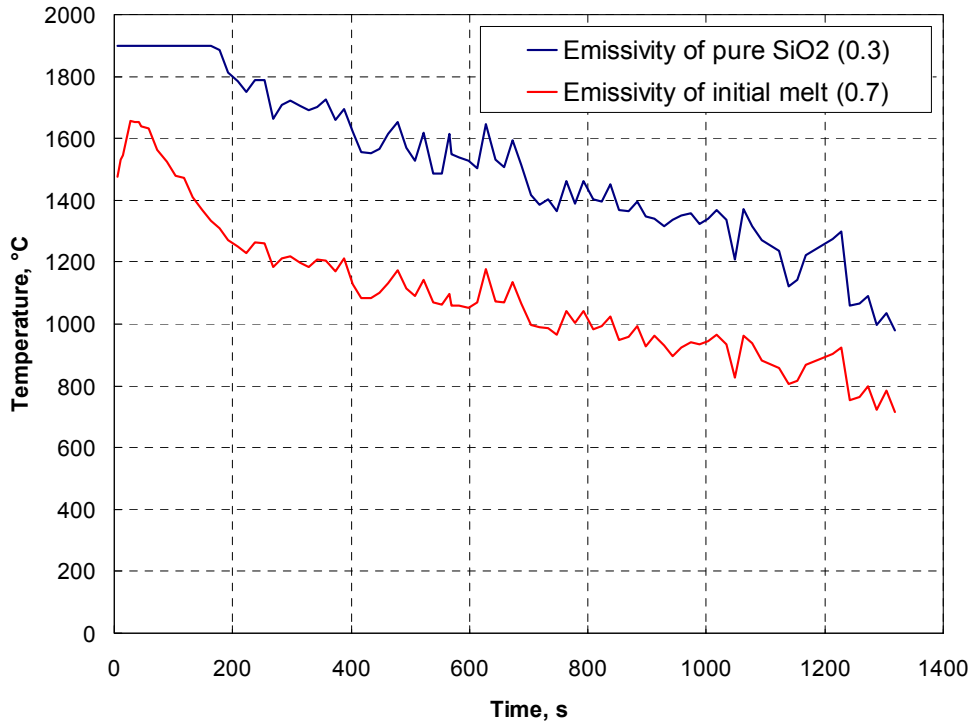

Fig. 34: Evolution of the maximum measured temperatures of the melt surface assuming the emissivity is 0.7 (lower curve: initial oxide) and 0.3 (upper curve: late oxide)

For a detailed analysis of concrete erosion rates and cavity shape, the failure times of thermocouples in the concrete cavity are evaluated. Based on the estimated contour of the erosion front the predicted cavity shape is shown for the SW-NE plane in **Fig. 35**.

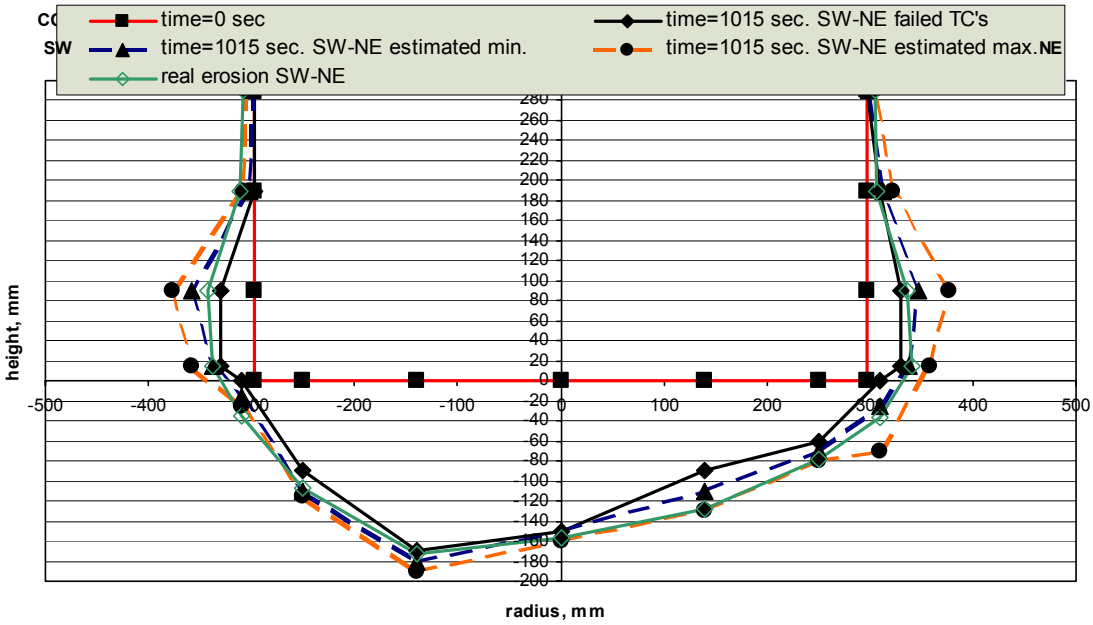

Fig. 35: Initial and final cavity shape in the SW-NE plane

Post-test analysis

After the test, the crucible was sectioned along the main instrumentation plane (**Fig. 36** and **Fig. 37**). The lower cavity is filled with the solidified iron melt, overlaid by oxide. The yellow line marks the original geometry of the crucible.

At the end of the experiment, a cavity was established in the centre of the crucible with 450 mm diameter and approximately 250 mm height. The dome collapsed due to residual stress and shrinking during the cooling period. The fragments were 10-50 mm thick consisting of pure oxide with small pores. The generation of the cavity started with water cooling resulting in a stable crust and release of gas bubbles from the melt. The bottom of the cavity consists of several bumps with a diameter between 8 and 10 cm which were generated by melt flowing through the already established crust. A small channel was found in which lava flew from the centre to the eastern rim of the crust.

The oxide melt contains a significant amount of unmelted silica gavels which is the consequence of low heat fluxes to the concrete surface. The heated concrete loses its mechanical strength, and the aggregates may be transferred into the melt before being melted. This may result in different heat flux distribution and erosion resulting from the lower “melting” enthalpy of concrete, and bulk cooling of the melt by aggregates.

The cavity erosion by the oxide melt is virtually zero in the upper cavity. The lower 30 cm of the sidewalls show a more pronounced radial erosion, maximum erosion about 3 cm, which is predominantly due to the attack of the metal melt. In contrast, downward erosion by the metal melt extends to some 17 cm with the maximum near the 10 cm radius. Although the uneven downward melt front is partly determined due to the inhomogeneous decay heat distribution. The more pronounced downward erosion seems to be imminent to the erosion by the metal melt for low heat fluxes. This is in agreement with the former BETA experiments V 3.1 to 3.3 [19] at low induction power. Induction heating was performed with a cylindrical induction coil with the result that a non-homogenous electromagnetic field was generated.

Fig. 36: Eroded concrete crucible

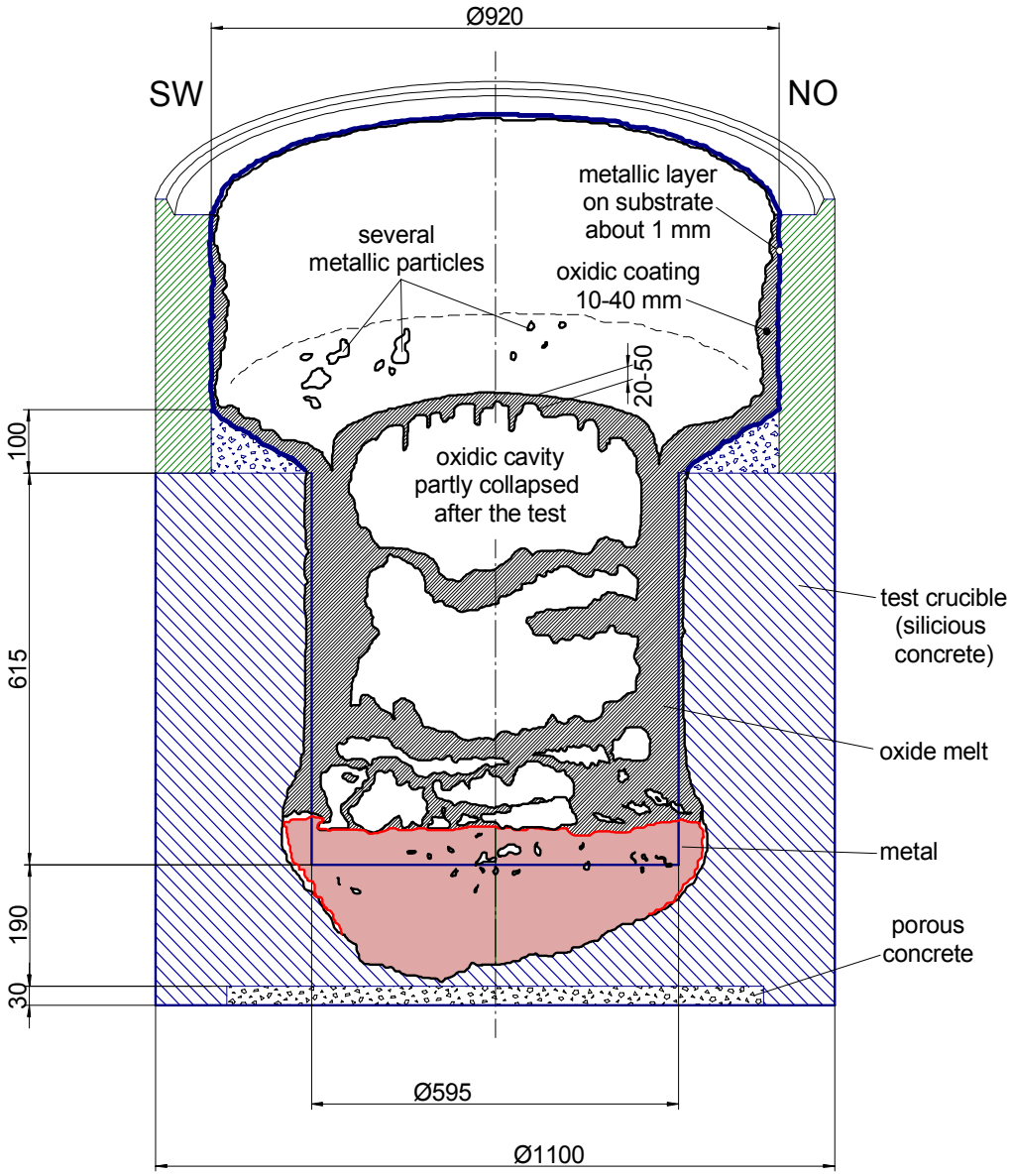

Fig. 37: Contour of the melt after the test

Evaluation and documentation of the experiment is ongoing. The data will complement existing and upcoming experiments, such as COMET-L1 test and the CCI experiments at ANL. The results are important for safety assessment and planning of accident mitigation concepts.

2.3. WP3: Large-scale Tests on Melt Dispersion (DISCO)

The DISCO-H test facility (
Fig. 38) at FZK is set up to perform scaled experiments that simulate melt ejection scenarios under low system pressure in severe accidents in pressurised water reactors (PWRs).

The experiments are designed to investigate the fluid-dynamic, thermal and chemical processes during melt ejection out of a breach in the lower head of a PWR pressure vessel at pressures below 2 MPa with an iron-alumina melt and steam. In the frame of these Direct

Containment Heating investigations the following issues are addressed: final location of corium debris, loads on the reactor pit and the containment in respect to pressure and temperature, and the amount of hydrogen produced and burned. The main components of the facility are scaled about 1:18 linearly to a large PWR: the containment pressure vessel (volume 14 m³), the RPV Reactor Coolant System (RCS) pressure vessel (0.08 m³), the cavity, the sub-compartment (1.74 m³), and the steam accumulator (0.08 m³). The sub-compartment is an annular space around the cavity with a volume of 1.74 m³.

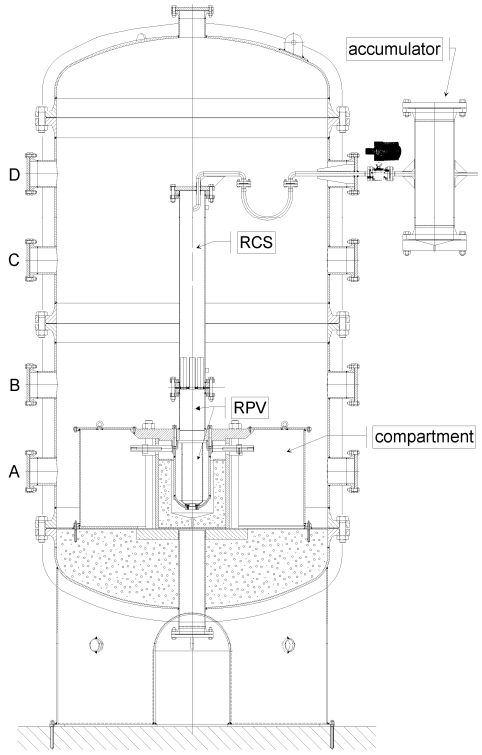

Fig. 38: Diagram of the DISCO test facility

The flow path from the cavity into the sub-compartment is along the eight stubs modelling the main cooling lines. The connection from the sub-compartment to the containment is by four openings in its top plate. The RCS-RPV pressure vessel models the volumes of both the reactor cooling system and the reactor pressure vessel. The RPV model, which serves as crucible for the generation of the melt, is bolted to a plate carrying the RCS-RPV pressure vessel. The hole at the bottom of the melt generator is formed by a graphite annulus. It is closed with a brass plate. The reactor pit is made of concrete and is installed inside a strong steel cylinder. Besides the flow path along the main cooling lines there is the option of a flow out of the cavity straight up into the containment through eight openings. Depending on the reactor design that is to be investigated, the cross section of the openings is variable.

In case of the modelling of a prototypical scenario, the containment vessel is heated by filling with steam additional to the atmospheric air until the pressure reaches 0.2 MPa. The average gas temperature and the wall temperature inside the vessel is 100 °C at the end of the heat-up. A metered amount of hydrogen gas (3 mol-%) is added to the vessel at the end of heat-up while fans are running inside the vessel. A gas sample is taken just before the start of the experiment.

The pressure vessel modelling the RPV and RCS volume is electrically heated to the saturation temperature of the planned burst pressure, e.g. to 180 °C at 1.0 MPa. It contains nitrogen at that temperature at 0.1 MPa. The steam accumulator is heated electrically to the saturation temperature of twice the planned burst pressure, e.g. 213 °C at 2.0 MPa. The accumulator is filled with a measured amount of water by a high pressure metering pump to reach that pressure. The RCS pressure vessel and the accumulator are connected by a 25 mm diameter pipe with an electro-pneumatically actuated valve.

The model of the RPV is filled with aluminium/iron oxide thermite. The experiment is started by igniting the thermite electro-chemically at the upper surface of the compacted thermite powder. When a pressure increase in the RPV-RCS pressure vessel verifies that the thermite reaction has started, the valve in the line connected to the accumulator is opened and steam enters the pressure vessel. When the pressure has reached a preset value the valve is automatically closed again. About 5 to 8 seconds after ignition the brass plug at the bottom of the RPV vessel is melted by the 2400 K hot iron-alumina mixture. That initiates the melt ejection. The melt is driven out of the breach by the steam and is dispersed into the cavity and the containment.

Standard test results are: pressure and temperature history in the RPV, the cavity, the reactor compartment and the containment, post test melt fractions in all locations with size distribution of the debris, video film in reactor compartment and containment (timing of melt flow and hydrogen burning), and pre- and post test gas analysis in the cavity and in the containment.

2.3.1. DISCO-L1 test

The experiment in the DISCO facility, proposed by IRSN, has been designed to investigate the fluid-dynamic and thermal processes during melt ejection out of a breach in the lower head of a French-type PWR pressure vessel at pressures below 2 MPa with an iron-alumina melt and nitrogen as a driver gas, thus, neglecting the chemical effects such as hydrogen generation and combustion.

The DISCO-L1 experiment was intended to contribute to solve the issue of Direct Containment Heating (DCH) at low RCS pressure in French 1300 MWe reactor plants. This experiment was carried out with nearly an inert atmosphere, thus avoiding hydrogen combustion and focussing on corium dispersion and on containment pressurisation induced by the debris to gas heat exchanges. The experiment has been performed on 4 November 2004. A scientist delegated from IRSN to FZK participated in the evaluation of the results and the preparation of the test report [21].

The reactor pressure vessel in the DISCO-L1 experiment is surrounded by a mostly cylindrical pit which has many three-dimensional elements (
Fig. **39**).

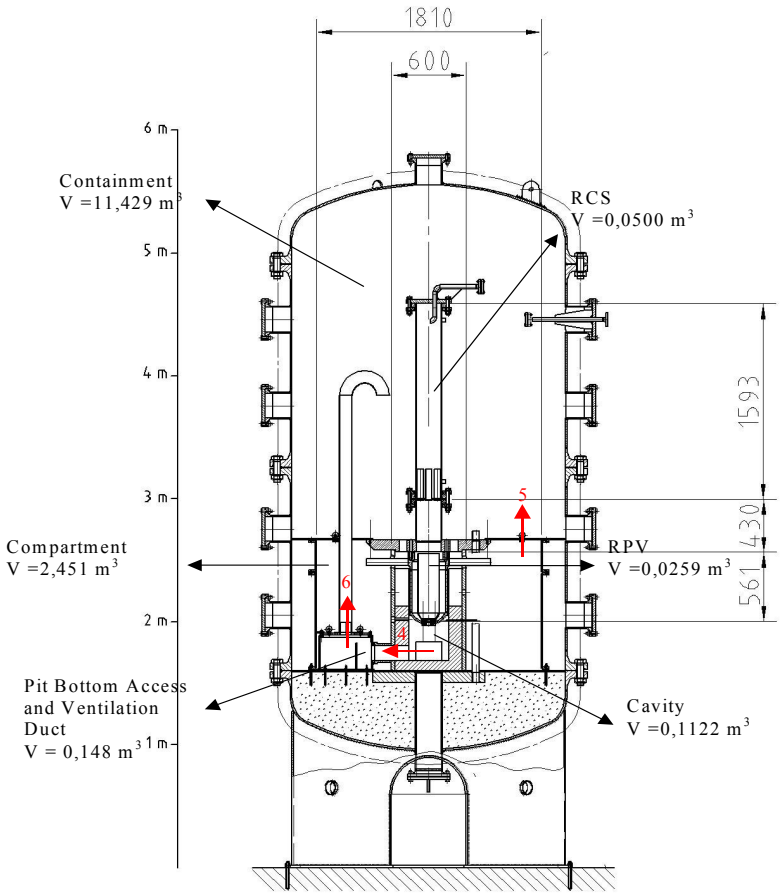

Fig. 39: DISCO facility with internal structures

Among these elements, there is a pit bottom access with a floor level at the same height as the pit bottom. It is vented into the reactor containment. Perpendicular to this a rectangular niche connects the pit bottom to a concrete wall which houses the penetrations of the instrumentation lines leading to the in-core reactor instrumentation.

Above the niche and up to the lower end of the pressure vessel, the pit is surrounded by a cylindrical wall. Further upwards begins a section, where eight rectangular volumes house the flux measurement chambers. These volumes are supposed to be empty. The gap that is formed by the pit around the pressure vessel and the measurement chambers ends up in the pit top annulus which is the pit volume above the vessel support ring. Through this annular space the main cooling lines lead from the vessel into the adjacent sub-compartments. The pit top annulus and the sub-compartments are connected to the containment.

The main differences to the European Pressurised Reactor geometry investigated up to now [16] are (1) the large height between pressure vessel bottom and cavity floor, (2) the direct connection from the reactor pit to the containment, and (3) the three-dimensionality of the cavity.

The initial conditions of the DISCO-L1 experiment are shown in **Table 3**.

Melt mass, kg	10.6
Melt temperature, °C	1930
Breach hole diameter at reactor scale, m	1
RPV pressure at failure, MPa	1.92
Gas composition in RPV	100 % N_2
Containment initial pressure, MPa	0.2
Containment initial temperature, °C	30
Initial gas composition in the containment	97 % N_2 3 % O_2

Table 3: DISCO-L1 initial conditions

The pressure vessel representing the RPV and RCS volumes was electrically heated up to 107 °C. Before the initiation of the experiment, the pressure vessel contained nitrogen at 8.5 bar. The temperature in the upper part was 80 °C and 33 °C in the lower part.

The experiment starts by igniting the thermite electro-chemically at the upper surface of the pressed thermite powder. The increase of temperature and pressure in the RPV-RCS pressure vessel shows that the thermite reaction has started. The thermite reaction progresses until it reaches the bottom of the RPV, 3.7 s after the ignition. At this time, the brass plug at the bottom of the RPV is molten and vaporised by the 1930 °C hot iron-alumina mixture.

At the breach opening, the pressure in the RPV was 19.2 bar. Measured pressures in the main locations are shown in
Fig. **40**. The maximum pressure was 3.3 bar in the containment, 5 bar in the cavity and 3.9 bar in the pit bottom access. However, it is noted, that with presence of H_2 and air in the containment, these pressures could be higher (due to the hydrogen combustion) than in the present experiment carried out in nearly inert conditions.

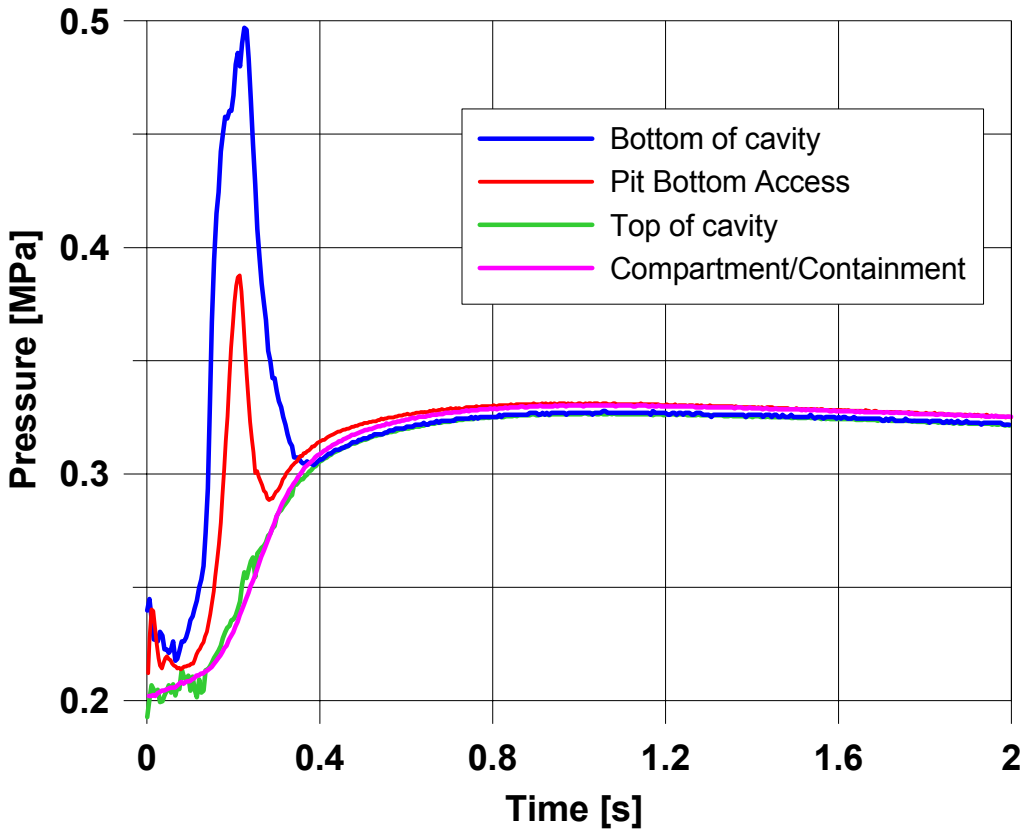

Fig. 40: Pressure transient in DISCO-L1

The temperatures in the RPV increase after the start of the thermite ignition. At the breach opening, the temperature in the RPV is 760 °C and 170 °C in the RCS. Due to the constriction between RCS and RPV, the homogenisation of the temperature is very slow and not achieved at the time of the breach opening. This results in a stratification of the temperature.

The maximum of the average temperature in the containment reached 190 °C. During the first 5 seconds, the temperature in the compartment is higher than in the containment. In the containment, after 3 seconds, the temperatures are approximately homogeneous around 170 °C and after 8 seconds, all temperatures in the containment and in the compartment are nearly equilibrated (
Fig. **41**).

All the surface of the cavity is covered by a film of solidified melt and 60.6 % of the initial mass of melt was ejected out of the cavity: 14.5 % was found in the containment, 28 % in the compartments and 18.1 % in the pit bottom access. In the pit bottom access 1860 g of the melt were located in the annular space, and 93.9 g in the chimney. The most of the melt is deflected to the right by the baffle. The melt separates in two phases: the oxide phase which is lighter is located on the corner in front of the entrance. The heavier and very compact part which is pure iron remains not so far from the entrance. Some melt was also spread in the opposite path (left side of the pit bottom access) where some droplets and dust on the wall, some pieces of pure iron on the floor and a black layer of oxide in the corner can be distinguished.

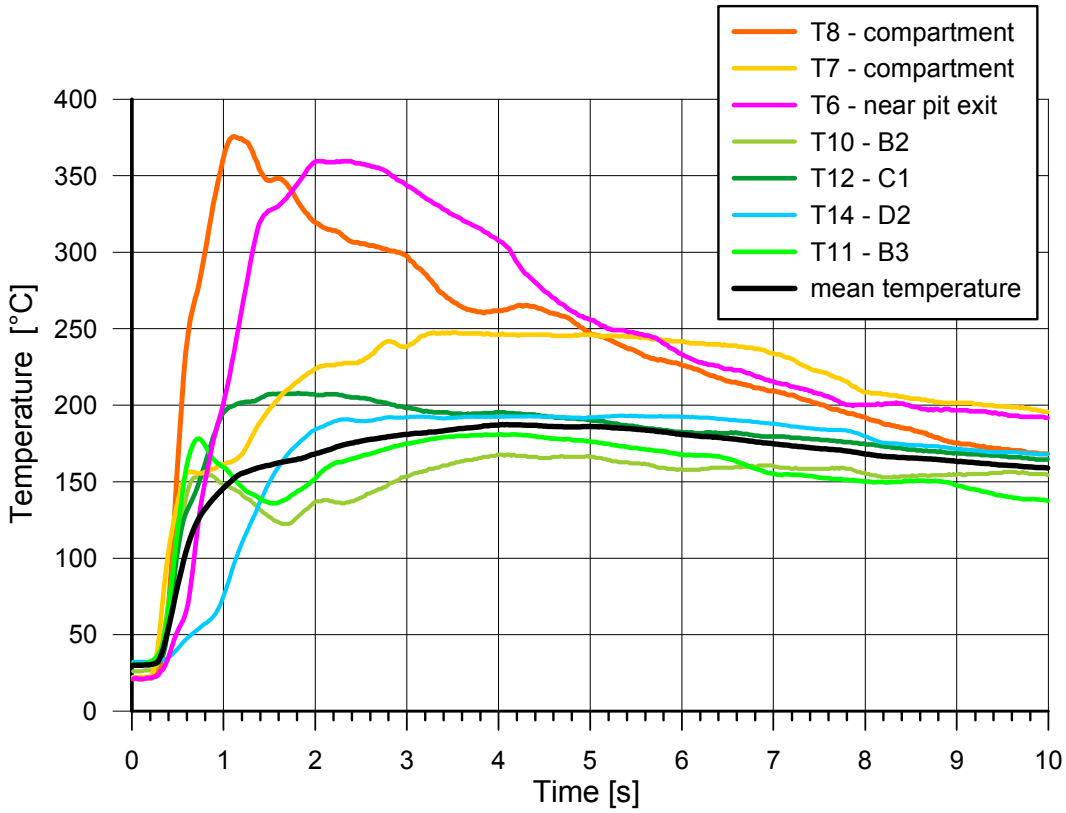

Fig. 41: Containment temperature in DISCO-L1

The compartment is also covered by dust but on the wall in front of each main cooling line, some melt impinged in form of droplets. The melt recovered in the compartment was ejected

from the pit via the cross section around the main cooling lines. The flow of melt diverges at the exit of the pit and impinges on the mounting parts in each side of the cooling lines.

During the blow down, the composition of the gas in the cavity was 20 % H_2, 15.6 % CO, 13.8 % CO_2, 5.8 % O_2 and only 43.6 % N_2. This might be the result of chemical reactions between the melt and the pit concrete or the graphite of the breach. These components are usual products measured during MCCI. Another source for the gas production could be an oxidation reaction with some water from the concrete or from the air. The gas composition in the containment did not change significantly during the experiment, except for a slight increase of H_2 to 0.7%.

2.3.2. DISCO-L2 test

After the third call for proposals, the experiment proposed by TUS in cooperation with the Kozloduy NPP, relating to the Kozloduy VVER-1000 plant, was accepted. The rationale was that the experiment [22] is designed for a reactor geometry, which has not been investigated before, neither in the DISCO facility nor elsewhere. The differences to geometries already investigated are large, and results cannot be extrapolated with the existing knowledge. The application of current models predicts a lower pressure increase in the containment, due to the geometry of the reactor pit. However, experimental data could lead to some necessary changes in modelling and improve the predictive capabilities of codes remarkably. This experiment is included in the Joint Programme of Activities (JPA-2) of the SARNET programme.

The geometry of the reactor cavity and its adjacent sub-compartments of the VVER-1000 plant are shown in **Fig. 42**. The experimental linear scale in DISCO-L2 experiment was 1:15 (**Fig. 43**). The most relevant characteristics of the cavity for DCH are the flow paths out of the lower pit. In a protracted process of clarification with the Kozloduy NPP team the proposer has conveyed the necessary information to the FZK team. There are three flow paths, all with small cross sections, and one potential flow path with a large cross section.

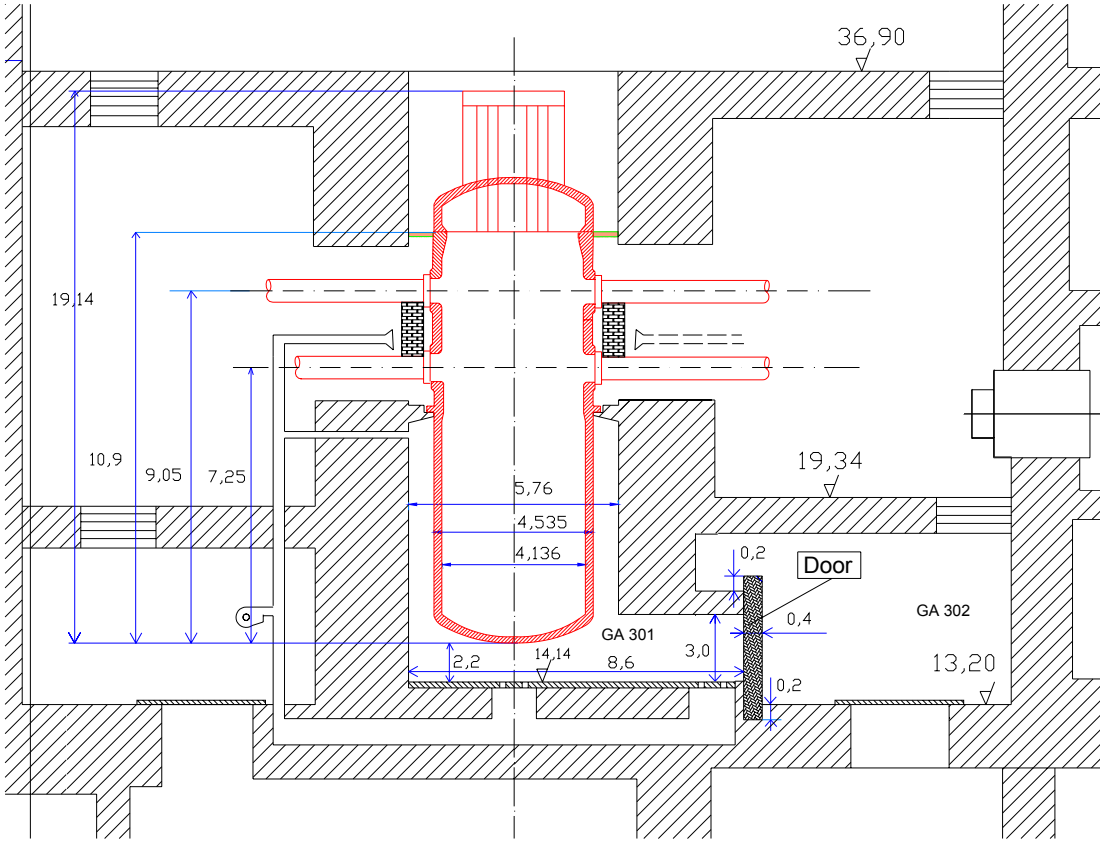

Fig. 42: The reactor cavity, sub-compartments and RPV of the VVER-1000 plant

At the vessel support, there are 30 venting openings with a total cross section of 0.16 m². They are connected to a ring line leading to the adjacent compartment. For the DCH test it is assumed that the venting lines will fail when melt enters the lines, and thereby an additional small flow path will be open to the compartment, provided the melt does not plug the lines. The third flow path is through the venting lines in the pit floor.

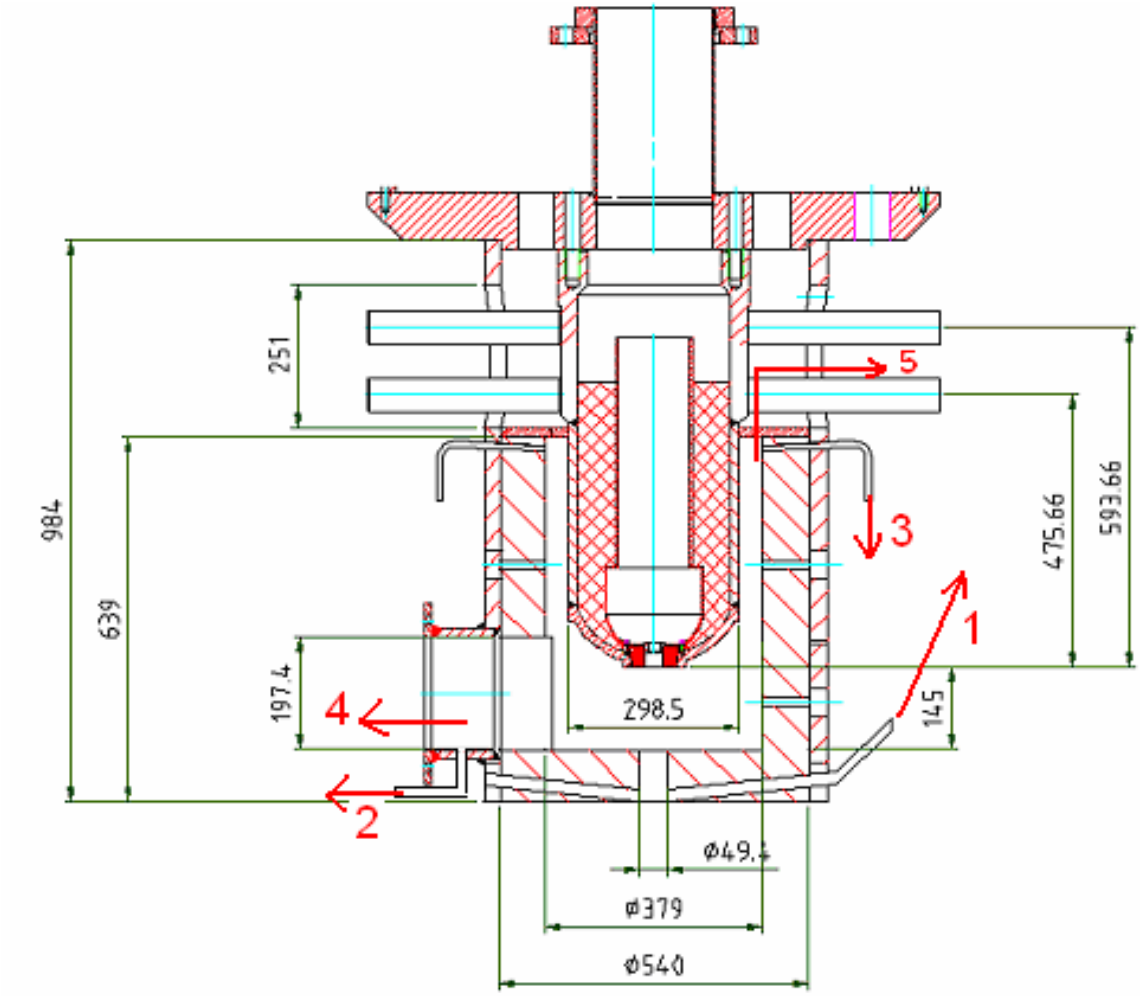

Fig. 43: The reactor cavity and RPV modelled in the DISCO-L2 experiment

The main venting access is at the centre of the pit floor with a diameter of 750 mm that is connected to four venting lines (I.D. 315 mm), which again are connected to a ring line with three exits (I.D. 315 mm) with a total flow cross section of 0.234 m². Another venting line in the pit floor exits close to a door in a pit niche (I.D. 250 mm), that has a cross section of 0.049 m². Both venting access holes are covered by a 5 mm thin perforated steel plate that will fail if melt hits it (scaled 0.33 mm thick).

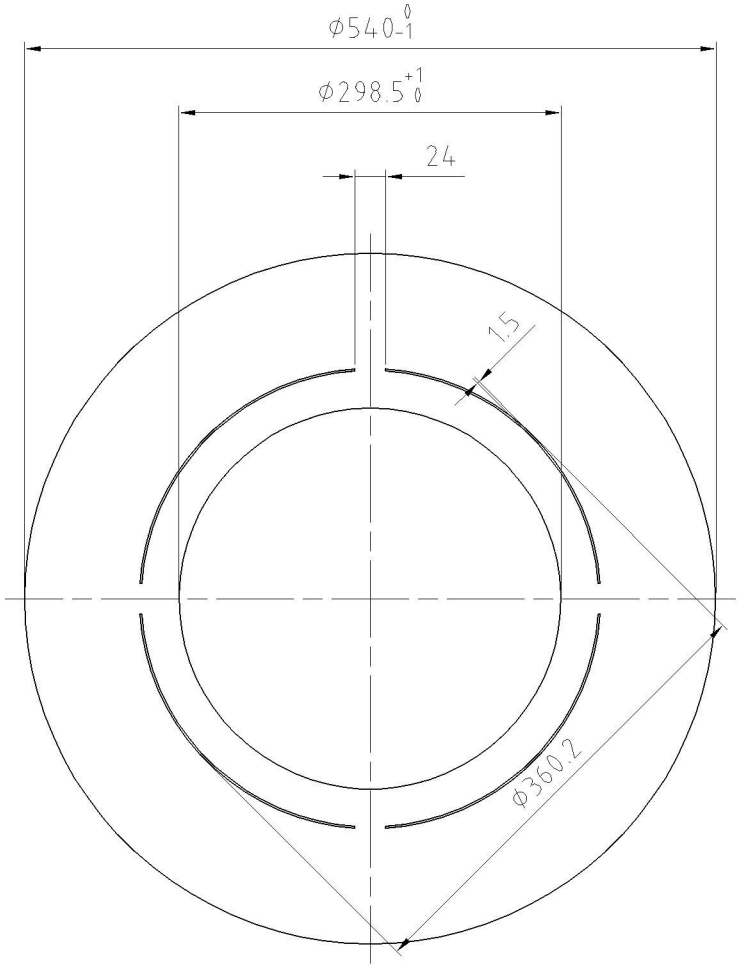

Fig. 44: Model of the small flow-cross section at the vessel support by a steel plate with four narrow slits

The potential large flow path is a door in the pit niche that closes an access to an adjacent sub-compartment that again is open to the containment dome. This door will withstand a differential pressure of 5 bar. If the pressure in the lower pit becomes higher, the door will give way and open a cross section of 5.4 m². If that happens early during blow down, this would be the main path for the melt and steam and for a possible heating and pressurization of the containment atmosphere. Table 4 shows all data and how they are modelled in the DISCO experiment.

	VVER-1000			**DISCO**		
	quantity	diameter [mm]	cross section [m²]	quantity	diameter [mm]	cross section [mm²]
RPV support	1	-	0.3500	-	-	1515
Venting lines at support	30	83	0.1623	16	8.0	804
Pit floor	3	315	0.2338	3	20.7	1010
V. l. Door	1	250	0.0491	1	17.0	229
Door		1.8 x 3.0 m	5.4000		197.4x125	24675
Total			**6.1952**			**28233**

Table 4: Flow path out of the reactor pit

The DISCO-L2 experiment was performed as close as possible to prototypic conditions, but with an iron-alumina thermite melt with initial temperature of approximately 2220 K. The driving gas was steam with some residual nitrogen, and the atmosphere in the containment was a mixture of air and steam at 2 bars with a content of 4 % of hydrogen (41 mole). The breach size at the centre of the lower head was small with a diameter of 16.5 mm (reactor scale 250 mm). The initial conditions of the DISCO-L2 experiment are shown below:

- Breach hole diameter: 16.5 mm (250 mm at reactor scale)
- RPV pressure at failure: 18.55 bar
- Gas composition in RPV: 1.8 mol N_2, 43 mol H_2O (0.778 kg)
- Containment pressure: 0. 216 bar
- Containment temperature: 96 °C (369 K)
- Containment gas composition: 440 mol N_2, 118 mol O_2, 366 mol H_2O, 38 mol H_2, 5 mol Ar (58.3 % air, 37.8 % steam, 3.9 % hydrogen)
- Melt mass: 10.5 kg
- Melt temperature 2300 ± 100 K

At the breach opening the pressure in the RPV was 18.6 bars. Measured pressures in the main locations are shown in

Fig. 45 and

Fig. 46. From the RPV pressure the three stages of the blow-down can be determined. Up to 0.62 s the melt jet is single-phase, up to 1.06 s it is a two-phase melt-steam jet and thereafter it is a pure steam jet. Due to the small breach size, the blow-down lasts 5 seconds, that is 75 seconds at reactor scale.

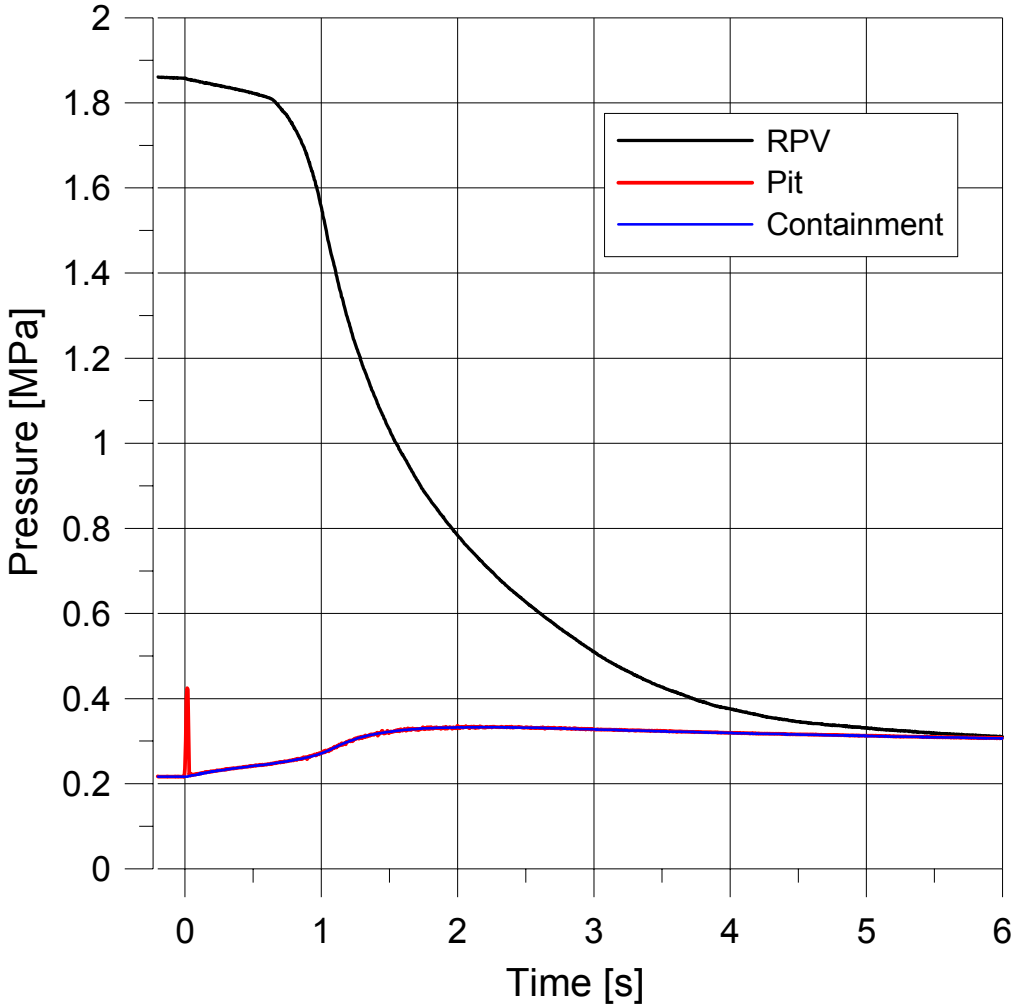

Fig. 45: Pressure histories in the DISCO-L2 test

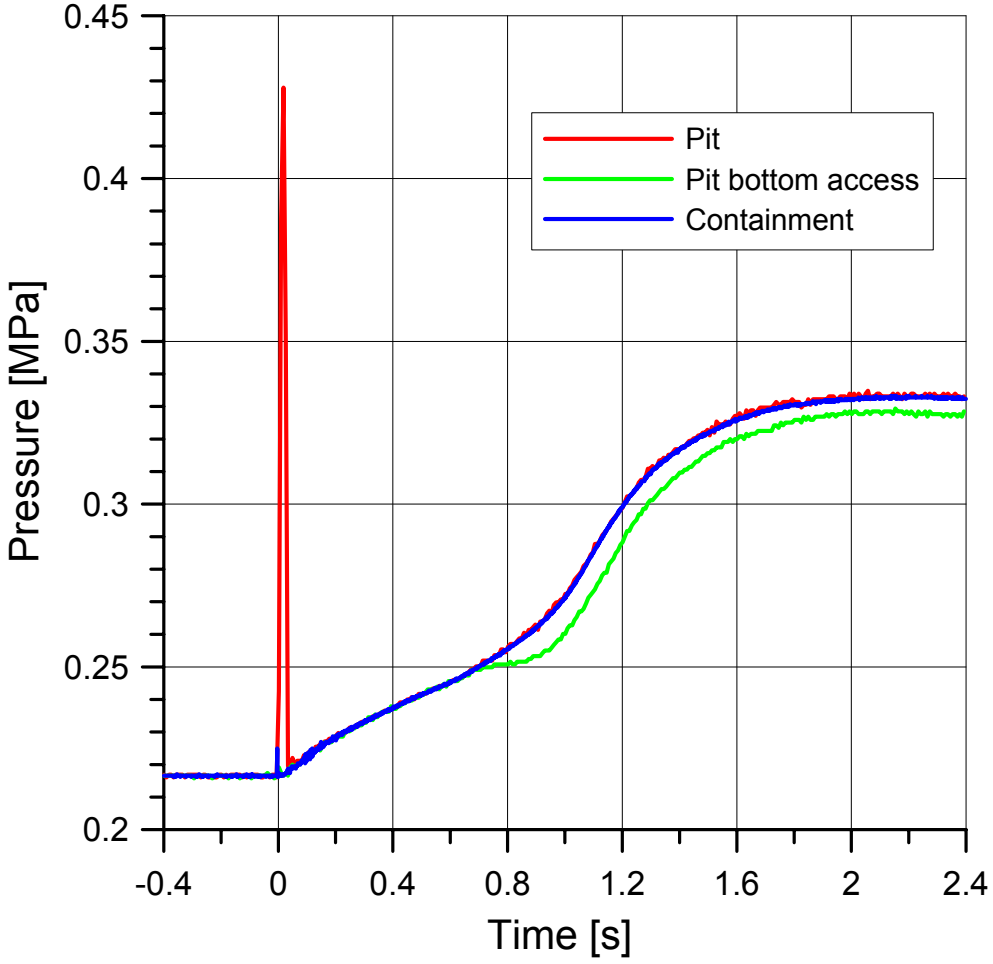

Fig. 46: Pressure in reactor pit and containment measured in DISCO-L2 test

Immediately after the melt has entered the reactor pit the pressure rises to 4.4 bars in the pit, and the door in the corridor opens (
Fig. **46**). With the open flow path into the neighbouring compartment the pressure drops again. All pressures in the pit, the compartment and the containment rise within 2 seconds to a moderate pressure of 3.3 bar. The pressure transducer in the pit bottom access compartment is affected by the high temperature, which is between 700 and 1400 °C in this room. The maximum temperature in the containment reaches only 300 °C after 1.5 seconds and remains at approximately 200 °C for a longer time.

The measured composition of the atmosphere as result of the gas samples taken before and after the test is given in Table 5. It shows that the dry gas atmosphere in the containment and in the sub-compartment before the test was similar, with 6.88 % hydrogen, 18.58 % oxygen and 74.54 % nitrogen.

Table 6 on the other hand shows the initial composition including steam. There are no data from the gas samples for gas composition during the blow down process and from the gas samples in the cavity during the whole experiment, due to some technical problems.

Table 7 shows the hydrogen mass balance in the experiment. The amount of hydrogen, that is produced and burned during the test, is determined by the nitrogen ratio method.

		H_2 (Vol. %)	O_2 (Vol. %)	N_2 (Vol. %)
Pre-test	Containment	6.88	18.58	74.54
	Sub-compartment	6.10	20.06	73.84
Post-test	Containment	6.98	16.68	76.34
	Sub-compartment	0	21.00	79.00

Table 5: Results of the dry gas samples in DISCO-L2

Mol% of hydrogen	%	3.89
Mol% of steam	%	37.80
Mol% of nitrogen	%	45.50
Mol% of oxygen	%	12.25
Mol% of argon	%	0.56

Table 6: Calculated initial gas composition in the DISCO-L2 containment vessel

Initial	H_2 kmol	0.041
Produced	H_2 kmol	0.020
Burned	H_2 kmol	0.025
Fraction burned	H_2 -	0.409

Table 7: DISCO-L2 hydrogen mass balance evaluated from the gas analysis

The result of the debris collecting process is shown in Table 8. The melt particles in the containment are less than 2 %, because the possibility for direct ejection of melts is small in the design of VVER 1000 reactors, as it is displayed in Fig. 43 and in Table 4.

	Mass balance		(kg)
a	Initial thermite mass		10,465
b	Cavity		4,683
c	Sub-compartment		4,122
d	Containment		0,120
e	Total ejected		8,925
f	Remain in RCS and RPV		1,29
g	Total recovered		10,215
	Recovery factor	frec = g/a	0,976
	Melt fractions based on total melt mass		
	Ejected out of RPV	f_{eject} = e/g	0.874
	Remained in cavity	f_{cav} = b/g	0.458
	Dispersed from cavity	f_{disp} = (c + d)/g	0.415
	Transported to sub-compartment	f_{subc} = c/g	0.404
	Transported to containment	f_{cont} = d/g	0.012
	Melt transport fractions based on ejected melt		
	Transported to cavity	f^t_{cav} = b/e	0.525
	Transported to sub-compartment	f^t_{subc} = c/e	0.462
	Transported to containment	f^t_{cont} = d/e	0.013

Table 8: DISCO-L2 debris data

The weight of RPV before the experiment was 207 825 kg, and after melt ejection – 197 360. The difference is the mass of termite blown down. The possibility for spreading the melt from cavity to containment depends on the area of the connection and on its location. The openings of the venting lines differ by their location in the cavity. After the experiment took place, a decrease of the openings was observed (they were filled with melt) according to the melt flux and to its thermo-physical properties.

The venting lines of the cavity were 100 % filled with melt, which lead to closing of the connection of the cavity with the containment and the pressure increased, reaching the level needed for the door to open. The development of DCH phenomenon of VVER1000 depends mostly on the opening of the cavity door. Theoretical, if the cross section of the venting lines does not change during the whole period of the accident, it is possible for the door to stay closed and the measured parameters may reach different values.

More than half the melt remained in the reactor cavity (46 %) and in the RPV (12 %) as crusts, and 40% went through the door into the compartment. Less than 2 % reached the containment as fine dust, with a particle mass median diameter of ~ 0.15 mm. Three quarters of the melt found in the compartment were crusts on the floor and on the wall opposite of the door. The rest had a particle mass median diameter of ~ 2.5 mm.

A post test sieve analysis was performed of the debris that was collected from the sub-compartment and separately from the collected debris from the containment. Out of the 4122 g found in the sub-compartment, only 797 g were small debris, the rest was in the form of

crusts at the walls and the floor. From the containment 99 g were used in the sieve analysis, out of 120 gram total. The remainder stuck to the hoses. The results of the sieve analysis are illustrated in
Fig. 47 and
Fig. 48. The particle size is larger in the sub-compartments than in the containment which is mainly covered by a thin dust. The mass mean diameter of the particles is approximately 0.2 mm in the containment and 2 mm in the sub-compartment.

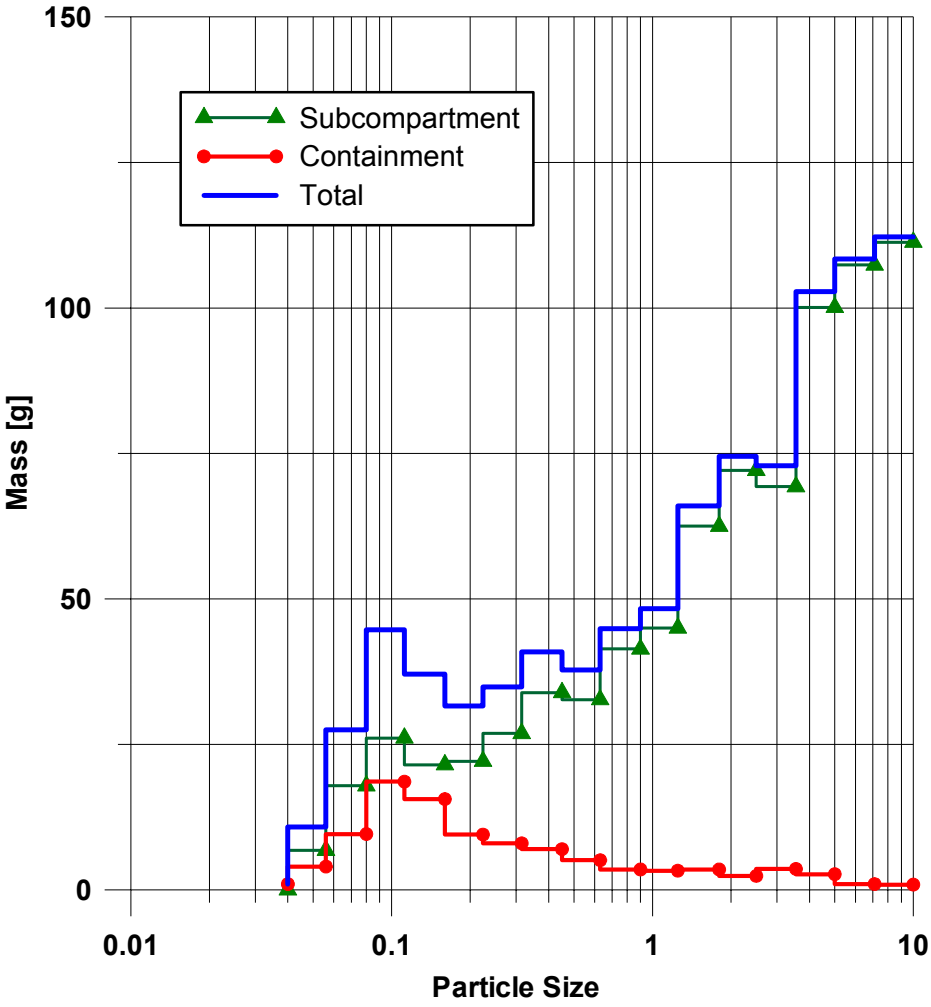

Fig. 47: Particle size distribution in the DISCO-L2 test

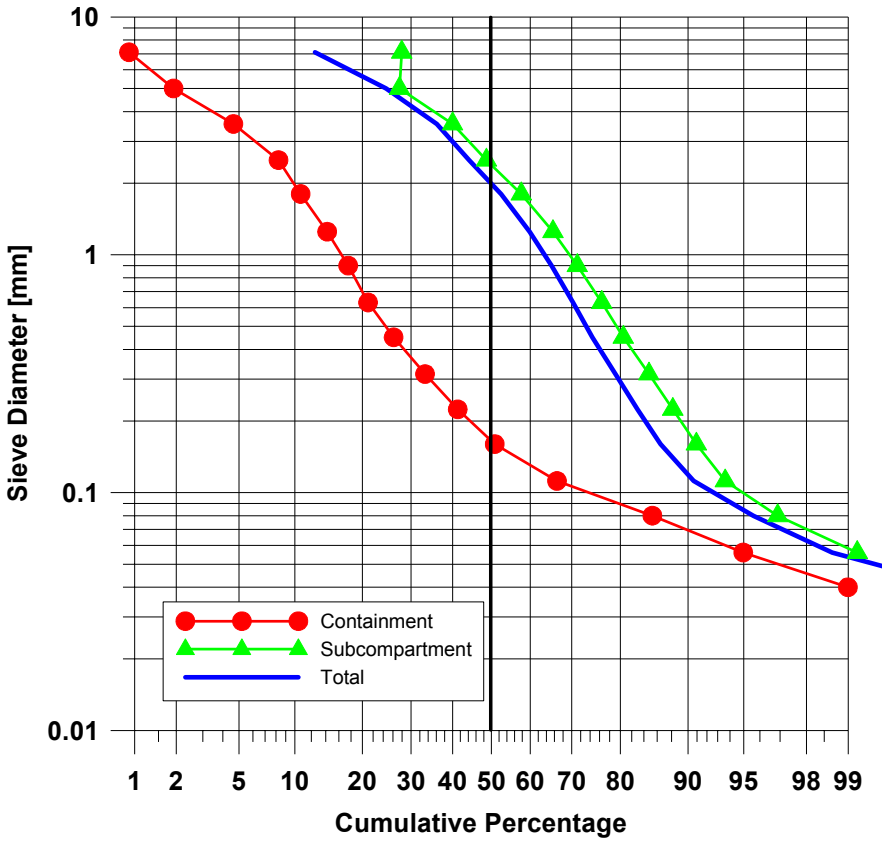

Fig. 48: Cumulative particle size distribution of debris in the DISCO-L2 test

The small amount of finely dispersed melt, especially in the containment, is the reason for the low pressure increase, and also for the small hydrogen production by metal oxidation. Only a fraction of 101 mole of the existing iron was oxidized, with part of 43 mole of blow-down steam. Gas samples, taken pre and post test, have shown that only 20 mole of hydrogen were produced and 25 mole burned, out of a total of 66 mole.

The experimental results show, that for the VVER-1000 reactor the pressure increase due to direct containment heating should not be a problem, because very little melt is finely dispersed and the debris-gas interaction is limited. The venting lines probably become plugged by frozen melt. Because almost all melt will gather in the reactor pit and the neighbouring compartment, corium concrete interaction will take place there.

2.4. WP4: Large-scale Tests on In-vessel Melt Relocation and Retention (LIVE)

The LIVE experimental facility (**Fig. 51**) is designed to study the late phase of core degradation, onset of melting and the formation and stability of melt pools in the RPV. Additionally, the regaining of cooling and melt stabilisation in the RPV by flooding the outer RPV or by internal water supply will be investigated. Steady state behaviour of debris and of molten pools in the lower head has been already investigated in several experimental studies (see also [23] and [24]). However, the database for the transient processes during core melting, melt relocation and accumulation is still very limited. For the melt released into the lower head of the vessel, there is a lack of information about e.g. transient heat fluxes to the vessel wall, crust formation, stability and re-melting of melt crusts, as may occur from melt release to steady state and under 3-d geometrical situations. An improved understanding of

these processes can help to define accident management procedures for accident control in present reactors.

The LIVE programme [25] is divided into three different phases. In the first phase (LIVE1) the investigations will concentrate on the behaviour of a molten pool, as it is poured into the lower head of the RPV, and take into account transient and possible 3-d effects, **Fig. 49**. The melt pool can consist of an oxide melt or both oxide and metal melts to simulate the components of a real corium melt. The melt masses and the conditions outside the test vessel can be varied to simulate different accident scenarios. Important phenomena, which are investigated, are:

- time dependent local heat flux distribution to the lower head,
- possible crust formation of the melt depending on the power density and the external cooling modes,
- gap formation between the RPV wall and the melt crust,
- role of phase segregation of a non-eutectic melt on the solidification behaviour.

In LIVE 2, pool formation and behaviour will be studied under the conditions of multiple pours of melt from the core region. The presence of water in the lower vessel head is an option for further studies, **Fig. 50**. The simulant melt can be pure oxidic or can be an oxide melt and a metal melt. The melt release can be in subsequent pours and at different positions (central and/or non-central). The phenomena, which will be investigated, are similar to LIVE 1.

The third phase (LIVE 3) will start with a simulated in-core corium pool. Main emphasis is on the stability of such melt pools during different cooling modes and subsequent relocation processes at crust failure.

Important phenomena to be investigated are crust growth around the pool, stability and failure modes of the crust, the release rates and flow paths of the melt from the in-core-melt pool, the accumulation of the released melt in the lower head and its coolability and finally necessary conditions to stabilise the melt pool in the core region.

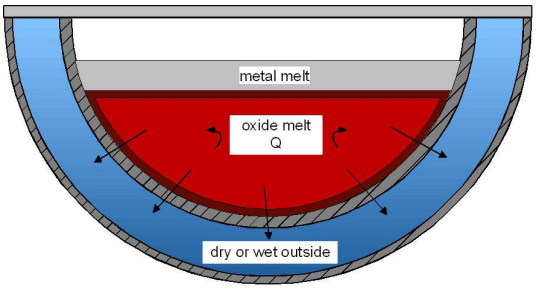

Fig. 49: Melt retention in the lower head (LIVE 1)

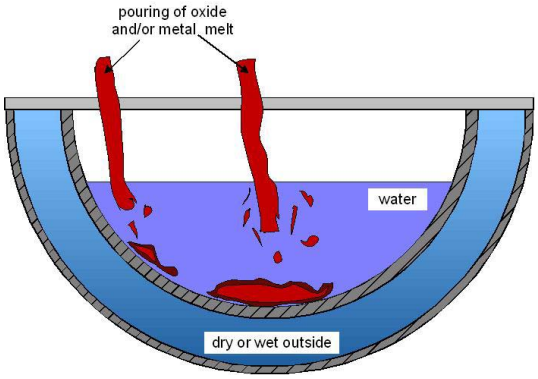

Fig. 50: Melt relocation to the lower head (LIVE 2)

The core of the LIVE test facility is a 1:5-scaled RPV of a typical pressurised water reactor (**Fig. 51**). For the first and second phase of the experiments (LIVE 1 and LIVE 2), only the hemispherical bottom of the RPV will be used. The inner diameter of the test vessel is 1 m and the wall thickness is 25 mm. The material of the test vessel is stainless steel. To investigate the transient as well as the steady state behaviour of the simulated core melt, an extensive instrumentation of the test vessel is realised, **Fig. 52**.

Fig. 51: LIVE test vessel

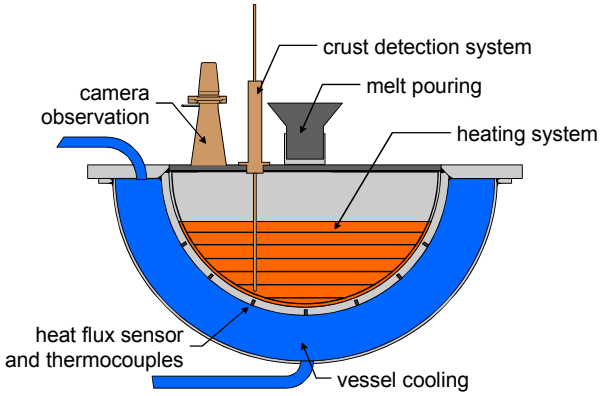

Fig. 52: Diagram of the LIVE test facility

The vessel wall is equipped with 17 instrumented plugs (**Fig. 53**) at different positions along 4 axes. Each plug consists of a heat flux sensor and 5 thermocouples. The thermocouples are protruding into the melt with different distances from the vessel wall (0, 5, 10, 15, 20 mm). The heat flux sensor is part of the vessel wall and is situated 1 mm below the inner surface of the test vessel. This sensor measures the heat flux and the corresponding temperature. To measure the temperature at the outer surface of the vessel wall, 17 thermocouples are located at different positions along 4 axes. In addition to the 85 thermocouples of the plugs, it is possible to place up to 80 thermocouples in the melt to measure the temperatures of melt and the crust growth.

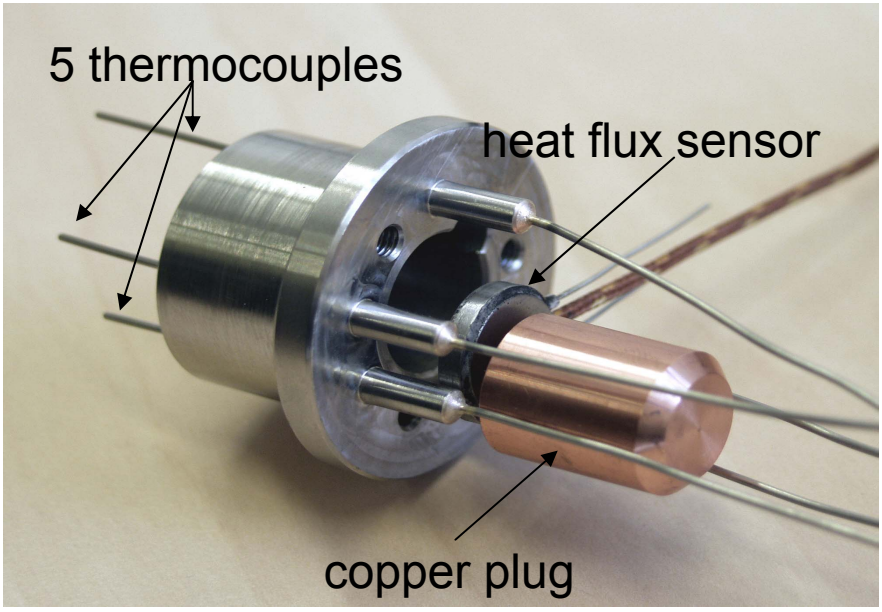

Fig. 53: LIVE instrumentation plug

The instrumentation of the test vessel includes also an infrared camera and a video camera to observe the melt surface, weighing cells to detect quantitatively the melt relocation process, and mechanical sensors to detect the melt crust thickness at the wall.

Decay power input into the melt is recorded and melt samples are extracted during the tests. Different openings in the upper lid of the test vessel allow pouring of the melt to the central region or close to the perimeter of the lower head. To be able to investigate the crusts, which are formed at the wall of the vessel, the residual melt is sucked out of the vessel at the end of the test.

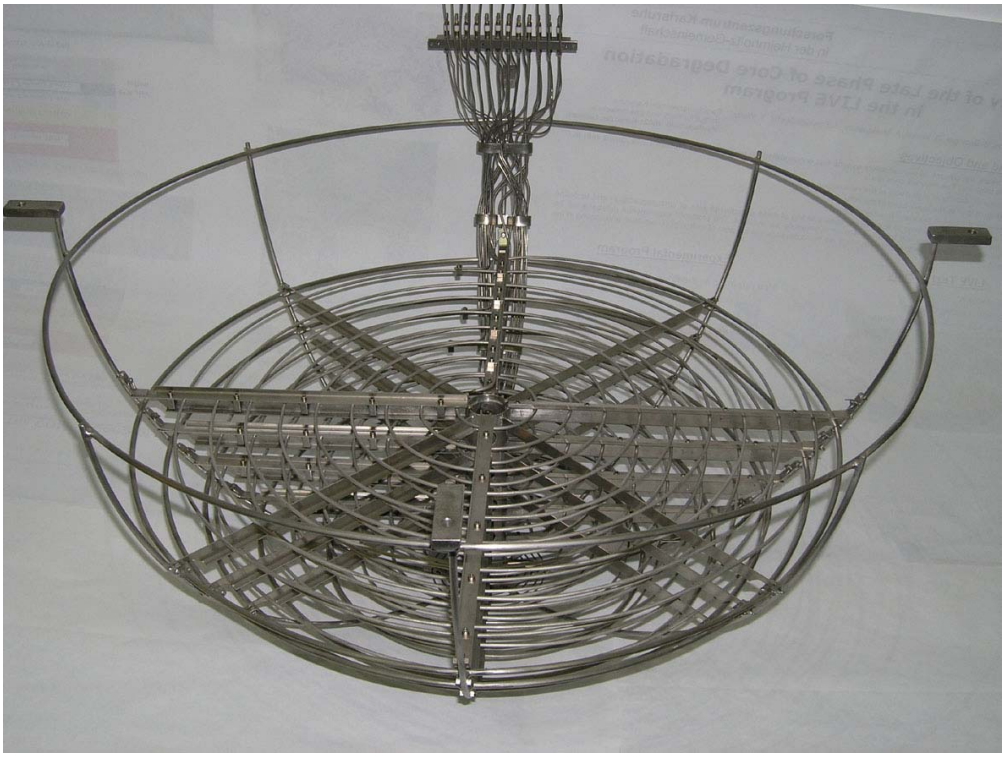

Fig. 54: LIVE volumetric heating system

To investigate the influence of different external cooling conditions on the melt pool behaviour, the test vessel is enclosed by a second vessel (cooling vessel) to be able to cool the test vessel at the outside by a cooling medium. The cooling medium is introduced at the bottom of the cooling vessel and leaves the vessel at the top.

The volumetric heating system (**Fig. 54**) has to simulate the decay heat released from the corium melt. Consequently, the heating system has to produce the heat in the simulant melt as homogeneously as possible. Therefore a heater grid with several independent heating elements was constructed. The heating elements are shrouded electrical resistance wires. The maximum temperature of the heating system is 1100 °C. The heating system consists of 6 heating planes at different elevations with a distance of about 45 mm. Each heating plane consists of a spirally formed heating element with a distance of ~ 40 mm between each winding. The heating elements are located in a special cage to ensure the correct position. All heating planes together can provide a power of about 28 kW. To realise a homogeneous heating of the melt, each plane can be controlled separately.

Fig. 55: LIVE furnace

To allow transient pouring of the melt into the test vessel, the melt is produced in a separate heating furnace (**Fig. 55**). The capability of this tilting furnace is 220 l volume. Therefore it is possible to produce the total amount of the scaled oxide melt mass and additionally the total amount of the scaled metallic part of the simulated corium melt. The maximum temperature of the heating furnace is 1100 °C. When the melt has reached the desired pouring temperature, the furnace is tilted and the melt is discharged with a specified pouring rate into the test vessel via a heated pouring spout. In addition, the heating furnace is equipped with a vacuum pump; so it is possible to suck the residual melt out of the test vessel back into the heating furnace.

Simulant materials should represent the real core materials in important physical properties and in thermo-dynamic and thermo-hydraulic behaviour as good as possible. Therefore, the applicability of several binary melt compositions as a simulant for the oxidic part of the corium has been checked.

Important criteria for the selection are that the simulant melt should be a non-eutectic mixture of several components with a distinctive solidus-liquidus area of about 100 K, and that the simulant melt should have a similar solidification and crust formation behaviour as the oxidic corium. Moreover, the simulant melt should not be toxic and aggressive against steel and vessel instrumentation. And finally, the temperature range of the simulant melt should not exceed 1000 °C distinctively because of the technical handling and the selection of the volumetric heating system and the heating furnace.

For the first series of experiments a binary mixture of sodium nitrate $NaNO_3$ and potassium nitrate KNO_3 was chosen, **Fig. 56**. The eutectic composition of this melt is 50-50 Mol% and

the eutectic temperature is 225 °C. The maximum temperature range between solidus and liquidus is ~ 60 K for a 20-80 Mol% $NaNO_3$-KNO_3 mixture. This melt can be used in a temperature range from 220 to 380 °C. Due to its solubility for water the applicability of this melt is restricted to dry conditions inside the test vessel.

For experiments, in which phenomena in the lower head are investigated under presence of water, another simulant melt has to be selected. Therefore several binary oxide melts, which are insoluble in water, have been investigated with respect to their applicability for simulant tests. In the temperature range between 800 and 1000 °C only a few oxides can be considered. These are the oxides MoO_3 and TeO_2 with melting temperatures between 700 and 800 °C and the oxide V_2O_5 with a melting temperature of about 660 °C. The investigations showed that MoO_3 starts to sublimate already at about 700 °C and is really aggressive against all types of steel. Both MoO_3 and TeO_2 show a pronounced increase of their vapour pressure with increasing temperature and are therefore not applicable. As V_2O_5 did not show this behaviour, this oxide was chosen as one of the melt constituents. Three binary mixtures with V_2O_5 have been found and were successfully tested with respect to their compatibility with steel: V_2O_5 with CuO, V_2O_5 with ZnO, and V_2O_5 with MgO. In **Fig. 57** the phase diagram of the mixture V_2O_5-ZnO is shown. The eutectic temperature of this mixture is 625 °C.

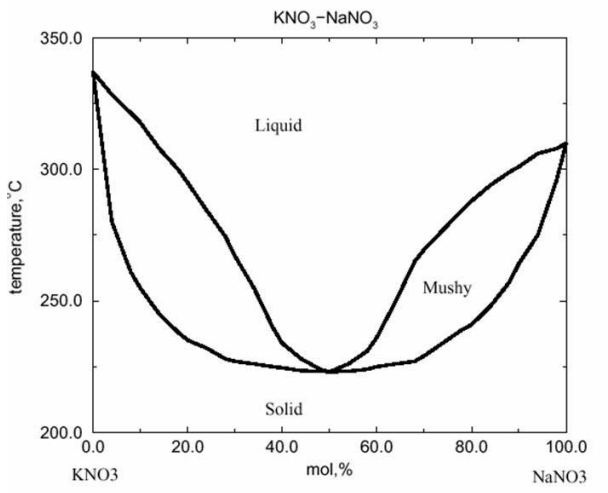

Fig. 56: Phase diagram of the melt KNO_3-$NaNo_3$

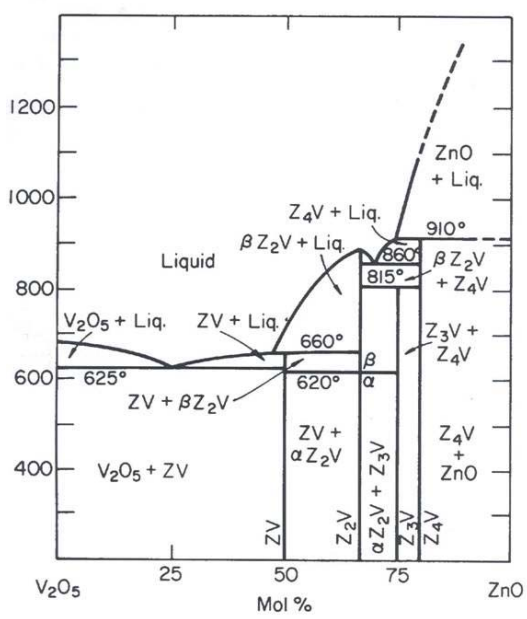

Fig. 57: Phase diagram of the melt V_2O_5-ZnO

Two experiments have been performed in the LIVE facility:

2.4.1. LIVE-L1 test

The experiment LIVE-L1 was dedicated to investigate the core-melt behaviour in the lower plenum of the reactor pressure vessel and the influence of the cooling of the vessel outer surface with water in the conditions that may occur during core-meltdown accident in the WWER-1000 plant. The test was proposed by TUS Sofia, Bulgaria and was successfully conducted on 22 June 2006. Test initial conditions and main parameters are summarised in **Table 9**.

To simulate the corium melt a binary mixture of 20 mole% of $NaNO_3$ and 80 mole% of KNO_3 with liquidus temperature of ~ 300 °C and solidification range of about 80 K has been used

(see also **Fig. 56**). The mixture has been melted in the separate heating furnace and when the temperature reached ~ 350 °C, 120 l of the melt has been centrally poured into the LIVE test vessel through the pouring spout preheated up to ~ 350 °C. Melt release rate and melt initial temperature are shown in
Fig. 58 and
Fig. 59. Maximum pouring rate derived from the analysis of the vessel weight was ~ 7 kg/s.

Melt characteristics		
Type	$NaNO_3$	KNO_3
Mole%	20	80
Mass%	17.37	82.63
Mass	58 kg	278 kg
Total mass	336 kg	
Furnace load	~ 390 l powder (at T = 20 °C)	
	~ 180 l melt (at T = 350 °C)	
Pouring mass	120 l (corresponds to ~ 31 cm melt height)	
Initial temperature	350 °C	
N_2 flow rate	20 l/min	
Melt pour		
Position	central	
Number of pours	1	
Furnace tilting velocity	0.5°/s	
Furnace target angle	80°	
Hold time	50 s	
Pouring spout temperature	350 °C	
Phase 1. Homogeneous heat generation (0-3724 s)		
Boundary conditions	air	
Heating planes	all	
Heating power	18 kW at the beginning, reduction to 10 kW	
Maximum melt temperature	350 °C	
Phase 2. Start of the outer vessel wall cooling (7230 s)		
Boundary conditions	water, continuous cooling	
Cooling water flow rate	~ 45 g/s	
Heating planes	all	
Heating power	10 kW	
Heat generation	homogeneous	
Phase 3. Reduction of heat generation (82675 s)		
Boundary conditions	water, continuous cooling	
Cooling water flow rate	~ 45 g/s	
Heating planes	all	
Heating power	7 kW	
Heat generation	homogeneous	
Phase 4. Test termination and melt extraction (102606 s)		
Test conditions	Reach of steady-state conditions in phase 3	
Heating power	0 kW	

Table 9: Main parameters and test phases of the LIVE-L1 experiment

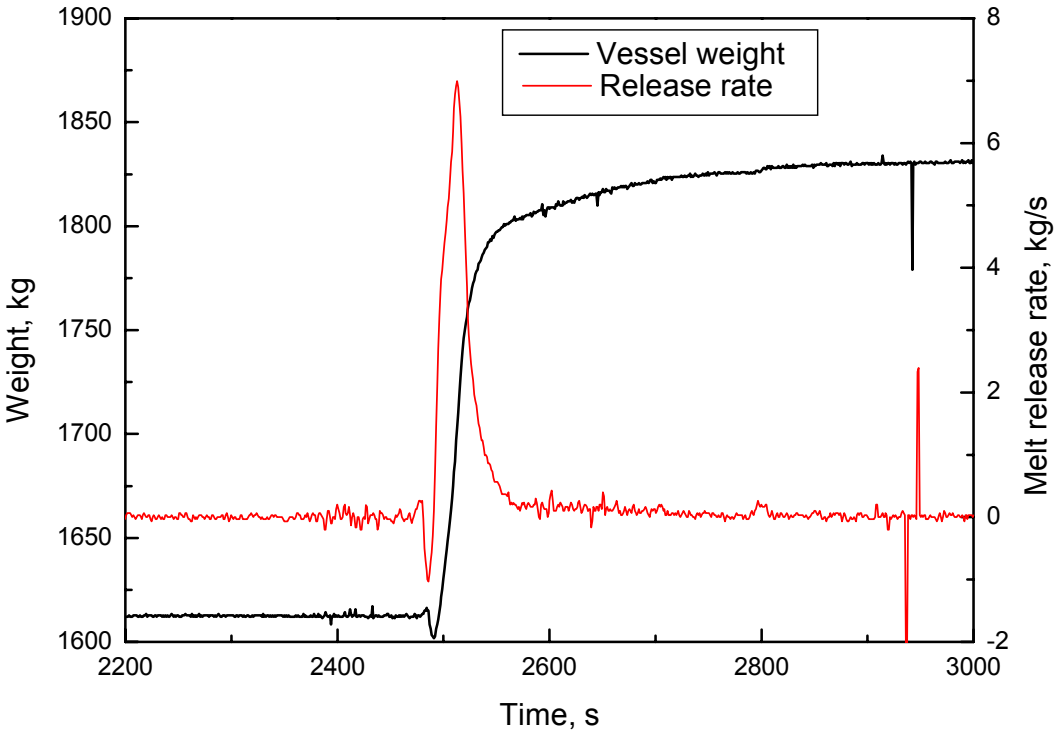

Fig. 58: LIVE-L1: melt release rate

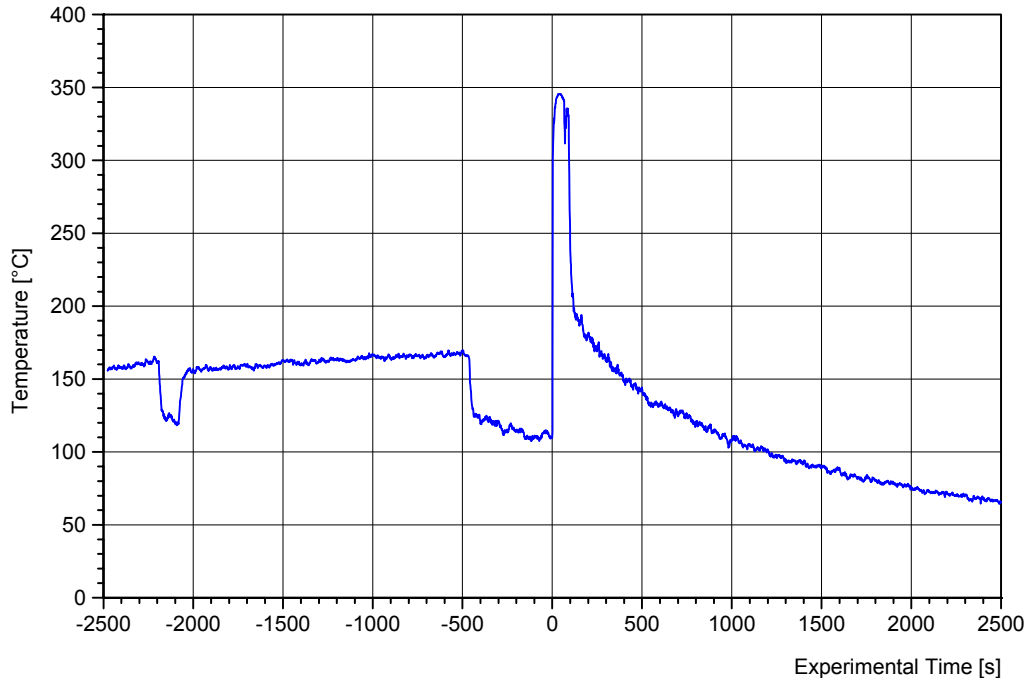

Fig. 59: LIVE-L1: initial melt temperature measured in the pouring spout

After the completion of the pouring process a heating power of ca. 18 kW was applied to homogeneously heat the melt by switching all six heating planes simultaneously. The heating power distribution is shown in **Fig. 60**. The distortions at the levels 1 and 2 located at the upper part of the melt pool are due to the automatic switch-off of the power when the heater temperatures exceed 380 °C in order to protect the melt from the overheating.

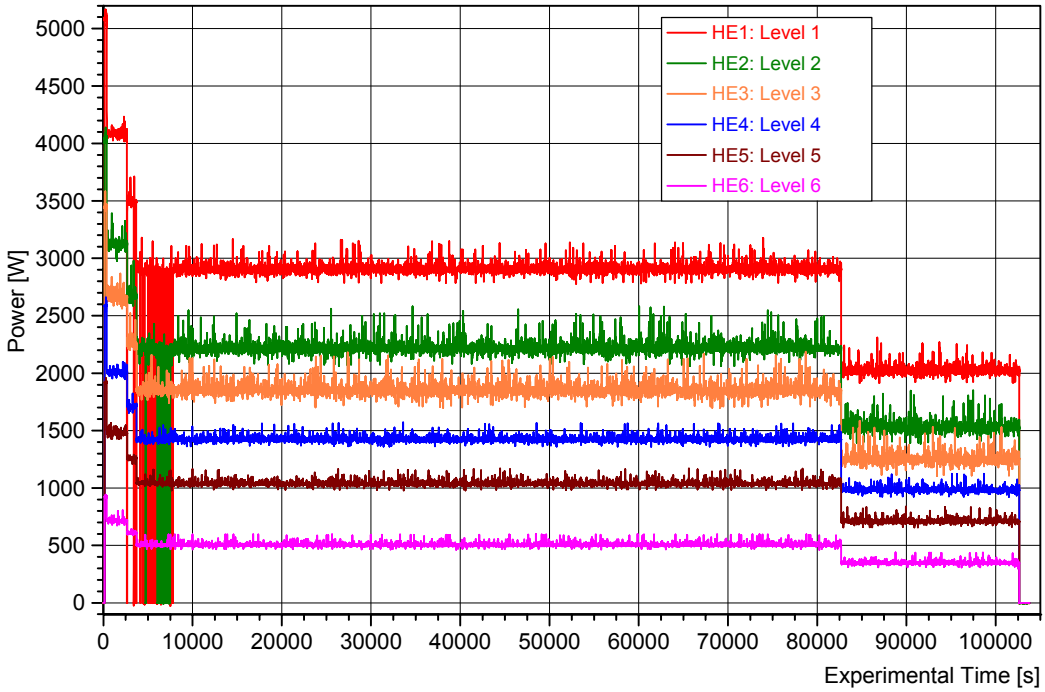

Fig. 60: LIVE-L1: heating power distribution between the heating planes

The melt temperatures measured inside the melt pool indicated that directly after the melt pour the pool temperature decreased to ~ 300 °C at the bottom of the test vessel and to ~ 330 °C near the melt surface. After the start of heating the maximum melt temperatures started to increase. To avoid the overheating of the melt the power was stepwise reduce to ~ 10 kW within 6200 s and was kept at this level. During this time, the maximum melt temperatures increased up to ~ 370 °C (**Fig. 61**).

Flooding of the outer vessel wall was started at 9700 s first with 1.5 kg/s to fill the gap between the cooling vessel and the test vessel wall and then with ~ 47 g/s (**Fig. 62**). This flow rate has been kept constant throughout the whole experiment. Water temperature at the inlet amounted to ~ 10 °C.

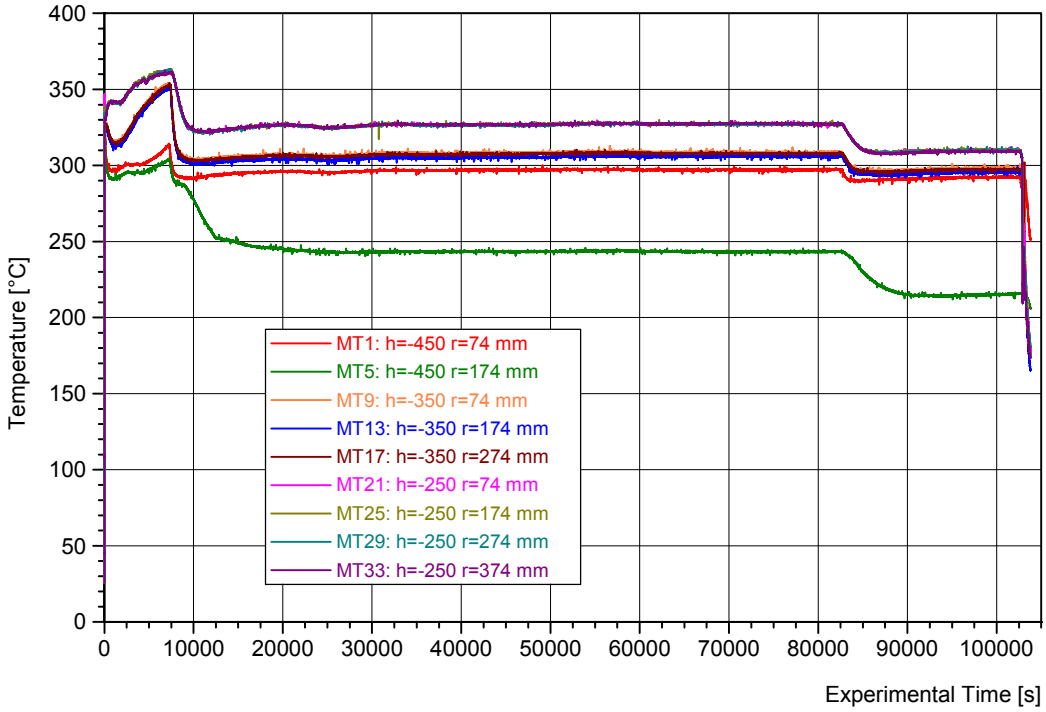

Fig. 61: LIVE-L1: melt temperatures

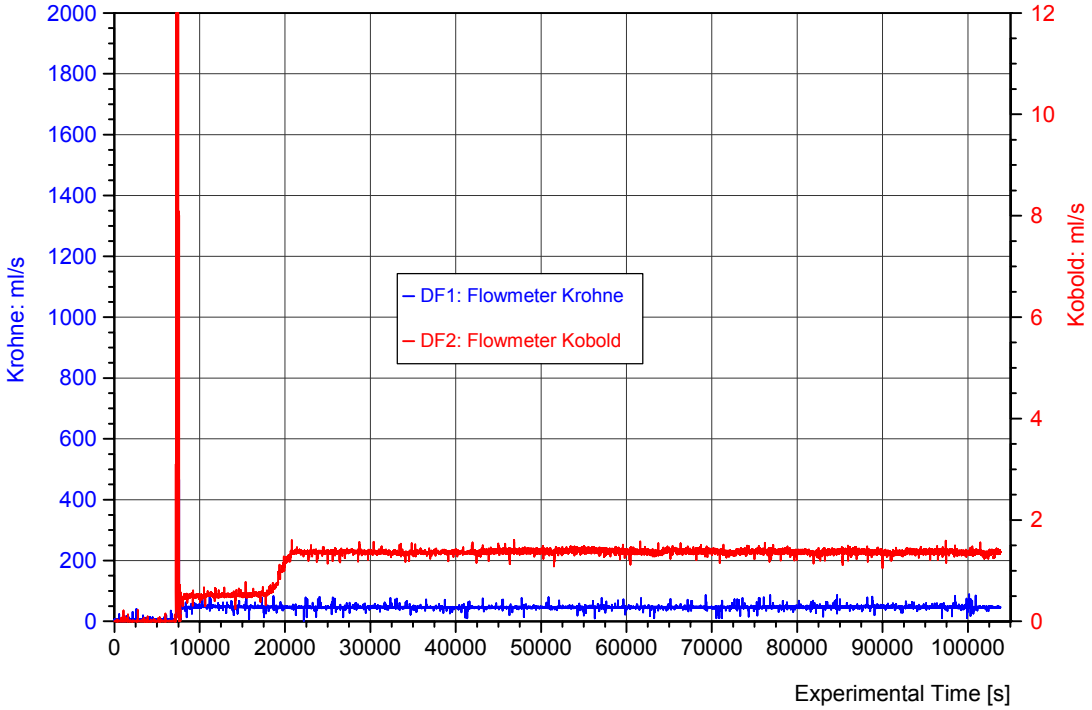

Fig. 62: LIVE-L1: mass flow rate of cooling water

After the cooling initiation the maximum melt temperatures at the upper part of the melt pool decreased to ~ 320 °C (**Fig. 61**). At the inner surface of the vessel wall the crust started to form and continued to grow which was clearly detected by the infrared camera installed at the vessel lid (blue stripe adjacent to the vessel wall in **Fig. 63**).

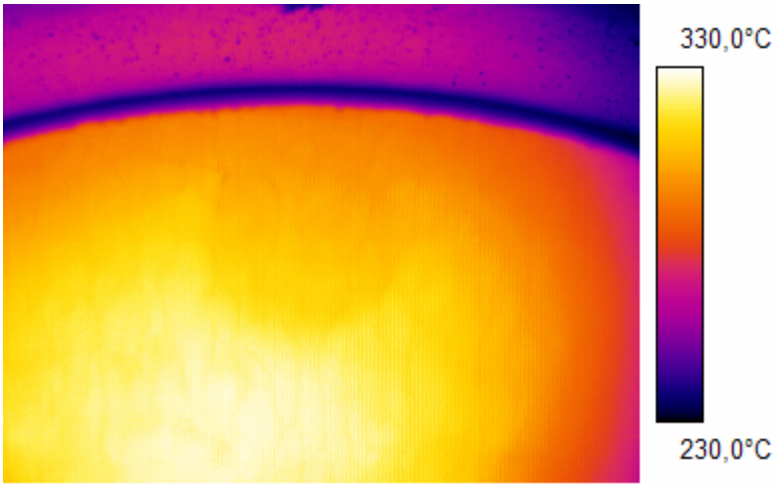

Fig. 63: LIVE-L1: thermogram of the melt surface

The homogeneous heating of the melt with ~10 kW was continued for about 20 hours to reach the steady state conditions. Afterwards the heating power was reduced to 7 kW to observe the influence of the power reduction on the crust growth and heat flux distribution and kept at this level for another 6 hours. During this phase the maximum melt temperature decreased to ~ 300 °C.

In LIVE-L1 only one half-axis of the hemispherical test vessel was equipped with the instrumentation plugs, which allowed to measure non-stationary heat fluxes through the vessel wall. The results of heat flux measurements are presented in **Fig. 64**. The measurements clearly show two peaks: one after the melt pouring and another one after the start of the outer vessel wall cooling. The maximum heat flux of ~ 30 kW/m^2 was measured during the vessel cooling by the heat flux sensor HF10 located just below the melt surface. In the steady-state phase, the value of the maximum heat flux through the vessel wall has been decreased to ~ 10 kW/m^2.

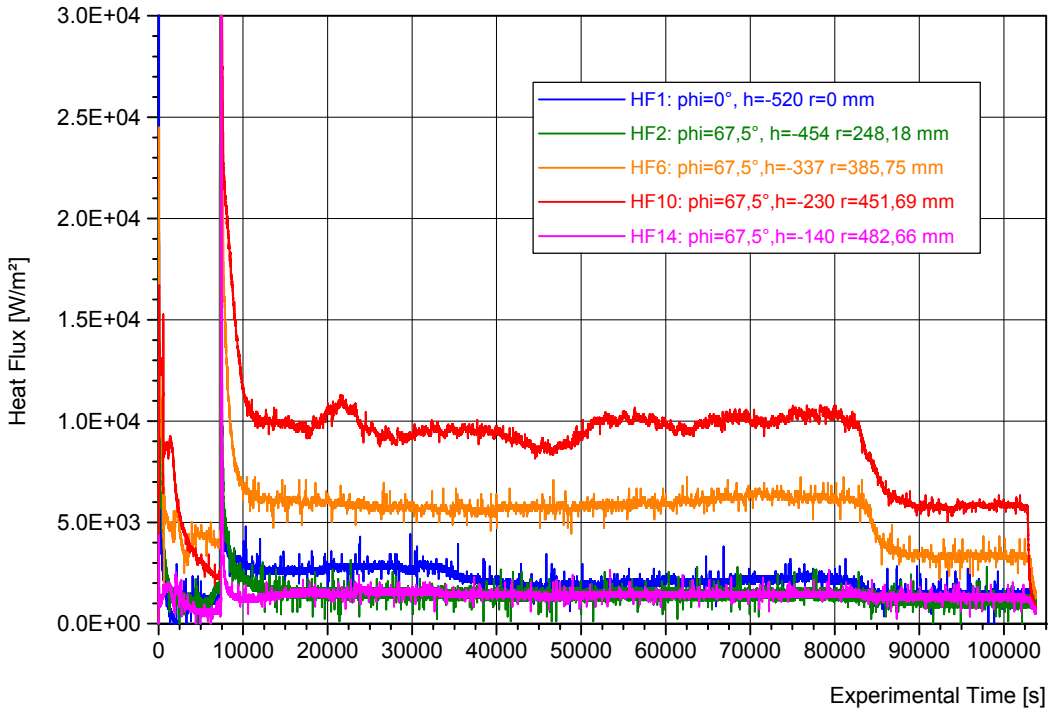

Fig. 64: Heat fluxes measured at different positions in the LIVE-L1 test

The experiment was completed by switching off the volumetric heating and by the extraction of the liquid melt back into the heating furnace to uncover the crusts formed during the test (**Fig. 65**).

Fig. 65: Crust formed during the LIVE-L1 test

The measurements of the crust thickness along the vessel wall are presented in **Fig. 66**. They show that the crust thickness varies between 11.7 mm at the position near to the melt surface and ~ 70.7 mm at the bottom of the test vessel.

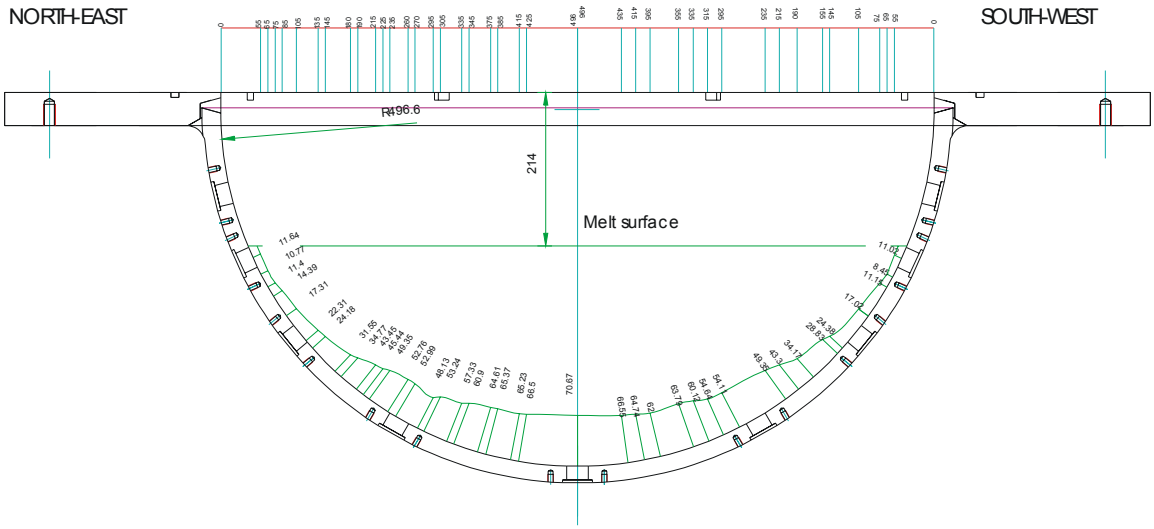

Fig. 66: Crust thickness profile measured in the LIVE-L1 test

During the test, two melt samples have been extracted from the melt pool, one at the beginning of the test and another one at the end just before the melt extraction from the test vessel. The analysis of the samples is important in two aspects: 1) comparison of the real melt composition with the composition planned for the test, and 2) evaluation of the changes in the melt composition caused by the crust formation and depletion of the high temperature melt component KNO_3. The results of the chemical analysis of the extracted melt samples are presented in Table 10. They clearly demonstrate that the real composition was very close to the planned one and that the initial KNO_3 fraction was reduced by ~ 1.7 mole-% during the experiment, as expected. This observation is in a good agreement with the post-test chemical analysis of the crust performed at two locations (Table 11), which indicated that the amount of KNO_3 in the crust has been increased to ~ 91 mole-% compared to initial value of 80 mole-%.

	Planned	**Before the test** (sample L1-M1)	**After the test** (sample L1-M2)
K [w%]	31.954	30.597	28.102
Na [w%]	4.697	4.511	4.584
Na/K [weight/weight]	0.14699	0.14742	0.16312
K [mole%]	80.0	79.954	78.283
Na [mole%]	20.0	20.046	21.717
Na/K [mole/mole]	0.25	0.25071	0.27741
KNO_3 [w%]	82.635	82.594	81.091
$NaNO_3$ [w%]	17.365	17.406	18.909

Table 10: Melt composition measured in LIVE-L1 experiment

	Before the test (sample L1-M1)	**After the test** (sample L1-M2)	**Crust** (sample L1-C1)	**Crust** (sample L1-C2)
K [w%]	30.597	28.102	38.883	37.960
Na [w%]	4.511	4.584	2.118	2.114
Na/K [w/w]	0.14742	0.16312	0.05447	0.05569
K [mole %]	79.954	78.283	91.522	91.349
Na [mole %]	20.046	21.717	8.478	8.651
Na/K [mol/mol]	0.25071	0.27741	0.09263	0.09470
KNO_3 [w%]	82.594	81.091	92.776	92.627
$NaNO_3$ [w%]	17.406	18.909	7.224	7.373

Table 11: Crust composition measured in LIVE-L1 experiment

2.4.2. LIVE-L2 test

The experiment LIVE-L2 was dedicated to investigate the transient melt spreading along the RPV lower head wall, the shape of the final melt pool and its impact on the steady-state heat fluxes in the conditions that may occur during core-meltdown accident in LWRs. The test was

proposed jointly by IRSN and CEA, France, and was successfully conducted on 28 August 2006. Initial test conditions and main parameters are summarised in Table 12.

Upper crust (non-symmetric melt release into the test vessel)		
Type	$NaNO_3$	KNO_3
Mole %	20	80
Thickness	~ 2 cm	
Gap to the vessel wall	~ 0.5 cm	
Location	upper heating plane	
Melt characteristics		
Type	$NaNO_3$	KNO_3
Mole %	20	80
Mass %	17.37	82.63
Mass	58 kg	278 kg
Total mass	336 kg	
Furnace load	~ 390 l powder (at T = 20 °C)	
	~ 180 l melt (at T = 350 °C)	
Pouring mass	120 l (corresponds to ~ 31 cm melt height)	
Initial temperature	350 °C	
N_2 flow rate	20 l/min	
Melt pour		
Position	near to the vessel wall	
Number of pours	1	
Furnace tilting velocity	0.5°/s	
Furnace target angle	80°	
Hold time	50 s	
Pouring spout temperature	350 °C	
Phase 1: Homogeneous heat generation with continuous outer vessel wall cooling		
Boundary conditions	water, continuous cooling	
Cooling water flow rate	~ 45 g/s	
Heating planes	all	
Heating power	10 kW	
Heat generation	homogeneous	
Phase 2: Test termination and melt extraction		
Test conditions	Reaching of the steady-state conditions in Phase 1	
Heating power	0 kW	

Table 12: Main parameters and test phases of the LIVE-L2 experiment

At the top of the upper heating plane at ~ 32 cm from the bottom of the LIVE test vessel, a ~ 2 cm thick disc was placed (see also **Fig. 70**a). This disc should ensure non-symmetric melt relocation into the test vessel in the beginning of the experiment and simulate the upper crust on the melt surface after the complete melt relocation. Disc diameter was so that about 0.5 cm free space was left from the edge of the disc to the vessel wall to allow the melt to flow downwards. Material of the disc was the same as of the melt (20 mole% of $NaNO_3$ and 80

mole% of KNO_3) in order to keep the melt composition after the disc melting as constant as possible.
To allow fast crust formation and growth, the flooding of the outer vessel wall was started already before the melt pour, first with 1.5 kg/s (to fill the gap between the cooling vessel and the test vessel wall) and then with ~ 47 g/s (**Fig. 67**). This flow rate has been kept constant throughout the whole experiment. Water temperature at the inlet amounted to ~ 10 °C.

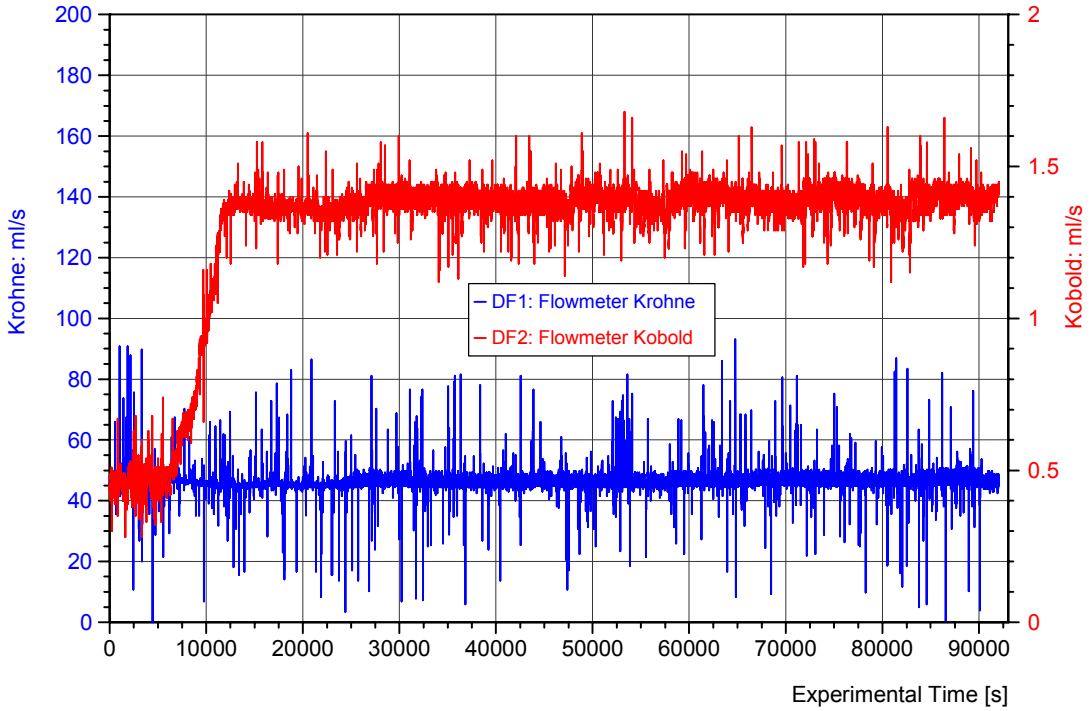

Fig. 67: LIVE-L2: mass flow rate of cooling water

To simulate the corium melt a binary mixture of 20 mole% of $NaNO_3$ and 80 mole% of KNO_3 with liquidus temperature of ~ 300 °C and solidification range of about 80 K has been used (see also **Fig. 56**). The mixture has been melted in the separate heating furnace and when the temperature reached ~ 350 °C, 120 l of the melt has been poured into the LIVE test vessel near to the vessel wall through the pouring spout preheated up to ~ 350 °C. Melt release rate and melt initial temperature are shown in **Fig. 68** and
Fig. 69. Maximum pouring rate derived from the analysis of the vessel weight was ~ 7 kg/s.

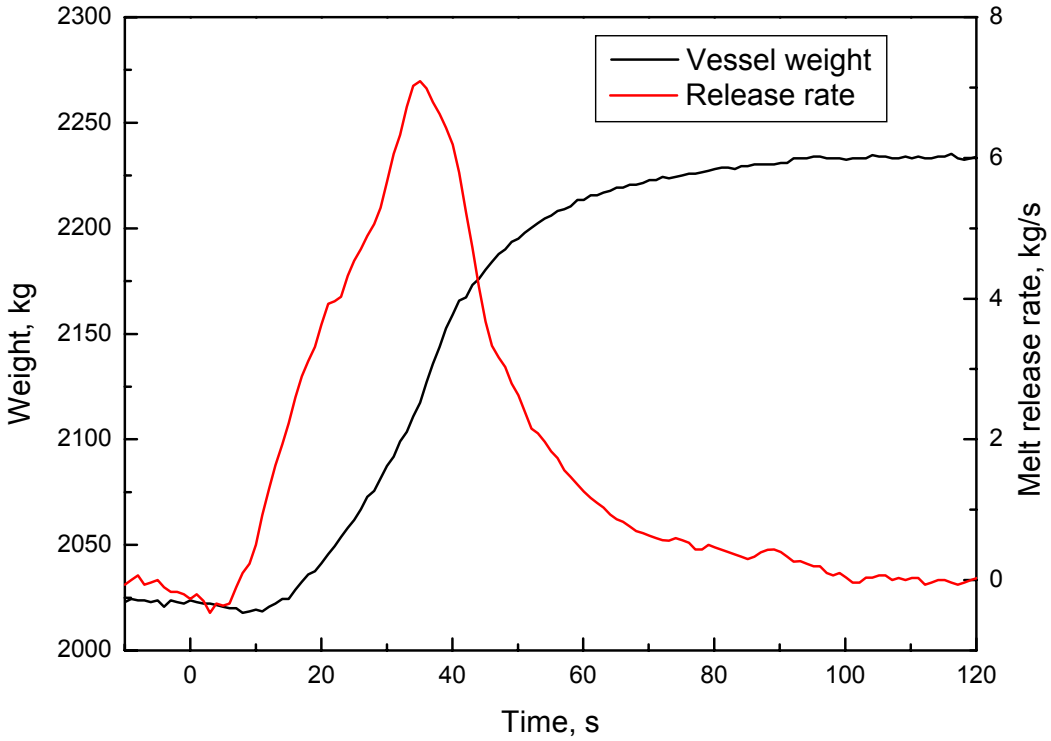

Fig. 68: LIVE-L2: melt release rate

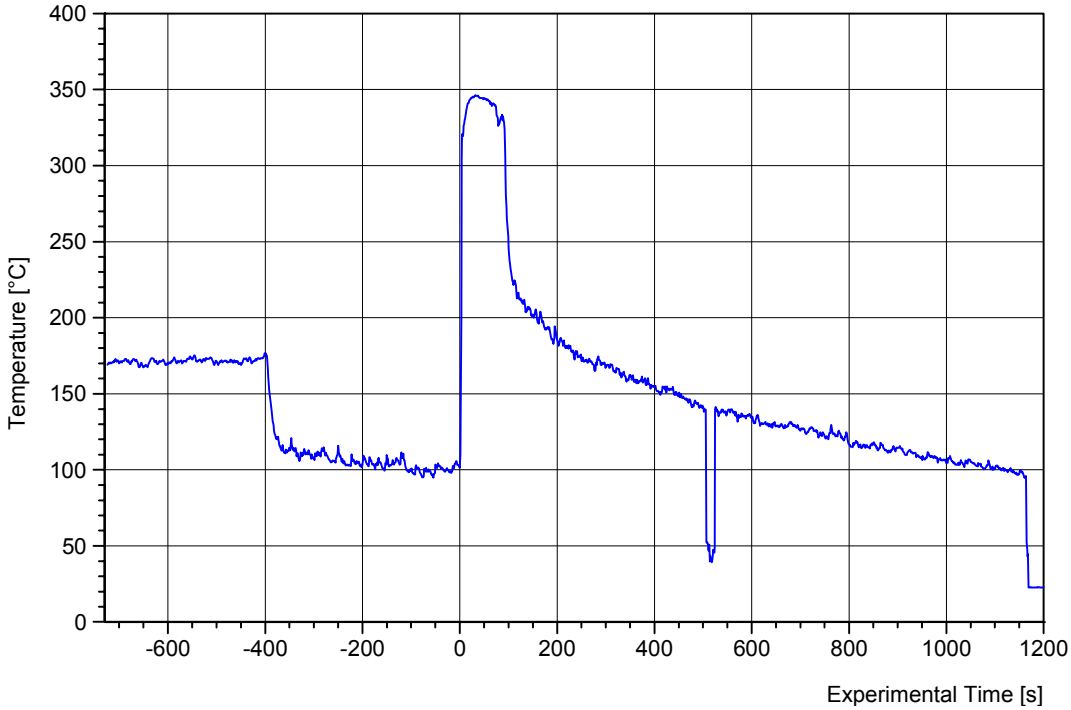

Fig. 69: LIVE-L2: initial melt temperature measured in the pouring spout

The behaviour of the melt and the upper crust is shown in **Fig. 70**. The melt coming from the poring spout (**Fig. 70**b) was first covered the crust surface and relocated downwards through the gap between the crust and the vessel wall (**Fig. 70**b and c). At the same time a hole in the crust was formed at the pouring position allowing the melt to relocate downwards also there. After the completion of the relocation process a firm contact between the crust and the

underlying melt pool has been established (**Fig. 70**d). At the same time, heating power of ca. 10 kW was applied to homogeneously heat the melt by switching all six heating planes simultaneously. The heating power distribution between the heating planes is shown in **Fig. 71**. During this time thinning and melting of the upper crust has been observed starting first at the position of the melt pour (**Fig. 70**e). Complete melting of the crust has been finished in approx. 30 minutes and the melt surface was completely uncovered (**Fig. 70**f).

The volumetric heating of the melt with ~ 10 kW was continued for about 24 hours to reach the steady state conditions. The temperatures measured in the melt pool are presented in **Fig. 72**. During the first 30 minutes of the test the heat generated in the pool was consumed by the crust melting, consequently, the melt pool temperatures were almost constant and even decreased. Only after the complete crust melting the melt pool temperatures started to increase and reached maximum values of ~ 330 °C.

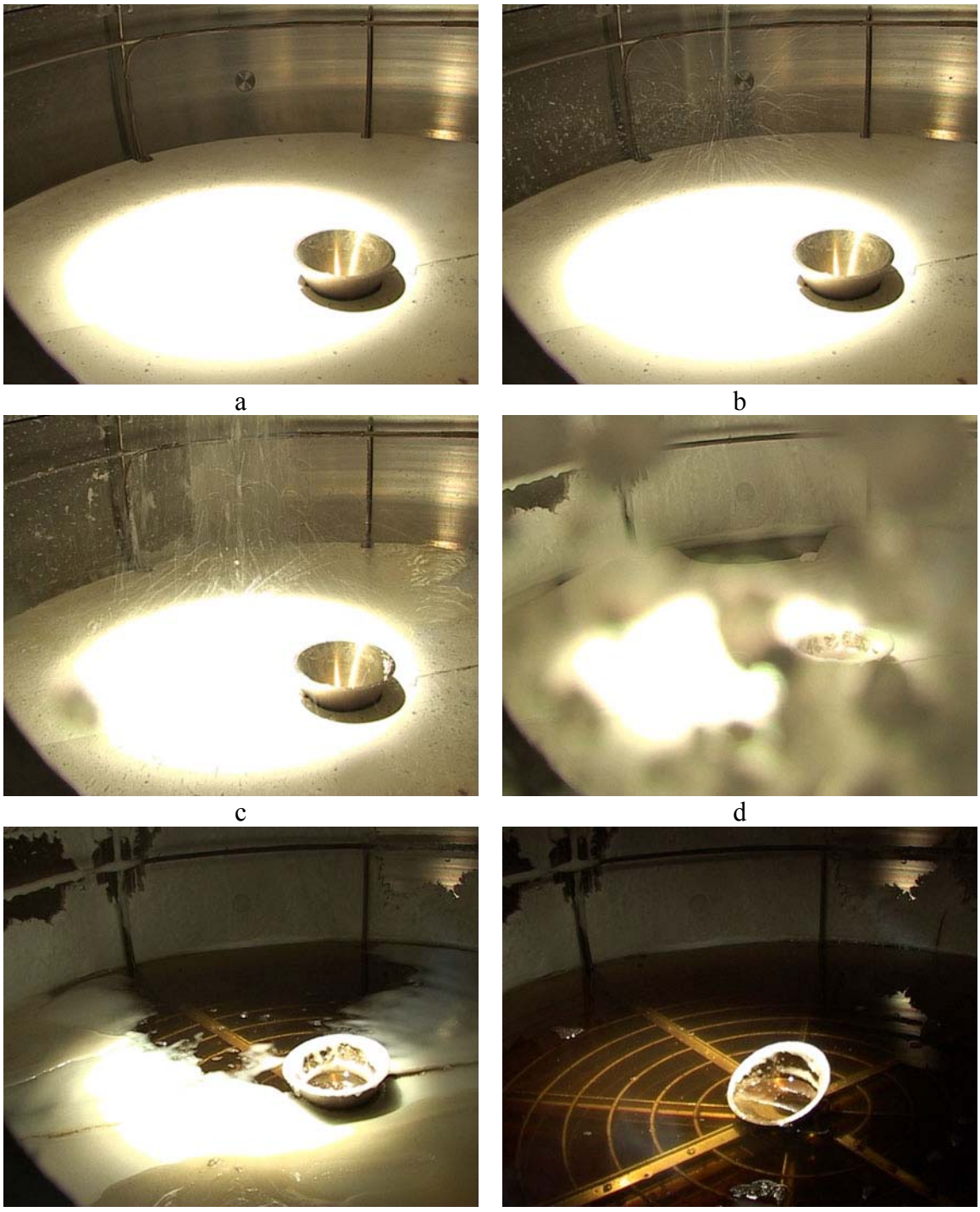

Fig. 70: Top crust behaviour during the LIVE-L2 test: a) before the melt pour, b) beginning of the melt pour), c) melt spreading on the crust surface, d) crust melting at the pour position, downward relocation of the melt, e) crust thinning and partial melting, f) complete crust melting after ~ 30 min from the begin of the melt pour

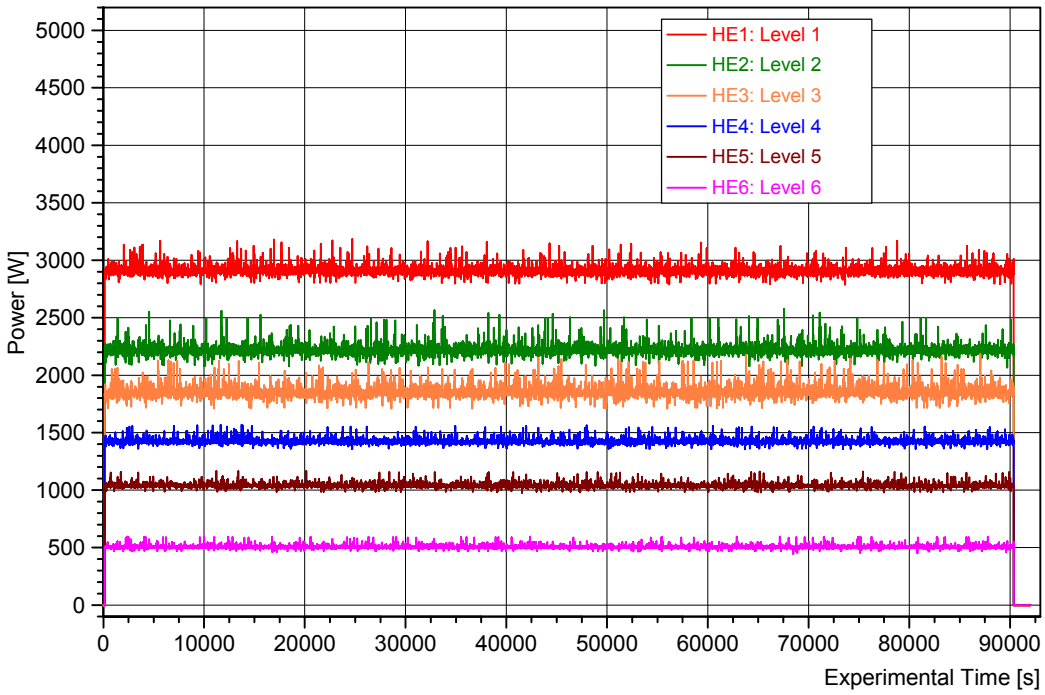

Fig. 71: LIVE-L2: distribution of the 10 kW heating power between the heating planes

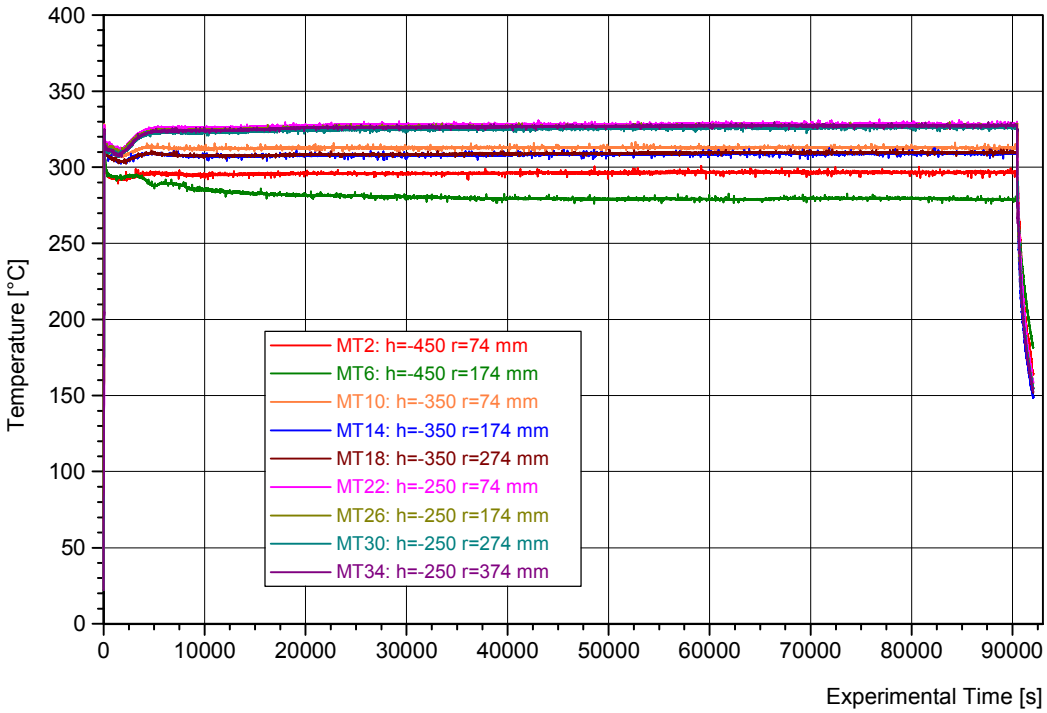

Fig. 72: LIVE-L2: melt temperatures

As in LIVE-L1, only one half-axis of the hemispherical test vessel was equipped with the instrumentation plugs, which allowed to measure non-stationary heat fluxes through the vessel wall. The results of heat flux measurements are presented in **Fig. 73**. In the steady-state phase the value of the maximum heat flux through the vessel wall amounted to ~ 10 kW/m^2 and was measured by the heat-flux sensor HF10 located just below the melt surface. This value is in a good agreement with the results obtained in the LIVE-L1 test.

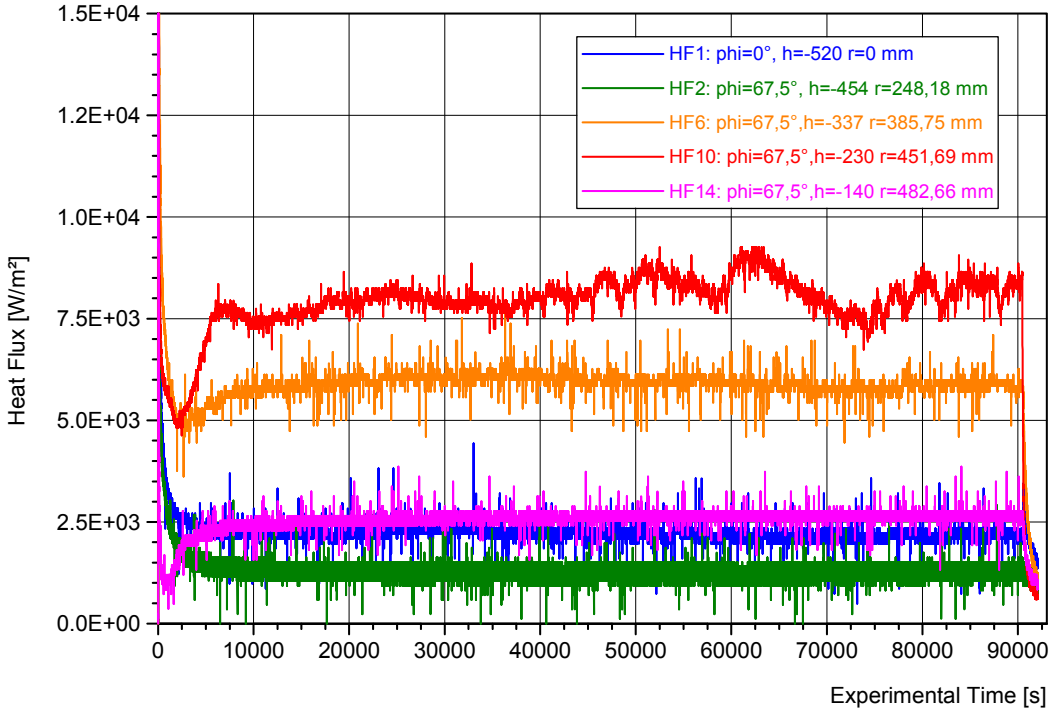

Fig. 73: Heat fluxes measured at different positions in the LIVE-L2 test

To measure the crust thickness and to quantify the crust growth three thermocouple trees were installed at the vessel inner surface at different locations. Each tree has seven thermocouples positioned at different distance from the inner vessel wall. The results of the measurements are presented in **Fig. 74** and **Fig. 75**. The measurements near to the vessel bottom (**Fig. 74**) indicate rapid decrease of the melt temperature and formation of a stable crust which was at least 30 mm thick. In the contrary, the thermocouples located near to the melt surface (**Fig. 75**) show the temperature drop below the solidus temperature immediately after the pouring followed by a temperature increase above the liquidus during the melt heating, thus indicating the re-melting of the crust initially formed during the pouring process. The fluctuations of the thermocouple TC32, which was located at approx. 3 mm from the vessel wall into the melt lead to the conclusions that the crust at this location did not exceed thickness of 3-4 mm.

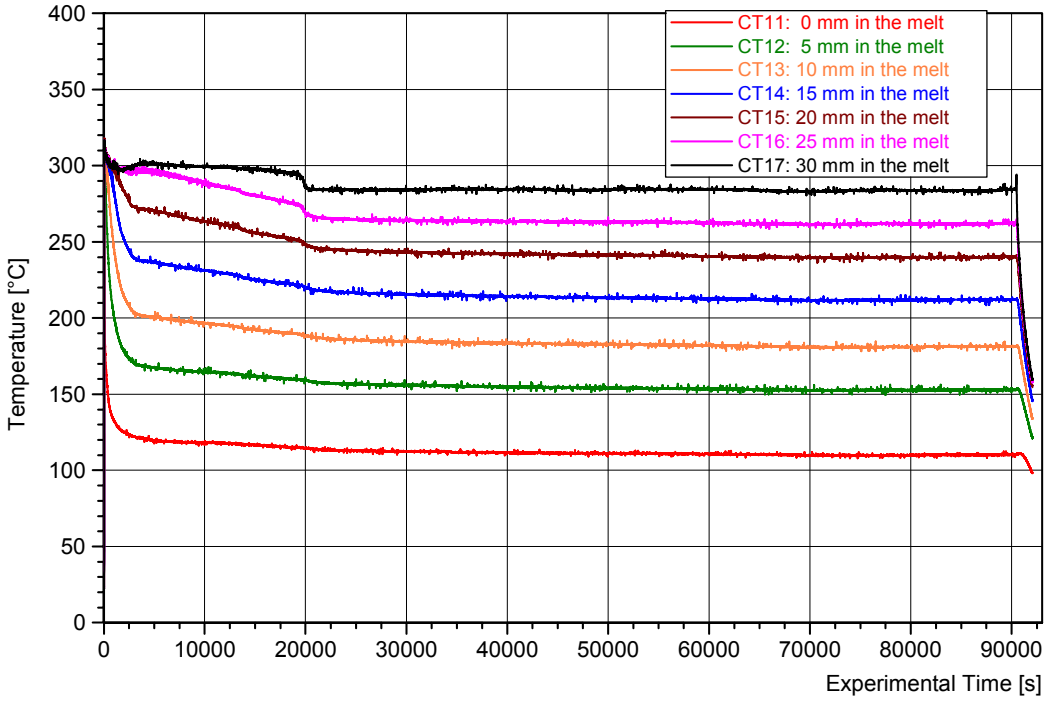

Fig. 74: Temperatures measured by the thermocouple tree TT1 in the LIVE-L2 test

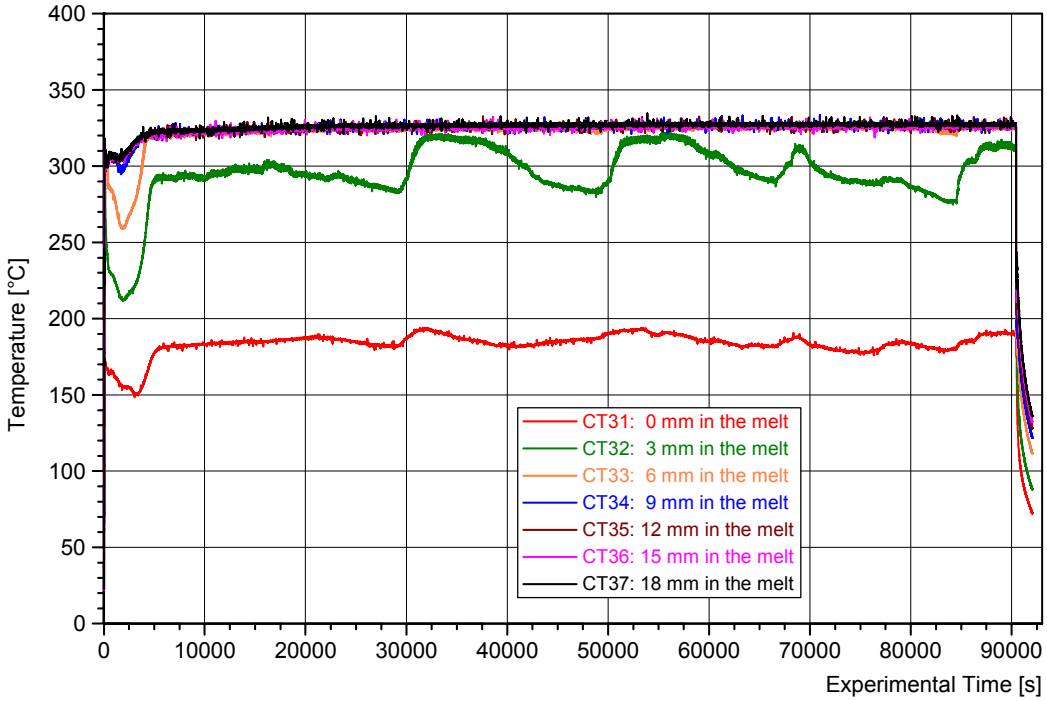

Fig. 75: Temperatures measured by the thermocouple tree TT3 in the LIVE-L2 test

The experiment was completed by switching off the volumetric heating and by the extraction of the liquid melt back into the heating furnace to uncover the crusts formed during the test. The measurements of the crust thickness along the vessel wall are presented in **Fig. 76**. They show that the crust thickness varies between 5 mm at the position near to the melt surface and ~ 46 mm at the bottom of the test vessel. These values are also in a good agreement with the results obtained by the analysis of the thermocouple trees measurements.

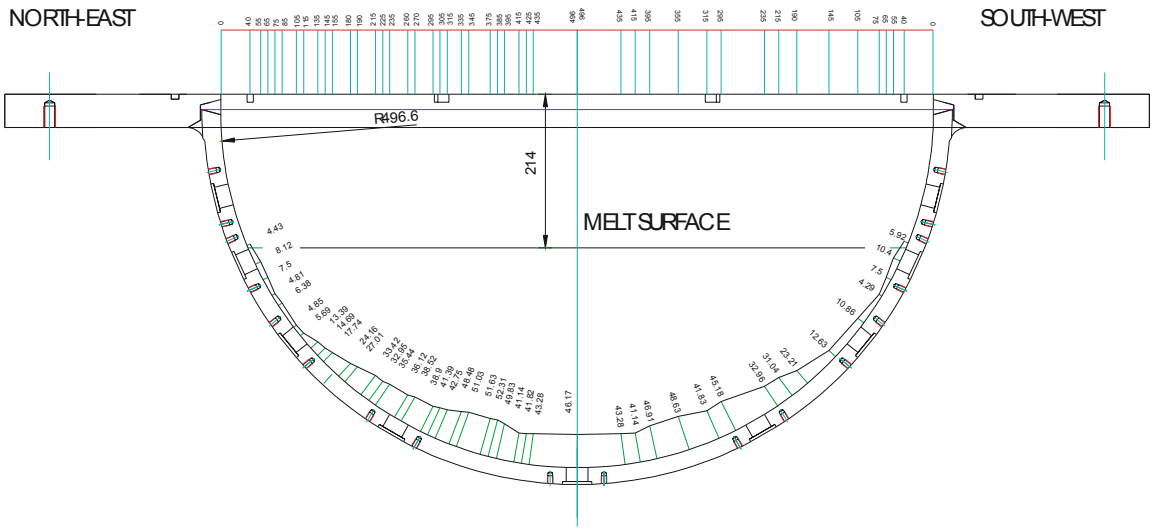

Fig. 76: Crust thickness profile measured in the LIVE-L2 test

3. Summary and conclusions

The LACOMERA project at Forschungszentrum Karlsruhe is a TALI action within the Fifth Framework Programme (FP5) of the EU. It started in September 2002. The overall objective of the project was to offer research institutions from EU Member Countries and Associated States access to four large-scale experimental facilities (QUENCH, LIVE, DISCO-H, and COMET) which can be used to investigate core-melt scenarios from the beginning of core degradation to melt formation and relocation in the vessel, possible melt dispersion to the reactor cavity, and finally corium concrete interaction and corium coolability in the reactor cavity.

The general aim of the LACOMERA project was to spread the experiments around different EU countries to achieve a balance amongst old and new members. As a result of three calls for proposals, eight organisations from five countries profited from the LACOMERA project by participating in the preparation, conduct and analysis of eight experiments. The results of these experiments were used for the validation of codes applied for safety assessment and planning of accident mitigation concepts. The main results obtained in these experiments are described below.

QUENCH-L1: Air-ingression impact on core degradation. Experiment QUENCH-L1 was intended to simulate air ingress during an anticipated accident in a spent fuel pool and its consequence on the fuel elements. In detail, it is assumed that water-cooling of the stored fuel elements is interrupted; the water inventory in the pool boils off, and oxidizes the fuel rods. Eventually, the water level is so low that a flow path for air into the fuel elements is opened through holes in the lower part of the shroud. If the water boils off even in the region of the bundle foot, a larger path is opened from below the shroud. The fuel element geometry is assumed intact up to this time. The test has provided unique data for the investigation of air ingress phenomenology in conditions as representative as possible of the reactor case regarding the source term.

– The bundle was pre-oxidised in steam to ~ 500 µm before the air ingression phase. After the oxidation in air the maximum oxide layer thickness prior to reflood amounted to more than 600 µm.

- Reflood was initiated when the bundle temperatures exceed 1800 °C, resulting in an almost immediate cooling of the rods, giving a total of ~ 53 g of hydrogen production, ~ 48 g of it being produced before reflood. About 60 % or 5 g of the nitrogen previously taken up was released.
- The bundle and its shroud appear completely oxidised in the region between 750 and 1000 mm. The surface of the rods shows a white oxide layer and some spots where nitride had formed by oxidation in air.

QUENCH-L2: Boil-off of a flooded bundle. The experiment QUENCH-L2 on boil-off and subsequent quenching is dedicated to investigate degraded core reflood situations with a rather low mass flow rate. The test conditions simulated a depressurised plant sequence in which the core would be essentially dried-out and with a limited steam flow due to boiling of residual water in contact with the hot structures in the lower plenum. In contrast to all the previous QUENCH experiments, the bundle was initially filled with water and slowly evaporated. Peak cladding oxidation after the transient prior to the reflood phase was about 170 µm. The total generation of hydrogen was ~ 140 g, of which more than 90 % was produced during the reflood phase. It is possible that the modest level of pre-oxidation, combined with the rather low reflood rate, led to conditions favourable for an enhanced oxidation during reflood.

LIVE-L1: Core-melt behaviour in the lower plenum of the reactor pressure vessel and the influence of the cooling of the vessel outer surface with water in the conditions that may occur during core-meltdown accident in the WWER-1000 plant. To simulate a corium melt a binary non-eutectic mixture of $NaNO_3$ and KNO_3 was used. The experiment provided significant information on the melt pool behaviour during the stages of air circulation at the outer RPV surface with a subsequent flooding of the lower head. Moreover, important data have been obtained regarding the dependence of the crust growth and crust composition on the internal heat generation and outside cooling regimes as well as the crust influence on the heat flux distribution along the vessel wall.

LIVE-L2: Transient melt spreading along the RPV lower head wall, the shape of the final melt pool and its impact on the steady-state heat fluxes in the conditions that may occur during core-meltdown accident in LWRs. The test addressed the questions of melt stabilisation and the effects of crust formation near the RPV wall for a non-symmetrical melt pool shape. To promote non-symmetric melt relocation into the test vessel and later on to simulate the upper crust at the melt surface after the complete melt relocation a ~ 2 cm thick disc was placed at the top of the upper heating plane at ~ 32 cm from the bottom of the LIVE test vessel. The test provided important data on the upper crust behaviour and heat flux distribution in the transient and steady state stages of the experiment.

COMET-L1: Long-term 2D concrete ablation in siliceous concrete cavity at intermediate decay heat power level with a top flooding phase after a phase of dry concrete erosion. This test investigates the situation of basement attack by the simulated corium melt The open questions which are addressed in this experiment are 1) long-term erosion of the concrete by a two component metal plus oxide melt during the absence of water, and 2) consequence of top flooding when water is added to the surface of the hot melt during concrete erosion. This experiment is complementary to the present OECD-CCI tests that are carried out at ANL with pure oxidic corium.

- In the early phase of the test initial erosion into axial and lateral direction is similar. The measurements show fast decrease of the melt overheat and reduction of the initially high concrete erosion rate.
- During the phase of equilibrium between decay heat and removed heat, there are indications for formation of a crust at the concrete interface. Erosion is then propagating mainly into the axial direction, as the encrusted metal melt tends to move like a solid body.
- After the end of heating the melt cools down very slowly. Late surface flooding has little effect to improve heat removal from the bulk of the (mostly solidified) melt.

COMET-L2: Long-term MCCI of simulated metallic corium under dry conditions with decay heat simulation of intermediate power; observation of downward and sideward cavity erosion. The experiment COMET-L2 concentrates on the study of a long-term metal/concrete interaction in cylindrical cavity for intermediate and low decay heat levels through the metal phase only, representing ex-vessel accident conditions some hours after the start of the basement erosion. In the early phase of the test, measurements show fast decrease of the melt overheat and reduction of the initially high concrete erosion rate. Initial erosion into axial and lateral direction is similar. During the subsequent phase of equilibrium between decay heat and removed heat, slow concrete erosion and slow gas release are interrupted by several phases of more intense gas eruptions and melt agitation and there are indications for formation of a metal crust at the concrete interface. Erosion is then propagating mainly into the axial direction, as the encrusted metal melt tends to move like a solid body. However, comparison with high power experiments shows that lateral erosion through the metal phase becomes more important when the heating power is reduced. The low power density in the present test favours the existence of metal crusts, which may have a strong influence on the shape of the cavity. Experimental results are important for real accident scenarios (metal at the bottom) and are required for code validation (e.g. ASTEC).

DISCO-L1: Thermal hydraulic behaviour of the corium melt dispersion neglecting the chemical effects such as hydrogen generation and combustion. The experiment DISCO-L1 was performed to contribute to solve the DCH issue at low RCS pressure in French-type PWR. This experiment was carried out with a nearly inert atmosphere, thus avoiding hydrogen combustion and focussing on corium dispersion and on containment pressurisation induced by the debris to gas heat exchanges.

- The maximum pressure was 3.3 bar in the containment, 5 bar in the cavity and 3.9 bar in the pit bottom access. However, it is noted, that with presence of H_2 and air in the containment, these pressures could be higher (due to the hydrogen combustion) than in the present experiment carried out in nearly inert conditions.
- The thermocouples in the containment show that the average temperature in the containment was around 170 °C, 10 s after the beginning of the ejection.
- All the surface of the cavity is covered by a film of solidified melt and 60.6 % of the initial mass of melt was ejected out of the cavity: 14.5 % was found in the containment, 28 % in the compartments and 18.1 % in the pit bottom access.
- The gas analysis showed some small hydrogen production and the existence of CO and CO_2 as usual products of melt concrete interaction.

DISCO-L2: The experiment DISCO-L2 aims at investigating the fluid-dynamic, thermal and chemical processes during melt ejection out of a breach in the lower head of a pressure vessel of the VVER-1000/320 type of reactor, which has not been studied before, neither in the DISCO facility nor elsewhere. The experimental results demonstrated that for the VVER-

1000 reactor geometry the pressure increase due to the direct containment heating should not be an issue, because only small amount of melt is finely dispersed and the debris-gas interaction is limited. The venting lines probably will become plugged by the frozen melt. Because almost all the melt will gather in the reactor pit and in the neighbouring compartments the corium-concrete interaction will take place there.

The LACOMERA project has attracted a great deal of interest because it concentrates on key safety related topics of particular interest for accident management and mitigation measures such as hydrogen generation not only during heat-up but also during cool-down and quenching, corium behaviour in the core lower plenum, and long-term corium concrete interaction. Project meetings held and linked with some QUENCH workshops provided a forum where the results could be widely discussed. In particular, results of the QUENCH-L1 test were used for the discussions of the future PHEBUS programme. Through various topical meetings and exchanges between EC projects like SARNET and PLINIUS, the project provided the opportunity to disseminate acquired knowledge and experience on core degradation and core-melt behaviour under severe accident conditions in the European nuclear energy community.

The importance of the LACOMERA project for European research is reflected in three aspects:

- The access to large-scale experimental facilities was proposed to investigate all processes from early core degradation to late in-vessel phase pool formation in the lower head and continuation to the long-term ex-vessel melt situations.
- The project considers the reactors on a European basis – taking into account the main light water reactors including Eastern ones (VVER design). A European vision was used to decide priorities in the experimental programme.
- The project offered a unique opportunity for Eastern experts to get an access to large-scale facilities in Western research organisation to improve understanding of material properties and core behaviour under severe accident conditions and to become familiar with high-level safety concepts in nuclear power plants.

Activities within the LACOMERA project also include the following achievements:

- An aerosol measurement system has been designed and installed at the QUENCH facility by AEKI, Hungary. It has been used in the QUENCH-L1 and QUENCH-L2 experiments. Measuring of aerosol production during the quenching process has not been done before. Although only loosely coupled to the melt formation and hydrogen production problem, the project partners thought it useful to measure the aerosols generated from these unique experiments so as to provide information to researchers working in the source-term area who are interested in knowing the size distribution of aerosols generated during quenching.
- The research activities within the LACOMERA project also incorporated valuable training aspects. A female student from Bulgaria was responsible for pre-test calculations of the COMET-L1 experiment and for the preparation of the experiment report. The evaluation of the experimental results was part of her diploma thesis. An engineering student from Bulgaria has been delegated to the FZK within the SARNET mobility programme to evaluate the results of the DISCO-L2 experiment and to write a final report on the test. The results of the DISCO-L2 experiment are part of his PhD thesis.
- In the DISCO-L2 experiment, a valuable link between the research organisations and the end-users has been established. This experiment was proposed by the Technical

University of Sofia, Bulgaria, in close co-operation with the Kozloduy nuclear power plant operator and was aimed at investigating the fluid-dynamic, thermal and chemical processes during melt ejection out of a breach in the lower head of the pressure vessel of a VVER-1000/320 type of reactor. The experimental results demonstrated that for the VVER-1000 reactor geometry, the pressure increase due to the direct containment heating should not be an issue, because only a small amount of melt is finely dispersed and the debris-gas interaction is limited.

Information about the project and the experimental facilities can be found at the LACOMERA website at http://hikwww9.fzk.de/lacomera.

4. Acknowledgements

The partners of the LACOMERA project warmly thank the European Commission for its financial support under the Fifth Framework Programme on Nuclear Fission Safety and in particular Alejandro Zurita and Michel Hugon for their deep interest, encouragement, comments, and suggestions that greatly improved the project.

5. References

[1] A. Miassoedov, H. Alsmeyer, L. Meyer, LACOMERA – Large-scale Experiments on Core Degradation, Melt Retention and Coolability at Forschungszentrum Karslruhe, 2003, *Nuclear Energy for New Europe* 2003 Conf. Proc., Paper 301, CD-ROM.

[2] A. Miassoedov, H. Alsmeyer, B. Eppinger, L. Meyer, M. Steinbrück, 2003, Large-scale Experiments on Core Degradation, Melt Retention and Coolability (LACOMERA). FISA 2003: EU Research in Reactor Safety, Luxembourg, Preproc. p. 239-244.

[3] A. Miassoedov, H. Alsmeyer, L. Meyer, M, Steinbrück, W. Tromm, 2006, An Overview of the Severe Accident Research Activities Within the LACOMERA Platform at the Forschungszentrum Karlsruhe, Technical Meeting on Severe Accident and Accident Management for Nuclear Power Plants, Tokyo, J, March 14-16, 2006, Proc. on CD-ROM.

[4] A. Miassoedov, H. Alsmeyer, L. Meyer, M, Steinbrück, Z. Hoser, I. Ivanov, G. Doubleva, M. Cranga, C. Carolli, D. Plassart, 2005, Results of the QUENCH-L1, DISCO-L1, and COMET-L1 Experiments Performed Within the LACOMERA Project at the Forschungszentrum Karlsruhe, Proc. of the 13th Internat. Conf. on Nuclear Engineering (ICONE-13), Beijing, China, CD-ROM Paper 50607.

[5] A. Miassoedov, H. Alsmeyer, L. Meyer, M, Steinbrück, P. Groudev, I. Ivanov, G. Sdouz, 2006, Results of the QUENCH-L2, DISCO-L2, and COMET-L2 Experiments Performed Within the LACOMERA Project at the Forschungszentrum Karlsruhe. Proc. of the 14th Internat. Conf. on Nuclear Engineering (ICONE-14), Miami, Fla., CD-ROM Paper ICONE14-89343.

[6] L. Sepold,, et al., 2004, Hydrogen Generation in Reflooding Experiments with LWR-Type Fuel-rod Bundles (QUENCH Programme), *Nuclear Technology*, vol. 147, p. 202-215.

[7] L. Sepold, et al., 2001, Reflooding Experiments with LWR-type Fuel-rod Simulators in the QUENCH Facility, Nuclear Engineering and Design, 204(2001) p. 205-220.

[8] L. Sepold, L. Steinbock, M. Steinbrück, U. Stegmaier, J. Stuckert, A. Miassoedov, S. Horn, Z. Hozer, I. Nagy, P. Windberg, L. Matus, 2004, QUENCH-10 Quick Look Report, PSF 3396, SAM-LACOMERA-D03, Forschungszentrum Karlsruhe.

[9] M. Steinbrück, A. Miassoedov, G. Schanz, L. Sepold, U. Stegmaier, J. Stuckert, 2006, Experiments on air ingress during severe accidents in LWRS. Nuclear Engineering and Design, 236(2006) p. 1709-1719.

[10] G. Schanz, M. Heck, Z. Hoser, L. Matus, I. Nagy, L. Sepold, U. Stegmaier, M. Steinbrück, H. Steiner, J. Stuckert, P. Windberg, 2006, Results of the QUENCH-10 Experiment on Air Ingress, FZKA 7087, SAM-LACOMERA-D09, Forschungszentrum Karlsruhe.

[11] C. Homann, W. Hering, J. Birchley, T. Haste, 2005, Analytical Support for the Preparation of Bundle Test QUENCH-10 on Air Ingress, FZKA 7086, SAM-LACOMERA-D01, Forschungszentrum Karlsruhe.

[12] L. Matus, I. Nagy, P. Windberg, N. Vér, M. Kunstár, A. Pintér, Z. Hózer, 2004, Aerosol Measurements in the QUENCH-10 Test, Experimental Data Report AEKI-FRL-2004-123-01/01, SAM-LACOMERA-D08, KFKI Atomic Energy Research Institute, Budapest, Hungary.

[13] W. Hering, 2004, Summary of pre-test calculations performed for test QUENCH-L2 (QUENCH-11), NUKLEAR 3397, SAM-LACOMERA-D05, Forschungszentrum Karlsruhe.

[14] G. Doubleva, H. Alsmeyer, T. Cron, B. Fluhrer, J. Foit, G. Messemer, A. Miassoedov, S. Schmidt-Stiefel, T. Wenz, I. Ivanov, M. Cranga, 2005, COMET-L1 Test Data Report, NUKLEAR 3399, SAM-LACOMERA-D04, Forschungszentrum Karlsruhe.

[15] G. Doubleva, H. Alsmeyer, T. Cron, B. Fluhrer, J. Foit, G. Messemer, A. Miassoedov, S. Schmidt-Stiefel, T. Wenz, I. Ivanov, M. Cranga, 2006, The COMET-L1 Experiment on Long-Term MCCI and Late Melt Surface Flooding, FZKA 7213, SAM-LACOMERA-D14, Forschungszentrum Karlsruhe.
[16] M. T. Farmer et al., 2004, Results of Reactor Materials Experiments Investigating 2-d Core-Concrete Interaction and Debris Coolability, Proc. ICAPP '04, Pittsburgh, PA, Paper 4102.
[17] G. Sdouz, R. Mayrhofer, H. Alsmeyer, T. Cron, A. Miassoedov, S. Schmidt-Stiefel, 2005, COMET-L2 Test Data Report, NUKLEAR 3404, SAM-LACOMERA-D07, Forschungszentrum Karlsruhe.
[18] G. Sdouz, R. Mayrhofer, H. Alsmeyer, T. Cron, B. Fluhrer, J. Foit, G. Messemer, A. Miassoedov, S. Schmidt-Stiefel, T. Wenz, 2006, The COMET-L2 Experiment on Long-Term MCCI with Steel Melt, FZKA 7214, SAM-LACOMERA-D15, Forschungszentrum Karlsruhe.
[19] H. Alsmeyer, 1995, Review of Experiments on Dry Corium Concrete Interaction, Molten corium/concrete interaction and corium coolability – A state of the art report, EUR 16649 EN,1995.
[20] L. Meyer, M. G. Gargallo, 2003, Low-Pressure Corium Dispersion Experiments with Simulant Fluids in a Scaled Annular Cavity, Nuclear Technology, 141, p. 257-274.
[21] D. Plassart, G. Albrecht, M. Kirstahler, L. Meyer, M. Schwall, E. Wachter, G. Wörner, 2004, DISCO-L1 Test Report, NUKLEAR 3397, IRSN-NT-DSR/SAGR/05-52, SAM-LACOMERA-D06, Institut de Radioprotection et de Sûreté Nucléaire, Forschungszentrum Karlsruhe.
[22] S. Kisyoski, I. Ivanov, D. Popov, G. Albrecht, M. Kirstahler, L. Meyer, M. Schwall, E. Wachter, 2006, DISCO-L2 Test Report, NUKLEAR 3408, SAM-LACOMERA-D12, Forschungszentrum Karlsruhe.
[23] O. Kymäläinen, H. Tuomisto, T.G. Theofanous, 1997, In-vessel retention of corium at the Loviisa plant, Nuclear Engineering and Design, 169 (1997), pp.109-130.
[24] S. Abalin, I. Gnidoi, V. Semenov, V. Strizhov, A. Surenkov, 2000, The Results and Analysis of the RASPLAV Salt Tests, Rasplav Seminar 2000, Munich, Germany, 14-15 November 2000.
[25] B. Fluhrer, H. Alsmeyer, T. Cron, G. Messemer, A. Miassoedov, T. Wenz, 2005, The Experimental Programme LIVE to Investigate In-Vessel Core-melt Behaviour in the Late Phase, Annual Meting on Nuclear Technology 10-12 May 2005, Nürnberg, INFORUM GmbH, 2005, Paper 312, p. 198-201.